

Energy Research and Development Division
FINAL PROJECT REPORT

Enhanced Skylight Modeling and Validation

Prepared for: California Energy Commission

Prepared by: Architectural Energy Corporation
Daylighting Innovations
California Lighting Technology Center

Project Management: New Buildings Institute



APRIL 2013
CEC-500-08-049



The CEC is in the process of completing the final review of this report.

Prepared by: Daylighting Innovations

Primary Author(s):

Zack Rogers (DLI)

Secondary Author(s):

Anothai Thanachareonkit (CLTC)

Luis Fernandes (CLTC)

Project Research Manager:

Judie Porter

Architectural Energy Corporation

Program Research Manager:

Cathy Higgins

New Buildings Institute

CLTC Principal Investigator

Konstantinos Papamichael

Contract Number: 500-08-049

Prepared for:

California Energy Commission

David Weightman

Contract Manager

Virginia Law

Office Manager

Energy Efficiency Research Office

Laurie ten Hope

Deputy Director

RESEARCH AND DEVELOPMENT DIVISION

Robert P. Oglesby

Executive Director

DISCLAIMER

This report was prepared as the result of work sponsored by the California Energy Commission. It does not necessarily represent the views of the Energy Commission, its employees or the State of California. The Energy Commission, the State of California, its employees, contractors and subcontractors make no warranty, express or implied, and assume no legal liability for the information in this report; nor does any party represent that the uses of this information will not infringe upon privately owned rights. This report has not been approved or disapproved by the California Energy Commission nor has the California Energy Commission passed upon the accuracy or adequacy of the information in this report.

ACKNOWLEDGEMENTS

The authors and the project manager wish to acknowledge the following in-kind collaboration partners:

- Bruce Mosher and Velux for the skylight photometric facility and product support.
- Kurt Levens with Daylight Technology
- Mark Jongewaard, Calvin Lanpher, Meg Tidd and LTI Optics for providing Photopia simulations, software access and tech support
- Michael Gauvin, Ed Freniere, Dave Jacobsen, and TracePro for software access and tech support.
- Jacob Jonsson with LBNL for goniophotometer measurements, data translation and support.
- Andy McNeil with LBNL and Greg Ward with Anywhere Software for genBSDF, BSDF material, and Radiance simulation support.

The support of the California Energy Commission/Public Interest Energy Research program staff, as well as the staff of New Buildings Institute is also gratefully acknowledged.

PREFACE

The California Energy Commission Energy Research and Development Division supports public interest energy research and development that will help improve the quality of life in California by bringing environmentally safe, affordable, and reliable energy services and products to the marketplace.

The Energy Research and Development Division conducts public interest research, development, and demonstration (RD&D) projects to benefit California.

The Energy Research and Development Division strives to conduct the most promising public interest energy research by partnering with RD&D entities, including individuals, businesses, utilities, and public or private research institutions.

Energy Research and Development Division funding efforts are focused on the following RD&D program areas:

- Buildings End-Use Energy Efficiency
- Energy Innovations Small Grants
- Energy-Related Environmental Research
- Energy Systems Integration
- Environmentally Preferred Advanced Generation
- Industrial/Agricultural/Water End-Use Energy Efficiency
- Renewable Energy Technologies
- Transportation

Enhanced Skylight Modeling and Validation is the final report for the Enhanced Skylighting Modeling and Validation project. This is a research project within the Evidence-based Design and Operations Project (CEC contract number 500-08-049) conducted by New Buildings Institute. The information from this project contributes to Energy Research and Development Division's Building End-Use Energy Efficiency Program.

When the source of a table, figure or photo is not otherwise credited, it is the work of the authors of the report.

For more information about the Energy Research and Development Division, please visit the Energy Commission's website at www.energy.ca.gov/research/ or contact the Energy Commission at 916-327-1551.

ABSTRACT

This report details all tasks, findings, and recommendations undertaken for the Enhanced Skylight Modeling and Validation project. The scope involved developing and validating computer simulation alternatives to physical measurements for producing optical daylighting system photometry. The project plan included comparing several physical photometric measurements of optical daylighting systems to computer models, and validating the use of computer simulation to produce this photometric information. The key activities were skylight device measurements and material testing, data processing, and computer simulations setup and analysis.

To achieve a robust validation of the computer simulation methods, it was ideal to have physical skylight system measurements from a wide variable range of sky conditions as well as skylight systems. The selected skylight devices were tested at a goniophotometer testing facility located in Greenwood, South Carolina.

One key step in creating accurate computer models of the skylight systems was to model accurate optical properties of the surfaces in those systems. Visible reflectance and transmittance measurements were made for any surface that interacts with the optics of the system. Samples of these materials were cut from the actual skylights tested for detailed measurements of the transmittance and reflectance.

The simulation process used the created sky sources, the geometric models, and material models to calculate an output photometric distribution for comparison with the measured photometric distributions. Three software platforms were used: Radiance, TracePro, and Photopia.

Findings indicate that it is possible to use computer simulations to accurately model and produce optical daylighting system photometry information. Further work is recommended to establish protocols for material testing and work with manufacturers to produce optical daylighting system photometry data for their products.

Keywords: Daylighting, Skylights, Photometry, TracePro, Radiance, Photopia

Please use the following citation for this report:

Rogers, Zack, (DLI), Luis Fernandes (CLTC) and Anothai Thanachareonkit (CLTC). 2013. Enhanced Skylight Modeling and Validation Report.

This page deliberately left blank

TABLE OF CONTENTS

EXECUTIVE SUMMARY	1
CHAPTER 1: Introduction.....	3
CHAPTER 2: Testing Facility and Skylight Systems	6
Velux Daylight Laboratory	7
Climate Information	8
Skylighting Systems.....	9
CHAPTER 3: Measurement Equipment, Settings and Procedure	12
Sky Measurement Equipment.....	13
Goniophotometer Equipment	16
Measurement procedure	17
CHAPTER 4: Measurement Results	20
Timeline of tests.....	21
Sky luminance mapping	24
Comparison of sky luminance at zenith	25
Horizontal illuminance	26
On-site Material Measurements.....	27
Luminous intensity	27
CHAPTER 5: Simulation Software and Setup.....	29
Sky Measurement Processing and Model Creation	29
Sky Source Ray Set Creation.....	32
Geometry Measurements and Creation.....	37
Near Field vs. Far Field Comparisons.....	70
CHAPTER 6: BSDF Measurements and Modeling.....	39
LBNL BSDF Measurements	41
Radiance BSDF Approach.....	42
TracePro BSDF Approach	52
Photopia BSDF Approach.....	59

BSDF Measurement Conclusions.....	64
CHAPTER 7: Simulation Setup.....	66
TracePro.....	67
Radiance	71
Photopia.....	78
CHAPTER 8: Simulation Results.....	83
Sunoptics Top Lens.....	86
Sunoptics Box.....	91
Sun Tunnel	96
CHAPTER 9: Conclusions and Recommendations.....	101
Sky Measurement and Processing	101
BSDF Measurement and Processing.....	102
Simulation and Modeling	103
Photometric Validation	104
Appendix A: BSDF Measurements	A-1
A.1 Theoretical Simulated BSDF Predictions.....	A-2
A.2 SunOptics Pyramid Measurement Comparison	A-4
A.3 SunOptics Reflector	A-13
A.4 Suntunnel Base Diffuser	A-13
A.5 Suntunnel Tube Walls.....	A-20
A.6 Suntunnel White Boot.....	A-21
Appendix B: On-site Material Measurements.....	B-22
Appendix C: Illuminance meter calibration	C-23
Appendix D: Sky Patching Study.....	D-24
Appendix E: References.....	E-25

List of Figures

Figure 1: Velux Daylighting Laboratory Location, Building and Surroundings	7
Figure 2: Velux Daylight Photometry Building and Equipment.....	8
Figure 3: Maximum Daily Horizontal Illuminance.....	9
Figure 4: Installation of the simple prismatic skylight system	10
Figure 5: Installation of the Sunoptics LightCube	11
Figure 6: Velux Sun Tunnel Installed.....	11
Figure 7: Equipment on the Roof.....	14
Figure 8: Sky luminance equipment: Luminance meter (left) and HDR camera for (right).....	15
Figure 9: Horizontal illuminance equipment: CLTC illuminance meter with shading disk (left) and Velux illuminance meter (right)	15
Figure 10: Skylight photometric measurement equipment schematic section.....	16
Figure 11: Goniophotometer control station	17
Figure 12: Measurement procedure diagram.....	18
Figure 13: Illuminance Meter Calibration.....	19
Figure 14: Measurement of the reflectance of the interior walls of the goniophotometer room and the light well panels	19
Figure 15: Measurement timeline diagram	22
Figure 16: Hemispherical photographs taken for Test 12	24
Figure 17: Final HDR image - raw sky luminance map for Test 12.	25
Figure 18: Luminous intensity of Sunoptics system (top only) under clear sky (test 27)	27
Figure 19: Luminous intensity of complete Sunoptics system under clear sky (test 31)	28
Figure 20: Luminous intensity of Sun Tunnel system under clear sky (test 29)	28
Figure 21: Locating and Mapping captured sky.....	29
Figure 22: Creating a negative mask, applying to capture sky and calibration.....	30
Figure 23: Creating a matching perez sky, performing a circumsolar adjustment, and a positive mask	31
Figure 24: Final Sky – 3202 fc.....	32
Figure 25: The “Sky Hat” and “Sun Hat” continuous ray-set sources	33

Figure 26: Common hemisphere mapping algorithms.....	34
Figure 27: TracePro Mapped Sky Candela Plot – 3203fc diffuse.....	37
Figure 28: Isometric diagrams of the Sunoptics Light Box and the Sun Tunnel Geometric Models	38
Figure 29: Section of physical measurement points and computer simulated near-field points .	70
Figure 30: Near field vs. far field photometry comparison.....	71
Figure 31: Definition of Polar Angles used in BSDF measurements	40
Figure 32: Illustration of the PAB Ltd Gonio-Photometer II used at LBNL	41
Figure 33: A diamond prism’s planes of symmetry (left) and measured planes (right).....	42
Figure 34: Laser Scan 3D Prismatic Lens Material Models	43
Figure 35: Rendering of the Sunoptics lens Radiance model.....	43
Figure 36: Klems Hemisphere Patches – Standard numbering and orientation.....	44
Figure 37: Klems coordinate system for incident, reflected and transmitted light.....	45
Figure 38: Orthographic projections of BSDF hemispherical division schemes a) full Klems basis – 145 patches b) 2x Klems - 580 patches, and c) 4x Klems – 2320 patches [ref andys paper]	45
Figure 39: Example of variable resolution BSDF tensor-tree representation.....	46
Figure 40: Sunoptics Lens: Perpendicular Front Transmission – Klems scatter Plot	48
Figure 41: Sunoptics Lens: Perpendicular Front Transmission – Variable resolution scatter plot	48
Figure 42: Sunoptics Lens: Perpendicular Back Transmission – Klems scatter plot	49
Figure 43: Sunoptics Lens: Perpendicular Back Transmission – Variable resolution scatter plot	49
Figure 44: Sun Tunnel Lens: Perpendicular Front Transmission – Klems Scatter Plot.....	50
Figure 45: Sun Tunnel Lens: Perpendicular Front Transmission – Variable resolution Scatter plot	50
Figure 46: Sun Tunnel Lens: Perpendicular Back Transmission - Klems scatter plot.....	51
Figure 47: Sun Tunnel Lens: Perpendicular Back Transmission – Variable resolution scatter plot	51
Figure 48: Harvey-Shack BSDF equation and angle definitions used	53
Figure 49: Sunoptics Reflector BRDF Measurements	53
Figure 49: Suntunnel reflective tube wall reflectance by incidence angle	54

Figure 50: SunTunnel white boot reflectance by incidence angle	54
Figure 51: Flat side Harvey Shack transmittance curve-fits.....	55
Figure 52: Prism side Harvey Shack transmittance curve-fits.....	56
Figure 53: Scatter Works scatter measurements and TracePro ABg Curve Fits	58
Figure 54: Definition of LTI Optics Relative Photometric Distribution Coordinate System.....	60
Figure 55: Diagram of LTI Optics goniophotometer.....	61
Figure 56: Sunoptics lens CAD model. - other side is flat.	62
Figure 57: Sun Tunnel lens CAD model - “flat” side	62
Figure 58: Sun Tunnel lens CAD model - prismatic side	63
Figure 59: Light scattering patterns from the Sun Optics prismatic lens material.	64
Figure 60: SunOptics Signature Series Barrel Vault Skylight	65
Figure 63: TracePro Sunoptics Top Model	67
Figure 64: Plot showing performance relative to the number of spawned rays	68
Figure 65: Radiance Sunoptics and Sun Tunnel System Models	72
Figure 66: Near Field Sensor points used in Radiance Simulations	73
Figure 67: Incoming patches used to illustrate system scatter at different incidence angles.....	74
Figure 68: Sunoptics Top System – Standard Klems BSDF distribution.....	75
Figure 69: Sunoptics Box System – Standard Klems BSDF distribution	76
Figure 70: Sun Tunnel System – Standard Klems BSDF distribution.....	77
Figure 71: Standard Photopia Sky Dome Model	79
Figure 72: Sky dome and sun ray sets for Test 18.....	80
Figure 73: Sunoptics Box CAD Model in Photopia	80
Figure 74: Vertical and horizontal illuminance planes.....	81
Figure 75: Polar candela plot for the Sunoptics Box Test 18	82
Figure 76: Simulated illuminance on a plane below the skylight	82
Figure 75: Polar candela plot for Test 18 using standard RP-21 sun and sky models.....	83
Figure 77: Photometric Coordinate System.....	85
Figure 78: Sunoptics Top photometric comparison, partly cloudy sky (Test 11)	87

Figure 79: Sunoptics Top photometric comparison, low sun angle sky (Test 15).....	88
Figure 80: Sunoptics Top photometric comparison, mid sun angle sky (Test 25)	89
Figure 81: Sunoptics Top photometric comparison, high sun angle sky (Test 28)	90
Figure 82: Sunoptics Box photometric comparison, partly cloudy sky (Test 9).....	92
Figure 83: Sunoptics Box photometric comparison, low sun angle sky (Test 18).....	93
Figure 84: Sunoptics Box photometric comparison, mid sun angle sky (Test 22)	94
Figure 85: Sunoptics Box photometric comparison, high sun angle sky (Test 32).....	95
Figure 86: Sun Tunnel photometric comparison, partly cloudy sky (Test 6)	97
Figure 87: Sun Tunnel photometric comparison, low sun angle sky (Test 16).....	98
Figure 88: Sun Tunnel photometric comparison, mid sun angle sky (Test 24)	99
Figure 89: Sun Tunnel photometric comparison, high sun angle sky (Test 30)	100
Figure 90: Error Comparison for Sky 9	105
Figure 90: Geometrical models of the prism skylight lens materials (angular and rounded prisms)	A-2
Figure 91: Examples of transmitted scatter for a perfect acrylic prism	A-3
Figure 92: Example of “Cross” distribution pattern common of all square prism materials.....	A-4
Figure 93: Comparison of SunOptics pyramid flat side transmittance measurements	A-6
Figure 94: Theoretical prism flat side Transmittance Measurements.....	A-7
Figure 95: Comparison of symmetric and asymmetric scatter data	A-8
Figure 96: Comparison of SunOptics pyramid flat side reflectance measurements	A-9
Figure 97: Comparison of SunOptics Pyramid prism-side transmittance measurements	A-10
Figure 98: Comparison of SunOptics Pyramid prism-side reflectance measurements.....	A-11
Figure 99: Sample results present the DAQ (BTDF/cos(theta_out) of Sunoptics pyramid prismatic skylight base material	A-12
Figure 100: Sample results present the DAQ (BRDF/cos(theta_out) of Sunoptics pyramid prismatic skylight reflector material	A-13
Figure 101: Comparison of SunTunnel Pyramid flat-side transmittance measurements.....	A-14
Figure 102: Comparison of SunTunnel Pyramid flat-side reflectance measurements	A-15
Figure 103: Comparison of SunTunnel Pyramid prism-side transmittance measurements	A-16

Figure 104: Comparison of SunTunnel Pyramid prism-side reflectance measurementsA-17

Figure 105: Sample results present the DAQ (BTDF/cos(theta_out) of Velux SunTunnel base material.....A-18

Figure 106: Sample results present the DAQ (BRDF/cos(theta_out) of Velux SunTunnel base material.....A-19

Figure 107: Sample results present the DAQ (BRDF/cos(theta_out) of Velux SunTunnel reflector material.....A-20

Figure 108: Sample results present the DAQ (BRDF/cos(theta_out) of Velux SunTunnel white material.....A-21

Figure 113: Standard sky types considered for shielded portion of measured sky.....D-24

List of Tables

Table 1: Skylight types and systems selected for study.....	9
Table 2: Equipment used for each measurement.....	14
Table 3: Measurement Sets Conducted.....	23
Table 4: Zenith luminance measured using calibrated luminance meter and HDR imaging.....	25
Table 5: Horizontal Illuminance measured using Velux and CLTC illuminance meters.....	26
Table 6: Measured reflectance for black wall, floor and Wood	B-22
Table 7: Results of first illuminance meter calibration.....	C-23
Table 8: Results of second illuminance meter calibration	C-23

EXECUTIVE SUMMARY

This report details all work undertaken for the Enhanced Skylight Modeling and Validation project: research aimed at developing and validating computer simulation alternatives to physical measurements for producing optical daylighting system photometry information. Current industry standards rely on physical daylighting system photometric labs which have inherent limitations in their measurement ability, including sky and size constraints, photometric resolution constraints, time constraints and geographical (solar altitude) constraints as well as questionable accuracy.

The research team was led by Architectural Energy Corporation (AEC) and the California Lighting Technology Center (CLTC). AEC's key subcontractor was Daylighting Innovations (DI) that performed the simulation work and validation analysis. The CLTC was responsible for the physical measurements with support from DI. Other key technical and match contributors included LTI Optics, Velux, Lambda, Lawrence Berkeley National Laboratory (LBNL) and Daylight Technologies.

The goal of the project was to develop and validate computer simulation methods as alternatives to the industry standard of physical measurements for producing accurate and useful optical daylighting system photometry. The project approach was to compare several physical photometric measurements of optical daylighting systems to computer models, validating the use of computer simulation to produce this photometric information. The project is comprised of two main groups of tasks to achieve this goal: measurement tasks and simulation tasks.

The goal of the measurement tasks is to obtain real-world skylight system photometric data along with simultaneous measurement of the sky and solar resource. The measurements were conducted, on July 21 and 22, 2010, at the Velux Daylighting Laboratory facility, in Greenwood, South Carolina. Three skylights configurations were selected for the study to represent a range of optical complexity: from very simple single optics to more complex systems with multiple optical layers. Each daylight system had a different installation configuration. Photometric files were obtained for 24 out of the 32 tests, of which 12 were chosen for final validation with computer simulation: four for each of the three skylight systems. For each skylight system, a test representing a low, mid, and high sun angle was chosen under a clear sky as well as a partly cloudy condition. This set of 12 skies was used to validate the computer simulated photometry (luminous intensity).

The goal of the simulation tasks was to develop modeling protocols and simulation methodologies and validate against the data provided in the measurement tasks. This involved creating representative computer models of all aspects of the daylighting system; the sky and sun source, the skylight system geometry and material characteristics, and the near-field meter locations. Three common lighting simulation tools were explored: TracePro, Photopia, and Radiance. Various simulation settings and methodologies explored for each simulation engine are presented and the final simulation results from each engine are compared to the measured data obtained. The following general conclusions can be drawn from the study.

The process of creating detailed reflectance and transmittance (BSDF) measurements of the main optical surfaces interacting was explored in detail. There are a number of different methods for creating and standards for documenting these BSDF definitions. A general measurement is discussed as well as the standard used in each of the three simulation engines.

In general, the modeling, measurement and simulation techniques presented here are shown to produce accurate optical daylighting system photometric information. This and other conclusions and recommendations are summarized in Chapter 9.

CHAPTER 1: Introduction

This report details all work undertaken for the Enhanced Skylight Modeling and Validation project: a project aimed at developing and validating computer simulation alternatives to physical measurements for producing optical daylighting system photometry information. Current industry standards rely on physical daylighting system photometric labs [1] which have inherent limitations in their measurement ability, including:

- **Size constraints** – it has been shown that to obtain reasonably accurate far-field photometric results the measurements have to abide by a 5:1 rule: they need to be taken at a distance of at least 5x that of the largest luminous element dimension. Given that many skylights are at least 5'x4' if not larger, this requires the measurements to be taken at [6.4'(diagonal) x 5 =] 32' away from the skylight inside aperture. This then requires either the use of mirrors and/or a building with a 32' roof height.
- **Sky constraints** – regardless of the physical location of the daylighting lab, there are limitations as to the solar angles and sky conditions that will be available. Unless the lab is between the tropics of Capricorn and Cancer, they will never experience sun angles directly overhead and the higher the latitude the lower the peak sun angle will be. Morning and evening conditions can suffice for measuring lower sun angles but the weather doesn't always cooperate. If sunny measurements are desired for a given time and day, there is no guarantee that condition will be available.
- **Photometric resolution constraints** – many of the prismatic and Fresnel optics used in skylight systems, in combination with the extremely intense parallel beam source of the sun, produce distinct luminous patterns with sharp peaks and valleys in the luminous intensity distribution. These variations require a high resolution of measurement points to capture. Ideally, this would come along with an integrating sphere measurement to ensure all light has been captured and accounted for.
- **Time constraints** – ideally, daylighting systems will have performance information for the range of sun and sky conditions that may exist. In order to obtain this full set of daylighting performance conditions, measurements often need to extend for several months. If the latitude is greater than 25°, then the measurements also need to encompass the summer solstice and often the winter solstice as well depending on the ability to rotate the skylight system.

It is the authors' hypothesis that clearly defined and validated computer simulation methods for analyzing the performance of optical daylighting systems would alleviate all these inherent limitations with the current industry standard of physical measurements in the following ways:

- **Size Constraints** – a computer simulation model has no constraints relative the geometric size of the daylighting system. In fact, absolute far field measurements are possible (an infinite measurement distance).
- **Sky Constraints** – standardized sky representations, such as those adopted by CIE or the Perez model, can be easily created, and consistently duplicated, in a computer simulation environment. Additionally, the real-sky luminance mapping techniques used in this study

and others can be used to convert these measurements into a source file to be used in ray tracing.

- **Photometric Resolution Constraints** – there is a minimal limit to the resolution a computer simulation can provide. For higher photometric resolutions, the total ray count/densities are increased resulting in increased rendering times but the overall simulation times are well within reason.
- **Time constraints** – computer simulations may take up to a day to perform which is still much quicker than a 6 month season of measurements.

The goal of the project is to develop and validate computer simulation methods as alternatives to the industry standard of physical measurements for producing accurate and useful optical daylighting system photometry. The project plan is to compare several physical photometric measurements of optical daylighting systems to computer models, validating the use of computer simulation to produce this photometric information. The project is comprised of two main groups of tasks to achieve this goal: measurement tasks and simulation tasks.

The goal of the measurement tasks is to obtain real-world skylight system photometric data along with simultaneous measurement of the sky and solar resource. The measurements were conducted, on July 21 and 22, 2010, at the Velux Daylighting Laboratory facility, in Greenwood, South Carolina. Three skylights configurations were selected for the study to represent a range of optical complexity: from very simple single optics to more complex systems with multiple optical layers. Each daylight system had a different installation configuration. The measurement facility and equipment are described in Chapter 2. In order to capture the luminance distribution of the sky, a sky luminance measurement system was developed based on high-dynamic-range photography and auxiliary zenith luminance and horizontal illuminance measurements. This equipment and measurement methodology are described in Chapter 3. The resulting sky measurements and skylight system photometry are presented in Chapter 4.

The goal of the simulation tasks is to develop modeling protocols and simulation methodologies and validate against the data provided in the measurement tasks. This involves creating representative computer models of all aspects of the daylighting system; the sky and sun source, the skylight system geometry and material characteristics, and the near-field meter locations. The measured sky luminance distribution and zenith luminance and horizontal illuminance measurements were processed to create representative daylight source computer models and geometric models were built to represent the different skylight systems and the near-field measurement locations, described in Chapter 5.

Three common lighting simulation tools were explored:

Two dominantly forward ray-tracers that excel at modeling optical lighting and imaging systems and offer numerous design tools:

- TracePro – TracePro is commercially available software from Lambda Research Corporation. From their website (lamdares.com) – “TracePro is a comprehensive, versatile

software tool for modeling the propagation of light in imaging and non-imaging opto-mechanical systems.”

- Photopia – Photopia is commercially available software from LTI Optics. From their website (www.ltioptics.com) - “Photopia is a fast and accurate photometric analysis program that produces comprehensive performance evaluations for non-imaging optical designs.”

One backward ray-tracer that excels at tail end illuminance calculations and renderings of product models or architectural spaces:

- Radiance – Radiance is a free software available from Lawrence Berkeley National Labs. From their website (www.radiance-online.org) – “Radiance is a suite of programs for the analysis and visualization of lighting in design.”

Chapter 6 describes the process of creating the necessary detailed reflectance and transmittance measurements of the main optical surfaces interacting with the daylight, namely the prismatic lenses and reflective side walls, and creating BSDF models for simulation. There are a number of different methods for creating and standards for documenting these BSDF definitions. A general measurement is discussed as well as the standard used in each of the three simulation engines explored. Chapter 7 discusses the various simulation settings and methodologies explored for each simulation engine including ray-tracing parameter settings, measurement locations, and sky and sun source size and resolutions. The final simulation results from each engine and comparisons to the measured results are presented and discussed in Chapter 8. Overall conclusions and recommendations are provided in Chapter 9.

This page deliberately left blank

CHAPTER 2: Testing Facility and Skylight Systems

To achieve a robust validation of the computer simulation methods, it is ideal to have physical skylight system measurements from a wide variable range of sky conditions as well as skylight systems. This section discusses the selected goniophotometer testing facility location, the climate of the facility, and the skylight systems used.

Velux Daylight Laboratory

The testing facility used in this project is an 18'x18'x18' building owned by the Velux Company and located in Greenwood, South Carolina, see Figure 1. The exact geographical coordinates of the building are 34° 13.057' N Latitude and 82 ° 6.501' W Longitude.

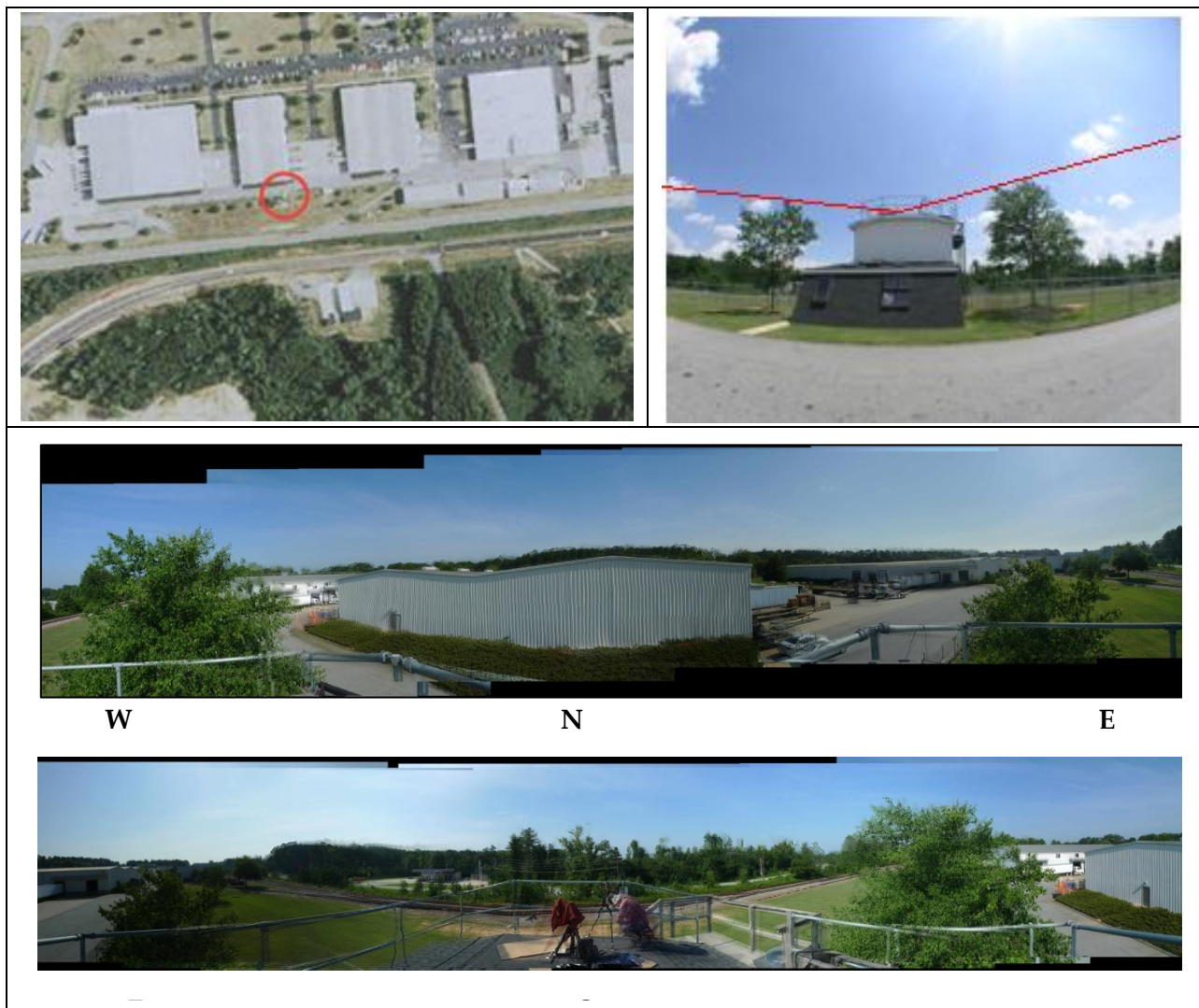


Figure 1: Velux Daylighting Laboratory Location, Building and Surroundings

This building was designed to house a custom-built goniophotometer for measuring the luminous intensity distribution that emanates from a maximum 2'x2' skylight, see Figure 2. The goniophotometer system is comprised of sensors, data logging equipment, and a computer that controls the overall measurement process and capture. To allow the roof to receive direct sunlight, the building is placed such that there are no significant obstructions. The angular height of surrounding buildings and trees was less than 10° above the horizon.



Figure 2: Velux Daylight Photometry Building and Equipment

Climate Information

The ideal testing period would include a range of sky conditions, from clear skies, to partly cloudy to overcast conditions, and for a range of sun angles from low to high. Climate information for Greenwood, shown in Figure 3, was reviewed to plan an optimal time for measurements. It can be seen that the sunniest days in Greenwood occur from early April to late October, with 65-70% sunshine. These days are also very humid with 80-90% relative humidity which results in a broader distribution of brightness around the solar disc. Cloud cover increases and clear days are less frequent into the winter months.

Because sun angles are high and there was a good chance of mixed conditions, measurements were performed in July and fortunately adequate sky conditions were present throughout the measurements. Overcast conditions were not present but some partly cloudy conditions were captured.

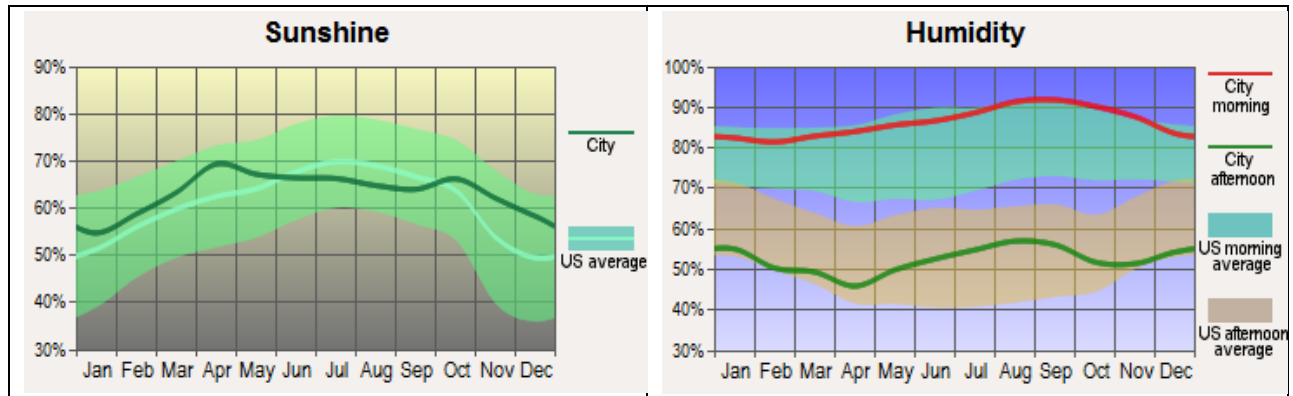
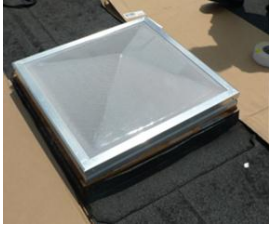
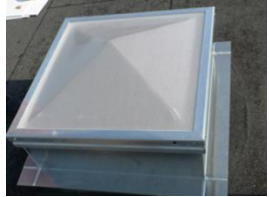



Figure 3: Maximum Daily Horizontal Illuminance

Skylighting Systems

Three skylights configurations were selected for the study to represent a range of optical complexity: from very simple single optics to more complex systems with multiple optical layers. Table 1 illustrates the different skylight configurations selected and products used. The systems and their installation are described in more detail in the following sections.

Table 1: Skylight types and systems selected for study

Skylight Type	Selected products	Image
1 Basic skylight: minimal optics, “low” aspect ratio	Sunoptics ¹ pyramid skylight Top prismatic lens White diffuse lightwell	
2 Moderate skylight: dual optics, “med” aspect ratio	Sunoptics pyramid skylight “light cube” Top and bottoms prismatic lens Reflective lightwell	
3 Advanced skylight: multiple optics, “high” aspect ratio	Sun Tunnel™ ² Top clear lens Bottom prismatic lens Reflective tubular lightwell	

¹ <http://www.sunoptics.com/>

² http://www.veluxusa.com/Consumer/Products/SUN_TUNNEL_skylights

Simple prismatic skylight

This configuration was achieved using only the top part of a Sunoptics prismatic skylight. A white foam core material was applied to the 2'x2'x2' wood-framed light well to better represent a real application and to allow the light well's optical properties to be accurately characterized. Figure 4 shows the installation of the simple prismatic skylight system and the white foam core applied to the vertical surfaces of the light well.

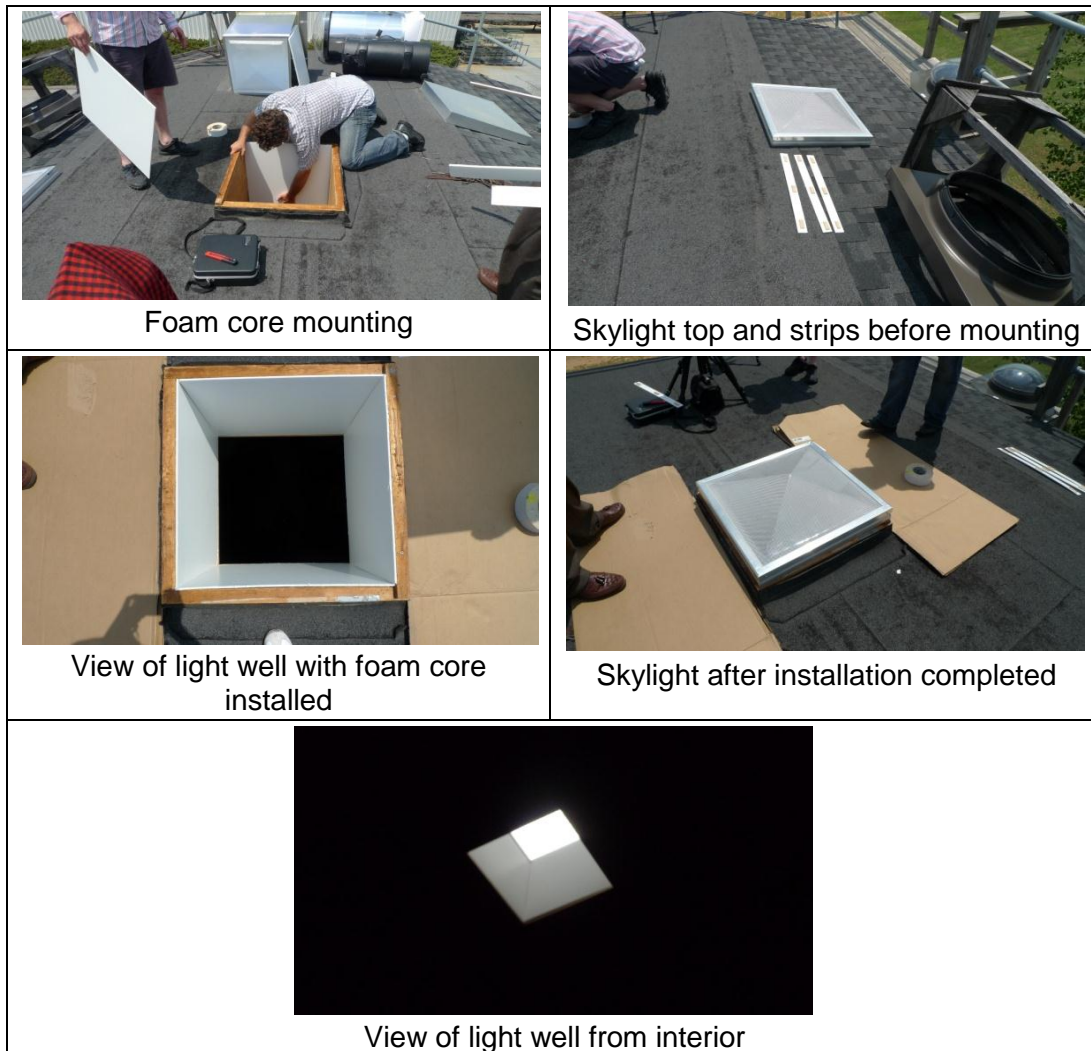


Figure 4: Installation of the simple prismatic skylight system

Prismatic skylight with integrated specular light well

For this configuration the complete (top and base) Sunoptics prismatic skylight system was used. This system has two prismatic diffusers, one at the top and the other at the bottom of the specular light well. In order to have a known reflectance in the vicinity of the bottom diffuser of this system, narrow strips of white foam core material were applied to the exposed parts of the wood-framed light well. Figure 5 shows the installation of the prismatic skylight with integrated specular light well and bottom diffuser and the foam core strips below.

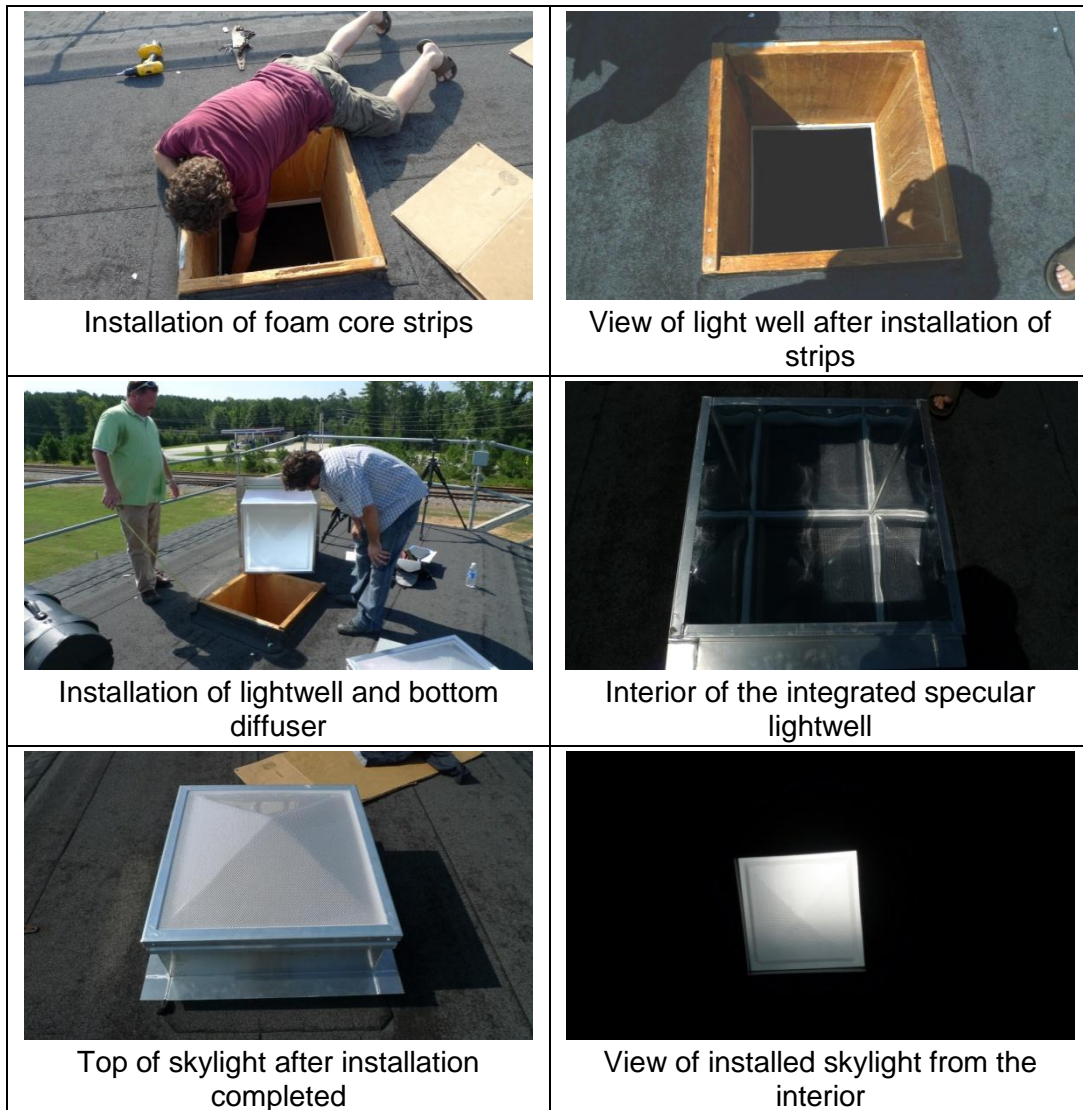


Figure 5: Installation of the Sunoptics LightCube

Tubular skylight

A 3' deep Velux Sun Tunnel skylight was used for this configuration as seen in Figure 6. It has a clear plastic dome, a three-foot highly specularly reflective tube, and a bottom diffuser. The bottom diffuser was flush with the bottom of the light well requiring no optical correction.



Figure 6: Velux Sun Tunnel Installed

This page deliberately left blank

CHAPTER 3: Measurement Equipment, Settings and Procedure

To ensure an accurate computer model representation of the physical test, simultaneous daylight resource and daylight system photometry information is needed. There is high variability in sky brightness distributions, especially under partly cloudy conditions, so for this study the sky distribution measurements were taken on the roof during the same time as the goniophotometer measurements in the building below. The equipment on the roof used to capture the sky resource, the goniophotometer measurements and computer controls, and the measurement procedure followed to collect all data is described in this chapter.

Sky Measurement Equipment

The variety of different measurement devices utilized to accurately capture the sky resource following the methods developed by Thanachareonkit et al., can be seen in Figure 7.



- 1) Nikon Coolpix 5400 camera
- 2) Nikon FCE9 Fisheye converter lens for the Nikon Coolpix 5400 camera
- 3) Nikon UR-E10 converter adapter for the Nikon Coolpix 5400 camera
- 4) Tripod for the Nikon Coolpix 5400 camera
- 5) Shading disk for the Nikon Coolpix 5400 camera
- 6) Konica Minolta luminance meter LS 110
- 7) Tripod for Konica Minolta luminance meter LS 110
- 8) Konica Minolta CL-200 Chromameter (Velux)
- 9) Konica Minolta CL-200 Chromameter (CLTC)
- 10) Tripod for Konica Minolta CL-200 Chromameter (CLTC)
- 11) Shading disk for Konica Minolta CL-200 Chromameter (CLTC)

Figure 7: Equipment on the Roof

The equipment was used to provide 4 groups of measurements, as described in Table 2. Sky zenith luminance measurements were taken to compare and calibrate the sky luminance mapping. In addition, horizontal and diffuse illuminance measurements were taken to further compare and calibrate the captured luminance maps.

Table 2: Equipment used for each measurement

Measurement	Equipment
Group 1: sky luminance at zenith	Using luminance meter (6+7) Using HDR camera (1+2+3+4+5)
Group 2: sky luminance mapping	Using HDR camera (1+2+3+4+5)
Group 3: Global horizontal illuminance	Using CLTC illuminance meter (9+10) Using Velux illuminance meter (8)
Group 4: Diffuse horizontal illuminance	Using CLTC illuminance meter with shading disk (9+10+11)

Sky luminance measurement system

High dynamic range (HDR) imaging was used to acquire the sky luminance distribution. The HDR imaging system was based on a Nikon Coolpix 5400 digital camera, equipped with a fisheye lens, and the Photosphere HDR imaging software. The camera was placed on a tripod, pointing upward, with its sensor in a horizontal position, see Figure 8. The camera location was adjacent to the skylight so that the view of the sky was approximately the same as that of the skylight to be measured without obscuring the skylight itself from the skydome. A moveable shading disk attachment was used to shield the camera sensor from direct solar radiation, which increases the accuracy of the measurement and reduces the risk of damage to the camera sensor. [2]

During the sky luminance distribution measurements, the luminance of the sky at the zenith was also measured using a Minolta LS-110 luminance meter, see Figure 8. This measurement was done for each HDR image capture. The luminance value of this point is then compared to the values obtained using HDR images, and used along with the illuminance measurements in the HDR image calibration.



Figure 8: Sky luminance equipment: Luminance meter (left) and HDR camera for (right)

Horizontal illuminance measurement system

To help determine the luminance of the shaded portion and to calibrate the overall magnitude of the HDR images, the global horizontal and diffuse illuminance were measured. Two illuminance meters, one from CLTC and one from the Velux facility, see Figure 9, were used. For the diffuse illuminance measurement, a moveable shading disk attachment was used in order to shield the CLTC meter from direct solar radiation. This disk shades the illuminance meter with approximately the same solid angle, a cone with a half angle of approximately 5° , as the disc shading the HDR camera lens. This fact was used to help calibrate the different components of the luminance map.



Figure 9: Horizontal illuminance equipment: CLTC illuminance meter with shading disk (left) and Velux illuminance meter (right)

Goniophotometer Equipment

Figure 10 shows schematically the geometry of the goniophotometer. The goniophotometer was controlled from an adjacent control station, see Figure 11. All the raw data gathered by the goniometer during each measurement was captured by a data acquisition system and stored in files. These files are converted to the IESNA standard photometric format, "IES files" (*.ies), by software that accompanies the data acquisition system. The testing procedures are documented in the recently developed IESNA approved method LM-81-10 for photometric testing of skylighting products [1].

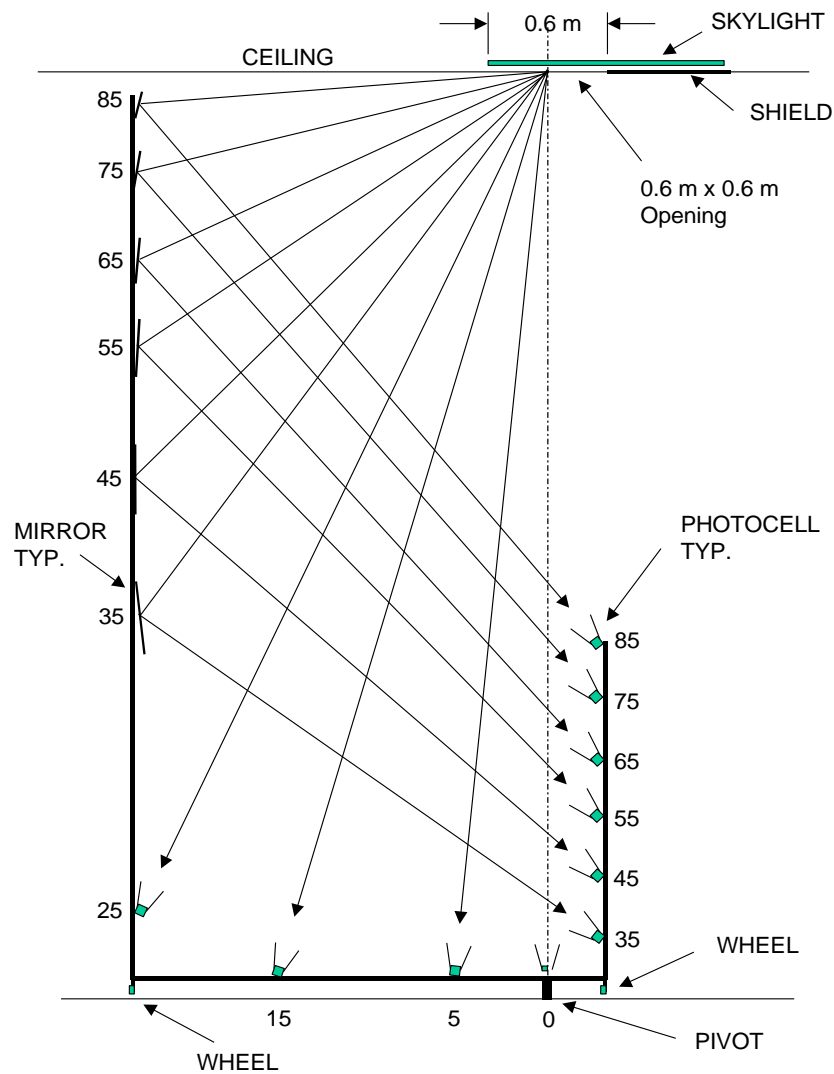


Figure 10: Skylight photometric measurement equipment schematic section



Figure 11: Goniophotometer control station

Measurement procedure

Measurements were taken simultaneously on the roof using the luminance camera, luminance meter, horizontal illuminance meter, and in the interior of the facility using the automated goniometer. Three people were required to operate equipment and record data on the roof, while automation allowed the goniometer to be controlled by a single person. The time of every measurement was recorded and referenced to a legal time server: <http://time.gov>. Figure 12 graphically depicts the general measurement procedure.

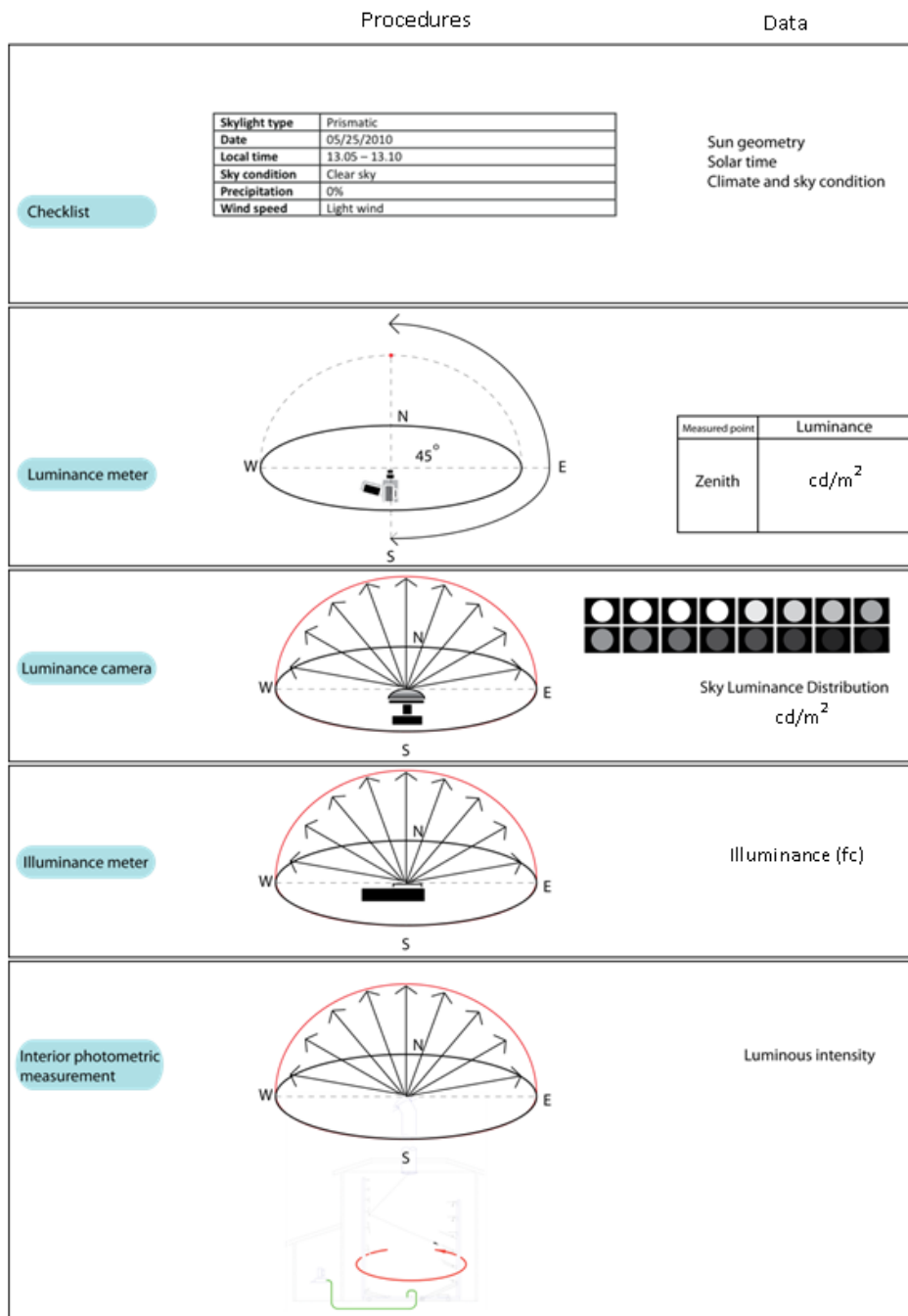


Figure 12: Measurement procedure diagram

Illuminance meter calibration

After the first tests, it was found that the CLTC illuminance meter, although being more precise and having been calibrated more recently, had the disadvantage of not having a measurement range beyond ten thousand footcandles. Since this global horizontal illuminance value was exceeded during the brighter parts of sunny days, several consecutive simultaneous measurements were taken (see Figure 13) in order to establish a relationship between measured values, so that both meters could be compared to each other.



Figure 13: Illuminance Meter Calibration

Material reflectance measurement

In order to determine the reflectance of the materials present in the measurement facility, luminance measurements were taken. A piece of white foam core was used as reference in the absence of a calibrated reference card. This reference material was stored for reflectance measurement at a later date using a calibrated reference card. Measurements were taken of the black walls inside the goniometer room and of the wood panels in the light well, see Figure 14.



Figure 14: Measurement of the reflectance of the interior walls of the goniophotometer room and the light well panels

This page deliberately left blank

CHAPTER 4: Measurement Results

A total of 32 sets of measurements were conducted over three days. The following sections present the timeline of these tests and the results obtained.

Timeline of tests

The measurements were conducted on July 21st, 22nd and 23rd, 2010. The goal was to make measurements with low, medium and high sun angles and with clear, partly cloudy and overcast skies in order to obtain a robust data set for a thorough validation. After a few preliminary tests in the morning of the 21st, measurements proceeded throughout the afternoon of the 21st and most of the day on the 22nd. By the afternoon of the 22nd, measurements had been performed for sunny sky conditions (all sun angles) and some partly cloudy sky conditions (mid-to-high sun angles). Overcast conditions were not available and few partly cloudy skies with no sun were available. Calibration and reflectance measurements were then performed. No measurements were performed the following day due to absence of desired sky conditions: July 23rd was a clear day. The measurement timeline is represented graphically in Figure 15.

Table 3 provides detailed information on each test performed.

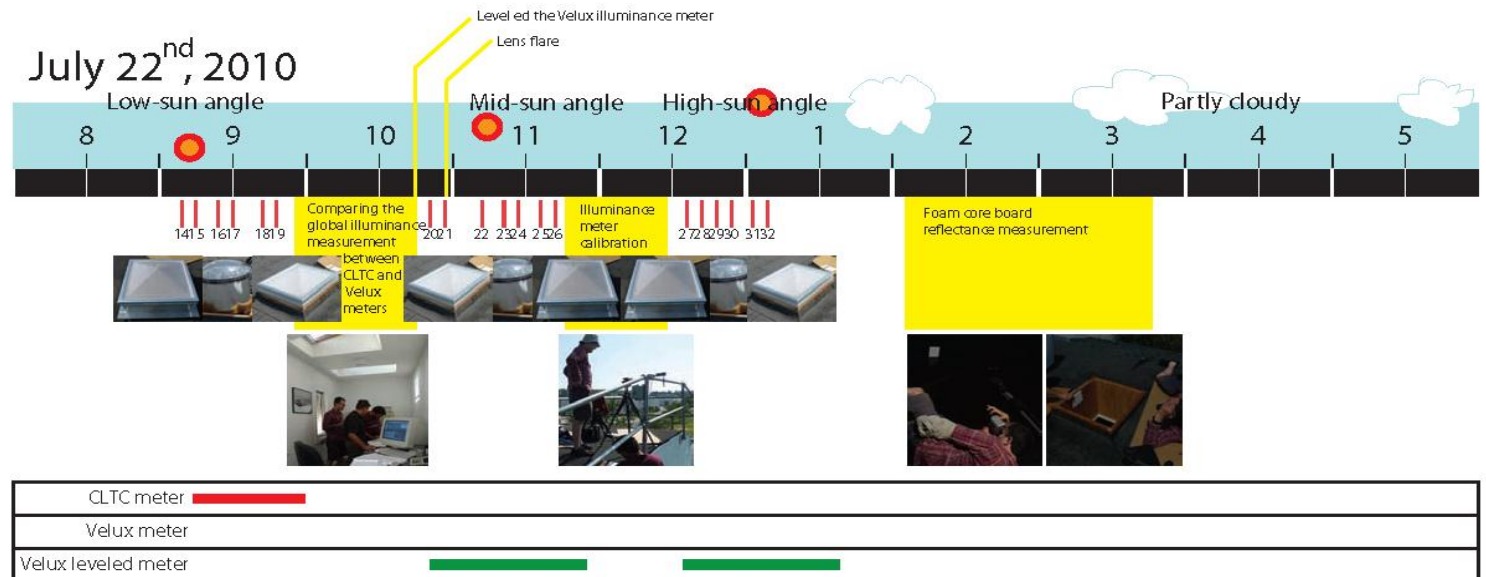
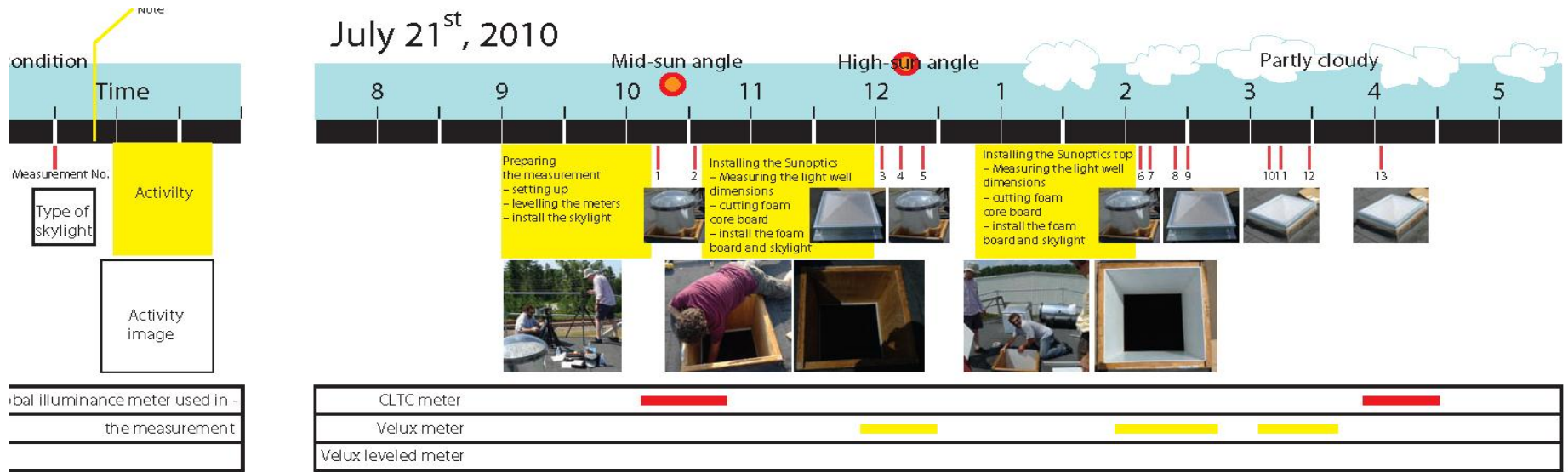


Figure 15: Measurement timeline diagram

Table 3: Measurement Sets Conducted

Test # ¹	Skylight Type	Start Time ²	End Time ²	Wind Speed ³	Sky Condition ³	Estimated Cloud cover ³
Test1	3' Velux Sun Tunnel	10.15am	10:18:45	10	Clear	2%
Test2	3' Velux Sun Tunnel	10.33am	10:36:48	10	Clear	2%
Test3	Sunoptics-Box	12.03pm	12:06:25	10	Clear	2%
Test4	3' Velux Sun Tunnel	12.13pm	12:15:35	10	Clear	2%
Test5	3' Velux Sun Tunnel	12.22pm	12:24:32	10	Clear	5%
Test6	3' Velux Sun Tunnel	2.07pm	2:09:25	10	Partly Cloudy w/ Sun	35%
Test7	3' Velux Sun Tunnel	2.13pm	2:15:33	10	Partly Cloudy w/ Sun	25%
Test8	Sunoptics-Box	2.23pm	2:25:28	15	Partly Cloudy w/ Sun	25%
Test9	Sunoptics-Box	2.29pm	2:31:22	15	Partly Cloudy w/ Sun	30%
Test10	Sunoptics-Top only	3.09pm	3:11:18	10	Partly Cloudy w/ Sun	30%
Test11	Sunoptics-Top only	3.16pm	3:19:17	15	Partly Cloudy w/ Sun	35%
Test12	Sunoptics-Top only	3.28pm	3:30:13	10	Partly Cloudy	20%
Test13	Sunoptics-Top only	4.04pm	4:06:03	10	Partly Cloudy w/ sun	25%
Test14	Sunoptics-Top only	8.39am	8:42:25	0	Clear	2%
Test15	Sunoptics-Top only	8.45am	8:47:52	0	Clear	2%
Test16	3' Velux Sun Tunnel	8.54am	8:57:18	0	Clear	5%
Test17	3' Velux Sun Tunnel	9.00am	9:03:01	0	Clear	5%
Test18	Sunoptics-Box	9.12am	9:14:45	0	Clear	5%
Test19	Sunoptics-Box	9.17am	9:19:48	0	Clear	5%
Test20	Sunoptics-Box	10.20am	10:22:53	5	Clear	10%
Test21	Sunoptics-Box	10.26am	10:28:50	5	Clear	10%
Test22	Sunoptics-Box	10.42am	10:44:44	5	Clear	10%
Test23	3' Velux Sun Tunnel	10.51am	10:53:41	5	Clear	5%
Test24	3' Velux Sun Tunnel	10.57am	10:59:42	5	Clear	5%
Test25	Sunoptics-Top only	11.07am	11:09:51	5	Clear	10%
Test26	Sunoptics-Top only	11.12am	11:15:03	5	Clear	5%
Test27	Sunoptics-Top only	12.06pm	12:08:15	10	Clear	15%
Test28	Sunoptics-Top only	12.11pm	12:13:07	10	Clear	15%
Test29	3' Velux Sun Tunnel	12.17pm	12:19:07	10	Clear	15%
Test30	3' Velux Sun Tunnel	12.22pm	12:24:02	10	Clear	15%
Test31	Sunoptics-Box	12.34pm	12:36:23	5	Clear (wispy clouds)	20%
Test32	Sunoptics-Box	12.39pm	12:41:08	5	Clear (wispy clouds)	20%

1 Test 1-13 performed July 21, 2010. Test 14-32 performed July 22, 2010

2 Start and end times are EDT

3 Estimated by the observers

Sky luminance mapping

Each measurement set yielded a sky luminance map, assembled from 16 hemispherical photographs taken with different exposures. These images were then assembled into a single high dynamic range (HDR) image using the Photosphere HDR software [www.anywhere.com]. An HDR image properly calibrated is an accurate luminance map of the scene. These photographs took 2-3 minutes each, approximately the same time it took the goniophotometer below to capture its hemisphere of measurements. A small shift of cloud cover was observed over this image capture period. When the images are combined, this shift gets averaged together creating the most representative sky possible for the 2-3 minute capture period. Figure 16 shows the 16 image exposures captured for Test 12. The resulting raw luminance map is shown in Figure 17.

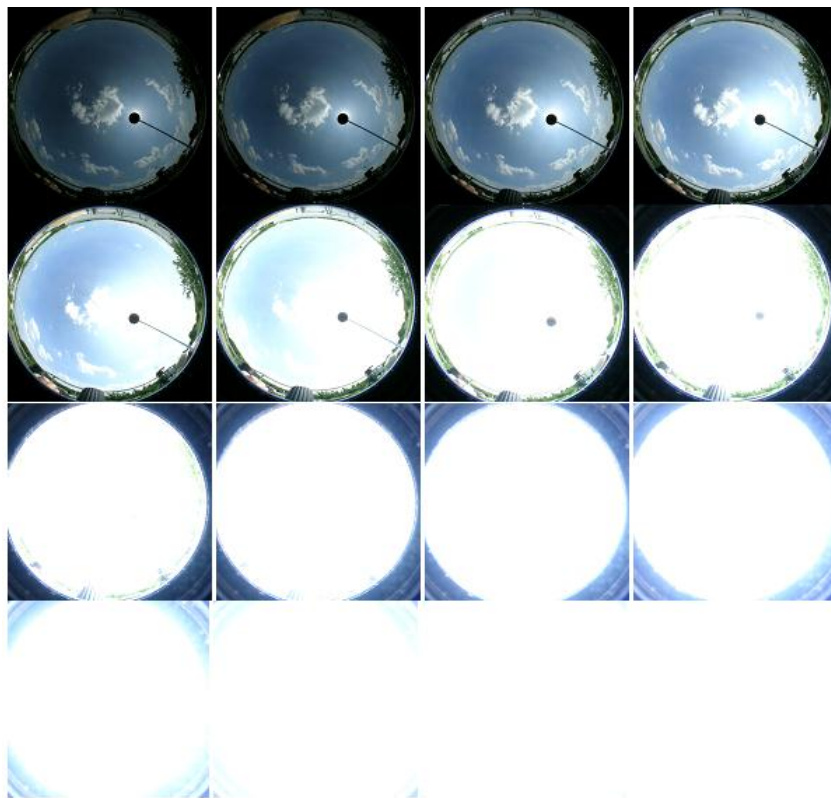


Figure 16: Hemispherical photographs taken for Test 12

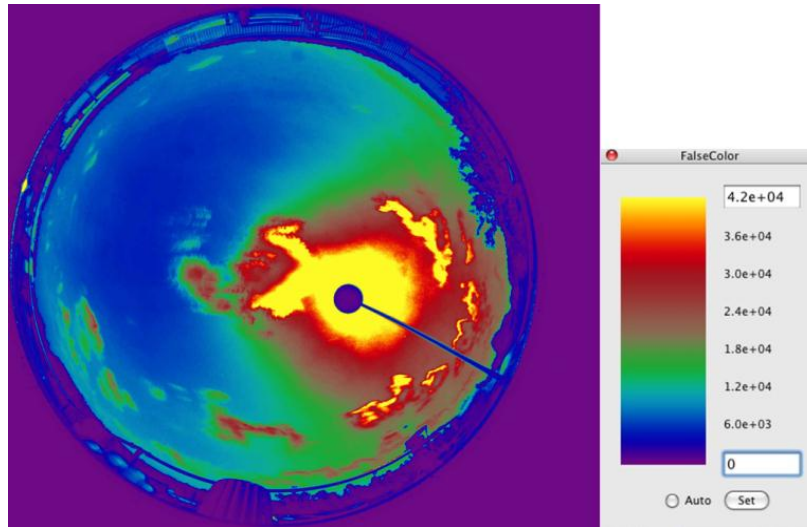


Figure 17: Final HDR image - raw sky luminance map for Test 12.

Comparison of sky luminance at zenith

Zenithal sky luminance was measured for each hemispherical image captured resulting in 16 measurements per test. These showed some variance, particularly for the higher sun angles with a bright zenith, and were averaged for each test. Table 4 shows the measured zenith luminance compared to those derived from the HDR images.

Table 4: Zenith luminance measured using calibrated luminance meter and HDR imaging

Zenith Luminance				Zenith Luminance			
Test #	Luminance meter	HDR	% Diff	Test #	Luminance meter	HDR	% Diff
Test1	3812	5541	69%	Test17	2414	3292	73%
Test2	4636	7145	65%	Test18	2564	3490	73%
Test3	11354	15488	73%	Test19	2727	3972	69%
Test4	12227	14965	82%	Test20	3929	5831	67%
Test5	14384	19818	73%	Test21	4240	6274	68%
Test6	21851	23758	92%	Test22	4638	7041	66%
Test7	18231	20393	89%	Test23	4750	7457	64%
Test8	16418	17696	93%	Test24	4930	7870	63%
Test9	18715	20265	92%	Test25	5258	8351	63%
Test10	17019	32911	52%	Test26	5744	8625	67%
Test11	16813	15031	112%	Test27	15431	18727	82%
Test12	16615	18470	90%	Test28	19135	21350	90%
Test13	4828	6182	78%	Test29	21643	22936	94%
Test14	2043	2690	76%	Test30	22653	24451	93%
Test15	2086	2825	74%	Test31	28224	30628	92%
Test16	2293	3218	71%	Test32	25281	45595	55%

Horizontal illuminance

Both global and diffuse horizontal illuminance measurements were taken in this study. Both were initially measured using the CLTC illuminance meter. However when the illuminance reached nearly 10,000 fc, the Velux illuminance meter was used in place of the CLTC meter which had reached its maximum reading threshold. Table 5 shows the values obtained with both meters.

Both the zenith luminance and horizontal diffuse illuminance measurements were captured for calibrating the sky luminance map. However, the diffuse illuminance measurements (taken with a 10° cone shading disc similar to the captured HDR images) proved to be the better measurement for calibrating the HDR luminance map than the zenith luminance which had greater variance. Also, since the ultimate goal was to have a matching amount of flux onto the surface of the skylights in our computer models, calibrating the source via measured diffuse and global illuminance ensured a more accurate estimate of the flux entering the system. Chapter 5 describes the sky map processing and calibration process in more detail.

Table 5: Horizontal Illuminance measured using Velux and CLTC illuminance meters

Test #	Illuminance (fc)		
	Velux meter	CLTC meter	
	Global	Global	Diffuse
Test1		6937.7	1853.3
Test2		7549.8	1857.2
Test3	9758		2151.8
Test4	9912		2217.8
Test5	10048		2267.4
Test6	11084		3270.2
Test7	10910		2891.8
Test8	10972		2912.2
Test9	10944		3128
Test10	10566		3093.4
Test11	10030		3012.2
Test12	9768		2919.8
Test13		3328.4	2822
Test14		3074.4	1342.2
Test15		3408.4	1368.4
Test16		3334.8	1433.4

Test #	Illuminance (fc)		
	Velux meter	CLTC meter	
	Global	Global	Diffuse
Test17		3577.2	1491.4
Test18		4247.2	1611.2
Test19		4636.4	1669.2
Test20	7338	7193.8	1665.2
Test21	7462	7295	1684.2
Test22	8018	7831.4	1670
Test23	8240	8053.8	1700.2
Test24	8490	8254.6	1710.4
Test25	8822	8582.8	1745.4
Test26	8982	8733.4	1781.4
Test27	10672		2665.2
Test28	11000		3032.2
Test29	11028		3133.2
Test30	10900		3349.8
Test31	10018		3615.2
Test32	9240		3640

During the measurements it was found out that the Velux meter was not leveled. In order to have a complete set of matching illuminance measurements, a correction factor was determined between the two meters by recording measurements between the two meters for a number of different times and conditions, these are shown in Appendix C. The determined correction

factor was used when calibrating the sky luminance maps with measured horizontal diffuse and global illuminance measurements.

On-site Material Measurements

Material measurements were taken for any on-site elements that would impact the optics of the skylight system, particularly for any exposed wood in the roof and skylight framing, the floor and walls of the goniophotometer room. The luminance measured for the different material and the calculated reflectance is provided in Appendix B.

Luminous intensity

Examples of the measured photometry (luminous intensity in units of candela – lumens/steradian) from the goniophotometer are shown in Figure 18, Figure 19, and Figure 20 for the three skylight systems under clear sky conditions: tests 27, 31 and 29, respectively. Photometric files were obtained for 24 out of the 32 tests. The remaining 8 tests had faulty or otherwise unreliable data and were not used for further validation. Of these 24 tests, 12 were chosen for final validation with computer simulation: 4 for each of the 3 skylight systems. For each skylight system, a test representing a low, mid, and high sun angle was chosen under a clear sky as well as a partly cloudy condition. This set of 12 skies is used to validate the computer simulated luminous intensity, discussed in the following sections, and compared in Chapter 7.

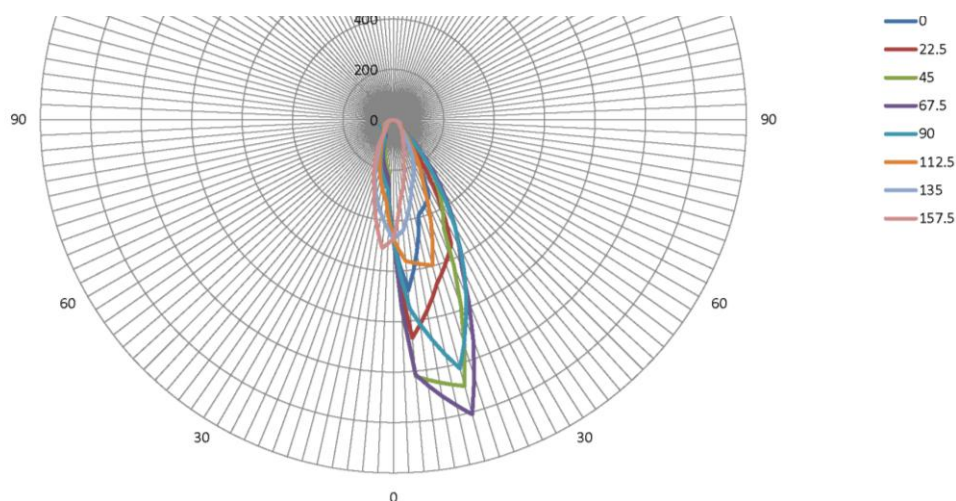


Figure 18: Luminous intensity of Sunoptics system (top only) under clear sky (test 27)

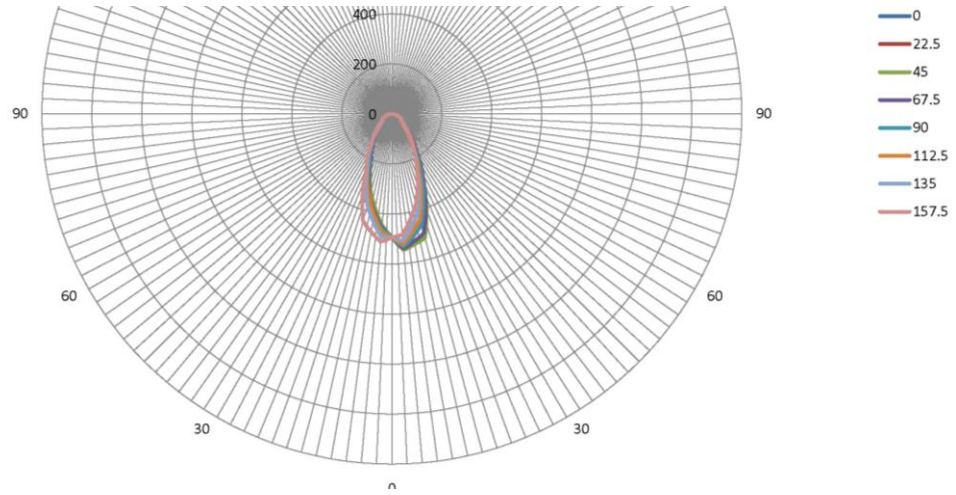


Figure 19: Luminous intensity of complete Sunoptics system under clear sky (test 31)

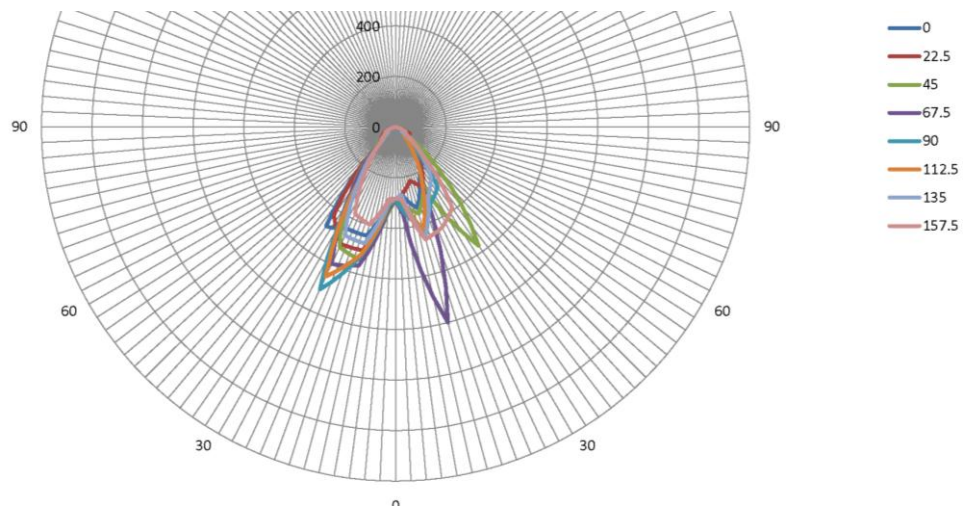


Figure 20: Luminous intensity of Sun Tunnel system under clear sky (test 29)

CHAPTER 5: Sky and Skylight Model Creation

This chapter discusses the development of both accurate sky models and skylight system geometric models using the captured field data. The first section describes the processing of the sky HDR images and recorded diffuse and global illuminance measurements into complete and calibrated sky luminance maps and sun sources. Next the creation of ray-sets for use in forward ray-tracing engines from the sky and sun sources is described. The last section describes the creation of the skylight geometric models.

Sky Measurement Processing and Model Creation

The steps below were followed to process the captured sky luminance maps into useable forms that represent a hemisphere of sky and are usable in raytracing software:

1. Crop raw photograph to represent a perfect hemispherical image with an angular mapping.
2. Create a negative masking layer, apply to cropped sky and adjust sky to match measured sky illuminance.
3. Create a matching Perez sky for current condition adjusted for “sky” shading and apply a positive masking layer to create a filler patch.
4. Combine the masked measured and Perez sky models and add sun definition to create a final sky.
5. Create a ray-tracing ray set describing the sky/sun source to be used in TracePro and Photopia.

The following sections describe this process in detail.

Raw image processing

It is important to map the captured sky luminance distribution in a computer model the same as it was captured in the field. The first step is to crop the original image down to a square shape that circumscribes a circle representing the actual hemisphere of the sky. The exact placement of the dome was determined by locating markers, such as the handrails, at the perimeter of the scene that were approximately the same height as the camera itself and placing those markers at the edges of the dome.

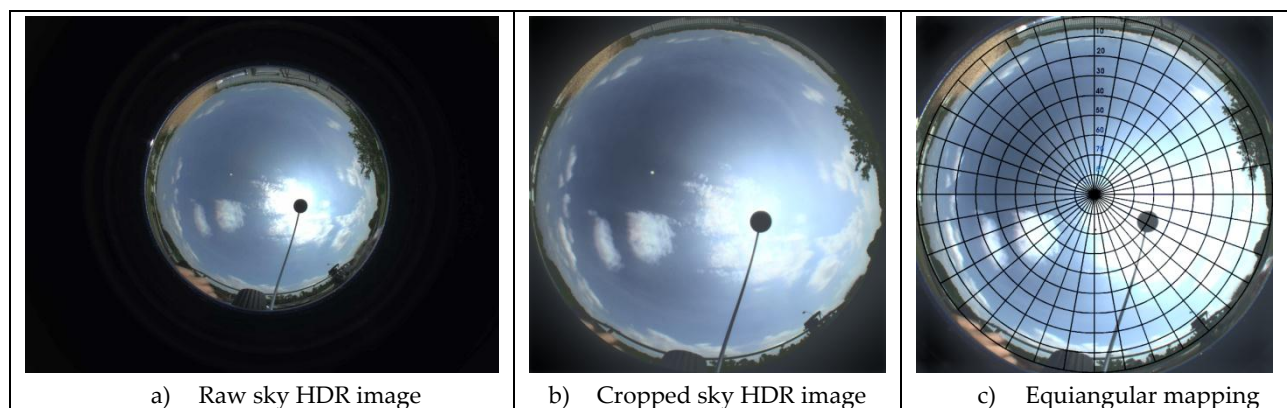


Figure 21: Locating and Mapping captured sky

Next, the appropriate angular mapping was applied. According to the camera lens manufacturer, the hemispherical lens used gives an approximately equi-angular mapping, shown as c in Figure 21, which gives equal weighting to each altitude angle. This exact mapping was not checked in the field and exact mapping data from the manufacturer was not available to verify [3].

Measured sky mapping and calibration

The sky luminance map was then calibrated against the diffuse sky illuminance measurements which provide a much more accurate description of the overall magnitude of the sky. A sky mask was first created by identifying pixels that fall well below the range of bright sky luminance image points around the shading disc. This identifies the location of the shading disc and arm allowing these out-of-range pixels which are not representative of any sky distribution to be removed from the luminance mapping. After this mask was applied, the illuminance of the remaining sky luminance map was determined. Since the diffuse illuminance measurements were taken with a similar shading disc with a cone angle of roughly 10°, the illuminance calculated from the masked luminance map should match up directly with the diffuse illuminance measurement taken on site. It is known that the captured sky luminance images are relative and not absolute, and hence this process of calibration to another better known quantity is necessary. This adjustment could be made based solely on our zenith luminance measurements, but it was found that there was too much variance in the zenith luminance in some cases. Especially when the sun was high in the sky and near zenith, which often led to significant differences in calculated illuminance versus the measured illuminance. In a number of other cases, the adjustments determined from either method were quite close, providing confidence in the measured numbers. Shown in Figure 22 is a) the blocking mask created, b) the captured sky with the mask applied, and c) the adjusted sky calibrated to match the measured total diffuse sky illuminance. The errors associated with this process involved differences in the shading disc spatial size between the HDR camera and the illuminance meter.

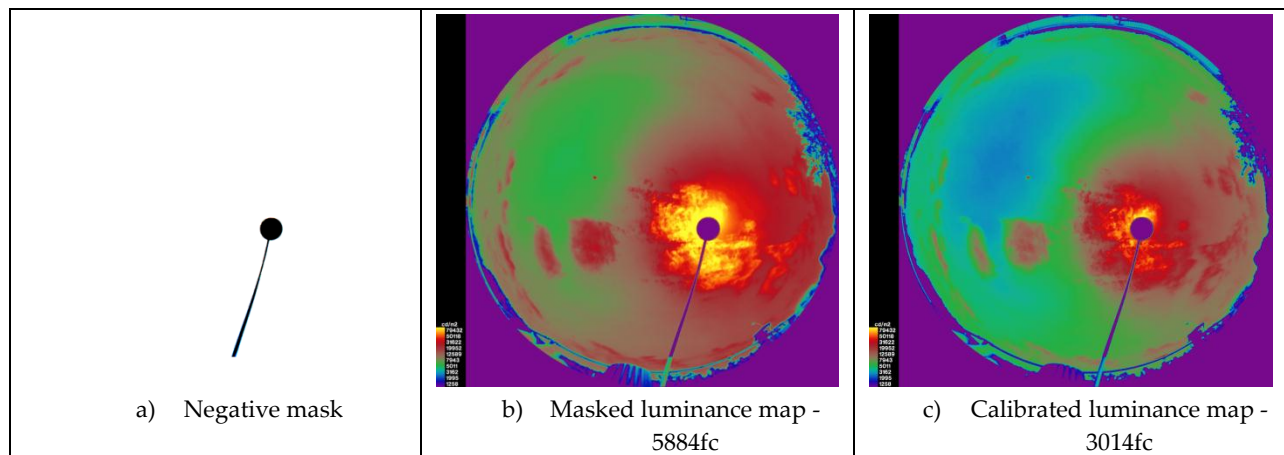


Figure 22: Creating a negative mask, applying to capture sky and calibration

Theoretical sky filler

Cutting out the portion of the sky luminance map obstructed by the shading disk and arm will introduce large errors in the final sky models since the approximately 10° cone obstructed by the shading disc is also likely the brightest portion of the daytime sky. To reduce these errors, the luminance of the blocked portion of the sky needs to be estimated and added back in to the sky model. A variety of theoretical sky models were explored as options to use for replacement the blocked portion of the sky. A study of these different sky models for Test Sky #1 was performed and is included in Appendix D. It was determined that using the Perez sky model, which is a common model used for weather based skies, would best fit the measured sky distributions, see a) in Figure 23. However, it was often seen that while this sky is most able to provide a fairly broad brightened circumsolar region, it still did not match the brightness of the measured circumsolar region. Hence, to best fill in the shaded disc, the Perez sky was then adjusted by matching the Perez sky luminance inside the shading disc to the measured luminance values directly outside the shading disc, see Figure 23 b). Once an adjusted sky was obtained, a positive sky mask shown in Figure 23 c) was used to obtain a piece of Perez sky that could fill in the area blocked. This resulted in a fairly well matched circumsolar region but resulted in overestimating the portion of the sky blocked by the shading disc arm. This was deemed acceptable as the very bright circumsolar region has a much greater impact on overall horizontal illuminance and skylight performance than the thin region further away from the sun blocked by the arm.

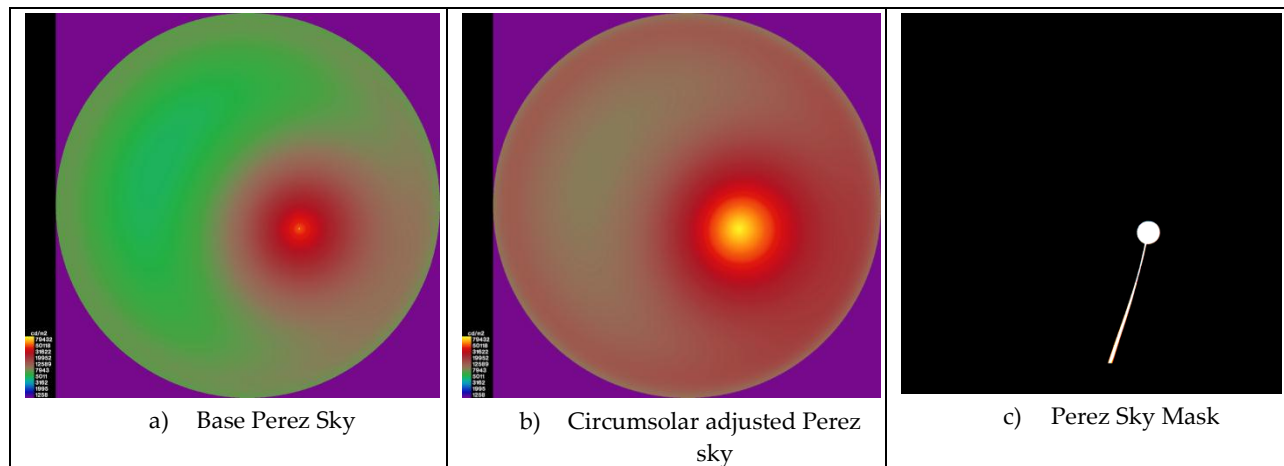


Figure 23: Creating a matching perez sky, performing a circumsolar adjustment, and a positive mask

This process resulted in a final sky model that provides a diffuse horizontal illuminance slightly larger than the measured diffuse horizontal illuminance, see Figure 24. This was expected since the measurement saw a $\sim 10^\circ$ shading disc while our new simulation sky is now filled-in and full. The simulated sky was adjusted one more time such that resulting diffuse illuminance is 10% higher than the measured diffuse illuminance with the $\sim 10^\circ$ shading disc. Calculations of the illuminance provided by the 10° circumsolar region for a several different skies showed an average 10% contribution from this portion.

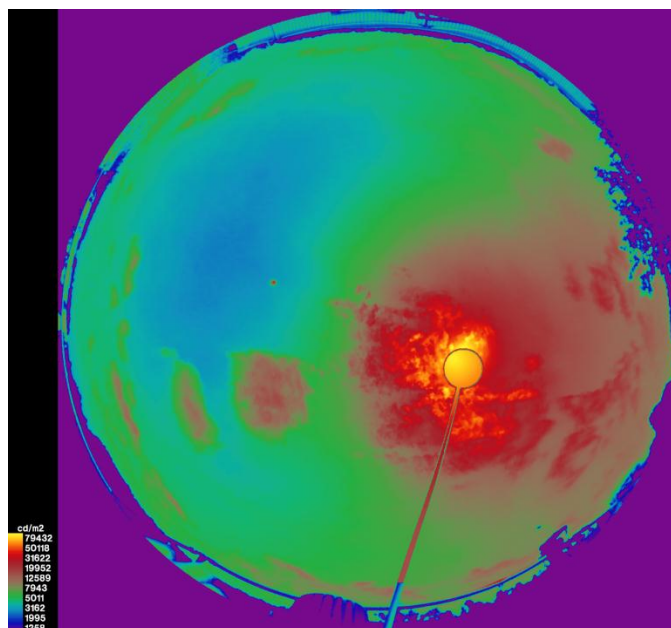


Figure 24: Final Sky – 3202 fc

A final step in the creation of a computer sky model was to add in the direct sunlight component. The direct sunlight component was calibrated to provide the remaining horizontal illuminance needed to obtain the exact global illuminance measured onsite as this measurement was the most accurate taken. The sun location and intensity was determined from the day, time and the direct illuminance and then added to the overall sky model.

Sky Source Ray Set Creation

The final step was to take our calibrated sky luminance map and direct sunlight source and turn them into a form usable by the forward ray-tracing programs. Two different approaches were explored; the creation of a “ray-set”, a data file containing each source ray to be traced, and the application of sky luminance patches to a Tregenza sky patch model. The “ray-set” approach allows for greater sky resolution and presumably better accuracy. This approach and was ultimately used for the Photopia and TracePro simulations and is discussed in the sections below. The Tregenza sky patch model approach available in Photopia is discussed in Chapter 7.

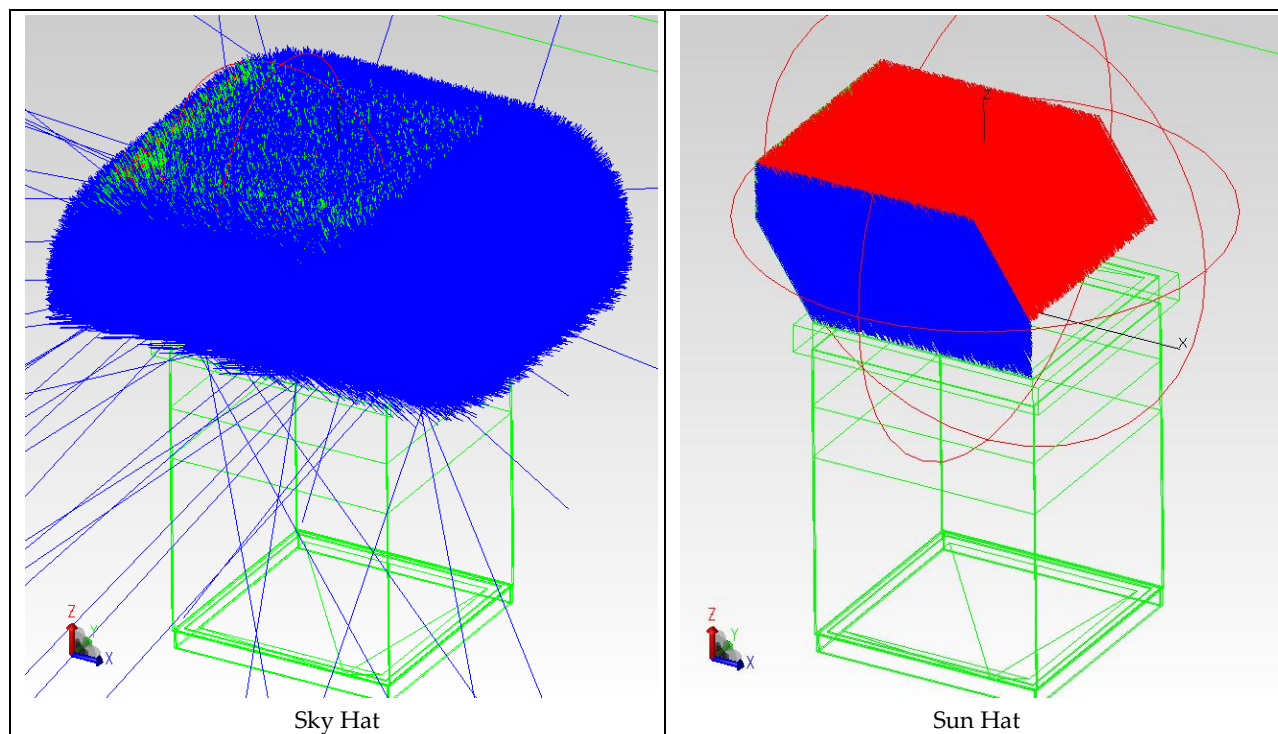


Figure 25: The “Sky Hat” and “Sun Hat” continuous ray-set sources

To create the continuous ray-set sky models, a custom script was developed that produces a large number of rays that start just above the skylight incoming aperture and direct all rays onto the skylight systems, see Figure 25.

The main challenge with physically-based forward ray-tracing has to do with the tremendous amount of “rays” that exist in reality and the still large number needed in a simulation for accuracy. Consider the 1250x1250 pixel resolution images that were captured of our source (the sky/sun). Each pixel in these images represents a different direction and solid angle of incoming light and a different brightness (luminance) for that given direction. If we were to treat each of these different directions as a distinct “ray” of incoming light, therefore taking advantage of the full resolution available, we would have $(1,250 \times 1,250 \times 0.785)$ 1,227,184 rays³. If we wanted to sample this angular density at a reasonable 1” spatial density for a 24”x24” sized product, for example, we would have $(24 \times 24 \times 1,227,184)$ 706,858,347 rays! This far exceeds most ray-tracing software and computer system abilities. A quick review of past TracePro and Photopia simulations have indicated that ray sets between 1,000,000 up to 20,000,000 result in reasonable accuracy and speed performance and larger ray sets begin to pose problems with computer memory resources.

The time and computer resource constraint to the size of a source ray sets poses several ray sampling and simulation questions:

³ 0.785 is the fraction of pixels in the square image that fall within the hemispherical circle, excluding the black corners.

- What hemispherical mapping algorithms most efficiently sample the important aspects of a sky source?
- What initial sky map resolution is required for accuracy?
- Should rays be sampled randomly or in a systematic grid? If randomized, should both the ray direction and ray location be randomized?
- How can the rays be limited to only those that interact with the skylight systems?
- What sky and sunlight sampling density on the skylight surface is required for accuracy?

Mapping Algorithms

The first question addressed was the mapping resolution to use in the sky sampling. A variety of hemispherical mapping algorithms have been developed for various purposes. Three of the most common algorithms were explored for mapping a sky for use as a ray-tracing source, see Figure 26. These were:

- Hemispherical mapping – this algorithm maps the hemisphere according to a cosine weighting (or Lambertian). The angular density of the mapping is determined by the cosine of the angle for each ray, hence the zenith is most dense and the horizon is the least dense with very little sampling. This mapping should best correspond with a horizontal illuminance as illuminance is also subject to a Lambertian weighting.
- Angular mapping – this algorithm maps the hemisphere with uniformity for all angles of sky patches. The zenith and horizon get mapped with relatively equal angular densities. This algorithm is similar to equi-**solid** angle mapping, which by definition provides the same angular density in all directions.
- Stereographic mapping – this algorithm provides the greatest angular density at the horizon and the smallest density at the zenith. This is a useful algorithm if the components around the edge of a hemisphere are of most concern. This could be the case in daylighting simulation for times of sunrise and sunset but is typically not the case throughout the days.

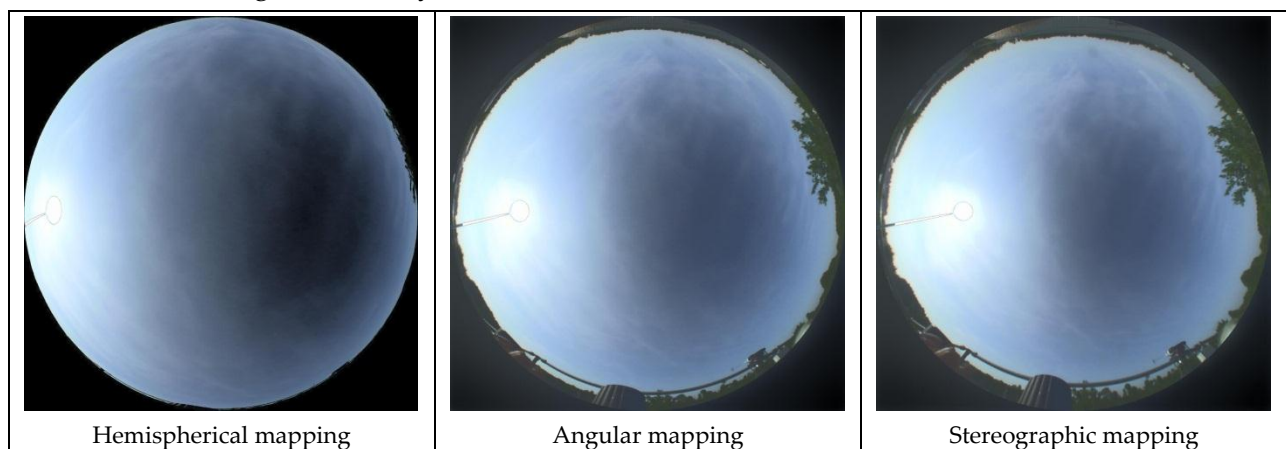


Figure 26: Common hemisphere mapping algorithms

Angular mapping was determined to be the best approach. It was the mapping closest to that of the lens used in capturing the sky images and hence minimized any translation density

issues. Also, since there are times of both low and high angle sunlight, angular mapping should provide adequate density for either. While hemispherical mapping would likely be best for cloudy skies or times when the sun is close to zenith and stereographic mapping would likely be best for sunrise and sunset times, angular is somewhere in between and should be adequate for either situation.

Sky Map Resolution

The next question addressed was the sampling resolution of the sky source. A quick study was performed translating different sky image resolutions into ray-sets and comparing illuminance estimates at 5 orientations (global, south, east, north, and west). Resolutions of 1250x1250, 512x512, 256x256, 128x128, and 64x64 were compared. The illuminance estimates maintained adequate accuracy down to 64x resolution. A 64x64 resolution image results in 3,215 sky sampling points. Recent research on Daylight Coefficient methods has indicated annual average accuracy for lower sky patch resolutions, such as the Tregenza distribution (145). However, a higher resolution of 2305+ patches is necessary for accuracy relative to glare prediction. Since our goal here is to capture specific daylight distribution patterns, not just simulate average skylight performance, a higher resolution may also be important. The 128x128 resolution was selected for these reasons; it is available, provides 12,861 sky sample points and should not introduce any resolution related errors into our simulation.

Random vs. Grid Sampling

There are several methods to consider for sampling these rays given both an angular distribution of the source (the hemispherical sky) and a spatial distribution of daylight onto the system in question. One could sample every single ray direction (12,861) for the array of points on the skylight system or randomize the directions samples, the array itself could be randomized or based on a grid, or the whole thing could be randomized. Randomization is generally deemed a good approach for any problem where many elements are being represented by fewer elements (a google of photons are being simulated via a mere millions of rays) and was pursued over an even grid layout of sampling. Furthermore, rather than sampling every single direction at a given point, every ray direction gets sampled an equal number of times but is always applied to a random location on the skylight. In this way, no two rays will strike the exact same point, yet every single sky direction will be sampled equally and rays will encompass the skylight system with high density and uniformity.

Ray Generation Focused on Skylight Systems

Before final densities could be explored, a method for ensuring enough “forward” rays would actually strike the skylight systems was needed to limit the amount of useless rays traced. Forward ray-tracers excel at simulating complicated optical systems, typically from a source through the system and out in the form of photometric data. When considering this kind of “source-side” forward ray-tracing problem, the majority of actual rays that leave a given source and scatter about the room but have no impact on a final point illuminance or view point calculation. This is the big advantage of backward ray-tracing algorithms: they only trace the rays that arrive at the illuminance point or view point of interest. These could be considered

“task-side” ray-tracing problems. In Radiance, the high resolution final sky luminance maps can simply be used and the backward raytracing algorithms will sample them as needed.

Borrowing from backward ray-tracing, a solution was developed so that all rays would fall onto a defined 5 surface box. A box, rather than a plane, was chosen so that three-dimensional daylighting apertures, such as the common pyramid and barrel domed lenses on skylights, could be encompassed. The rays are randomized on the 5 surfaces of this box that perfectly encompasses the skylight lenses: a 6”x2’x2’ box was used. The magnitude and direction of each ray is determined according to the sky luminance map and direct sun source and the ray is set to originate a unit vector away from the box intersection point, and aimed right back at the box. In this way, the sky and sun “hats”, see Figure 25, are created with all rays falling onto the 5 surfaces of the box. Since the box does not perfectly match any of the skylight domes, there are still rays that will miss the system, ranging from 10-50% depending on the sun angle. This is a reasonable loss and can be accounted for with a corresponding increase in initial rays.

Sun and Sky Source Density

Finally, the density of sunlight and skylight sampling falling onto the skylight systems was explored. As stated earlier, a target between 1,000,000 and 20,000,000 total rays was determined as reasonable relative to accuracy and computer ability. A 128x128 resolution was determined to be an adequate angular sampling density. With the randomization technique to apply each sky sample equally, the sky resolution density will be a multiplier of 12,861.

In TracePro, a density of 10 full sky samples per square foot ($10 \times 12,861 = 128,610$ samples per sf) was used which results in roughly 501,000 rays on the top surface of our 2’x2’x6” box. Including the sides, each sky produced roughly 734,000 rays. Sun ray density was separated from the sky rays so that the two sources could be sampled at different ratios. A sun ray density of 100,000 rays per sf was selected to closely match that of the sky ray density. This resulted in 592,210 sun rays total. Ray splitting was used in the TracePro simulations which resulted in double the amount of rays after the first scatter at the collector, and doubling again each consecutive bounce.

Photopia functions more optimally with a higher initial ray set and no ray-splitting. For the Photopia ray sets, a sky ray density of 30 was used giving roughly 2,200,000 rays and a sun density of 600,000 was used giving roughly 3,400,000 rays.

Final Sky and Sun Source Ray Set

A python script was written to create sky and sun source ray sets based on the parameters and decisions discussed above. The scripts create two ray set files, one for the sky and one for the sun. In forward ray-tracing software, these ray sets describe the source ray-by-ray. A view of a final ray set sky is illustrated below in Figure 27. It can be seen that this ray set accurately picked up the bright circumsolar region, brighter regions of cloud cover, and the darker horizon with tree obstructions. Final illuminance checks were performed for global, south, east, north and west orientations to ensure the ray sets produced an equivalent amount of light onto our encompassing box as was measured in the field.

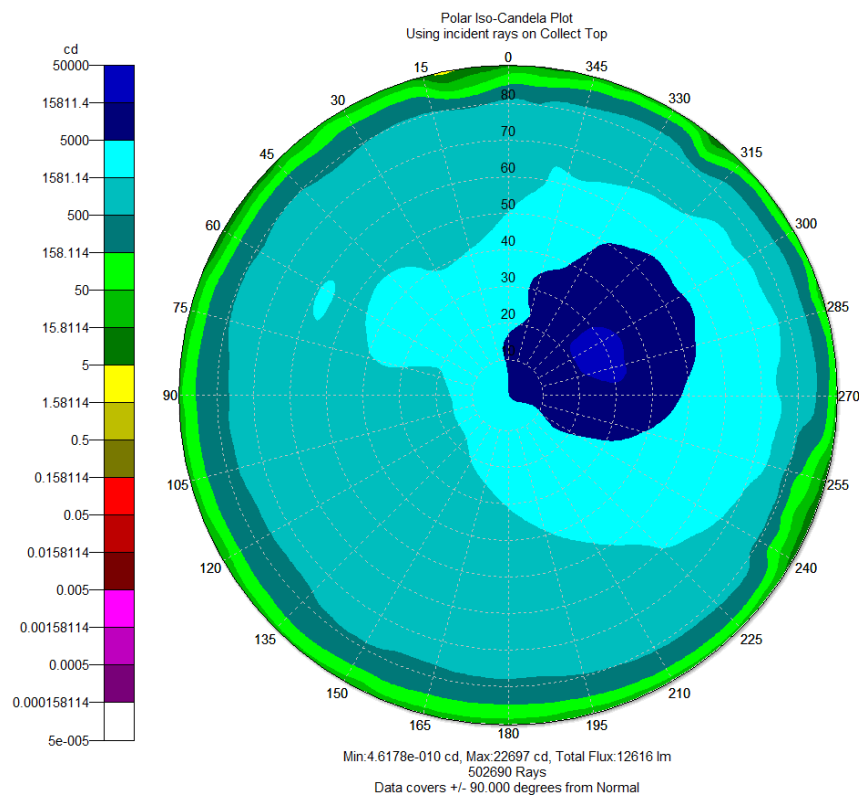


Figure 27: TracePro Mapped Sky Candela Plot – 3203fc diffuse

Geometry Measurements and Creation

Three-dimensional geometric models were created of the three skylight systems tested. The geometric model for the SunOptics light cube and the 22" Sun Tunnel systems are shown in Figure 28. The other system tested just consisted of the SunOptics pyramid skylight with white foam core walls and is not shown here. After the rooftop testing, the tested skylight systems were measured and modeled as a system of faces in Sketchup. These were then converted to solid element models for use in TracePro and Photopia and mesh models for use in Radiance.

In addition to the geometry shown, a roof element, a photometric collection plane, and an array of near field collection points were included in the models. The roof element blocks any stray rays that don't make it into the system from finding their way to the photometric collection plane. The approach of collecting exiting photometric data on a plane assumes a perfect far field photometric condition. For this reason, near field collection points were also included and the variance between simulated far-field and near-field photometry is explored in Chapter 5. The field measurements taken are near-field and so should align better with a matching near-field simulation.

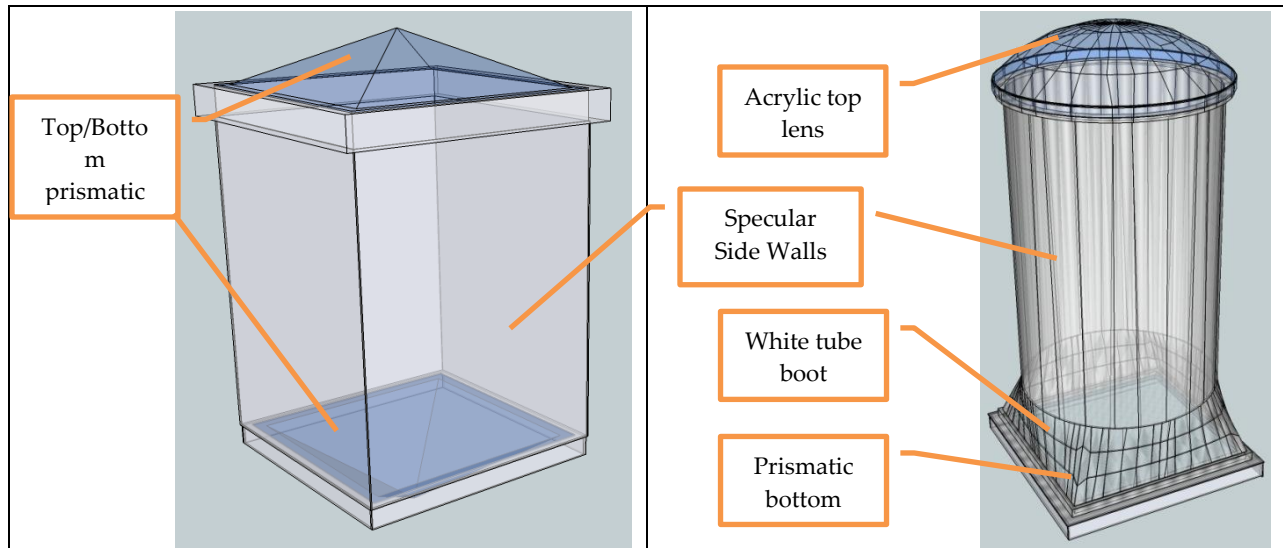


Figure 28: Isometric diagrams of the SunOptics Light Box and the Sun Tunnel Geometric Models

A fairly simple model was created for each skylight system that includes the basic elements as perfect geometric forms (i.e. pyramids, prisms, etc.) There were few noticeable imperfections in the geometry (out of plane walls, imperfections in the lens, etc.) that were not measured or modeled. However, it is expected that there are minor imperfections in the geometry throughout the systems both due to manufacturing variation and damage or marring during shipping, handling and installation. The differences introduced by the geometric imperfections will result in both over and under predictions with no tendency for errors to consistently be one way or another expected. In reality, these imperfections will always exist in field equipment and will rarely be modeled accurately. Therefore, it is acceptable to have these differences and worthwhile to validate the use of “perfect” computer geometry models to predict the performance of real field equipment.

CHAPTER 6: BSDF Measurements and Modeling

An important component of accurate computer models of the skylight systems is the accurate and detailed representation of the optical characteristics of the surfaces and materials involved. A detailed definition of this scatter of light is necessary, particularly for materials that exhibit broad and varied scatter of light and for daylighting systems that often see a very intense light source come from one incident direction.

A variety of different visible reflectance and transmittance measurements were taken and simulations performed for the main optical materials in our systems: the most important being the top and bottom prismatic lenses and the highly reflective side walls of the skylight systems.

The information required is the behavior of light scatter for every incoming direction of light or a Bi-Directional Scatter Distribution Function (BSDF). BSDF is the general term that includes both Bi-Direction Transmittance Functions (BTDF) and Bi-Directional Reflectance Functions (BRDF). In the simplest terms, the BSDF is the ratio of luminance in a specific direction divided by the illuminance from a specific direction. The following equation defines the BSDF as a function of both incoming illuminance (E_i) per incidence angle and outgoing luminance (L_s) per outgoing angle.

$$BSDF(\theta_i, \phi_i, \theta_s, \phi_s) = \frac{dL_s(\theta_s, \phi_s)}{dE_i(\theta_i, \phi_i)} \quad [1/ster]$$

Figure 29 illustrates the standardized angles used to describe BSDF measurements. There are four angles used to describe the incident and exitant light directions relative to a sample normal (ZB) and a designated orientation (XB). Two angles, a horizontal ($\phi_i - \phi_s$) and vertical ($\theta_i - \theta_s$) angle, define the direction of incoming light and two define the direction of scattered light (ϕ_s and θ_s). The angles encompass an entire sphere around the sample, ϕ ranges from 0° to 360° and θ ranges from 0° to 180° , and so can describe incoming light on both sides of the sample and outgoing light, both transmitted and reflected, in all directions. These annotations will be used to discuss these angles throughout the rest of the report and are defined in the ASTM E2387 Standard Practice for Goniometric Optical Scatter Measurements [4].

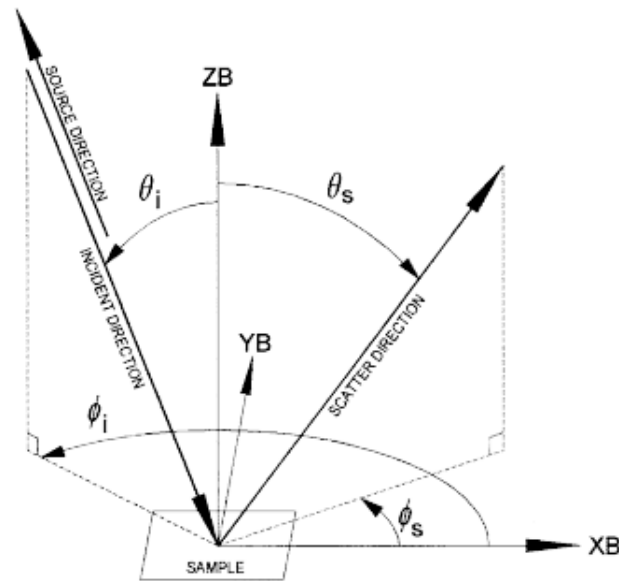


Figure 29: Definition of Polar Angles used in BSDF measurements

The terms isotropic and anisotropic are used to describe the nature of light transmission and reflection. Isotropic surfaces exhibit symmetry relative to the **incident** horizontal, ϕ_i , angles: they are rotationally symmetric. Many surfaces are uniform and behave in this way such as glossy paint or foam core. Anisotropic surfaces have different behavior depending on the horizontal direction of the incoming light. These surfaces typically have non-symmetrical characteristics, such as striations, ridges, or prisms and the reflectance/transmittance scatter changes as the surface is rotated about its normal.

Isotropic measurements are most common and just require a range of incident vertical, θ_i , angles from 0° to near 90° . Anisotropic measurements are more extensive as they require a range of ϕ_i to be measured as well. Depending on any symmetry to the anisotropic surface, a quarter or half of the hemisphere can be measured and mirrored to represent the whole hemisphere. In cases of no symmetry, the full 360° needs to be measured.

The reflected or transmitted scatter can also be symmetric or asymmetric. Most isotropic materials will exhibit a symmetrical scatter around the incident / mirror ray plane. In these cases, only a hemisphere of outgoing scatter needs to be measured. Anisotropic materials often have asymmetric scatter requiring a full hemisphere of exiting light to be measured.

Samples of the prismatic lenses were cut from the actual skylights tested and shipped to Lawrence Berkeley National Laboratory (LBNL), LTI Optics, and The Scatter Works for detailed BSDF measurements of the transmittance and reflectance. In addition, samples of the SunOptics box sidewall, Sun Tunnel sidewall, and white Sun Tunnel boot were measured at LBNL. BSDF simulations were also performed using high-resolution 3d models of the lenses which included many of the minor imperfections due to the manufacturing process, such as the dimple marks left likely from the injection molding process.

While these various labs and simulation approaches all measure BSDF information, they all utilize a different data format, different definition standards, and have varying ability to

measure anisotropic and assymetrical BSDF data. This makes the comparison and sharing of the data difficult. Because of this, each BSDF generation method was used with the simulation engine it was most suited to; Radiance, TracePro or Photopia. The following sections describe the various BSDF methods explored and the simulation approaches used with each.

LBNL BSDF Measurements

LBNL uses a PGII Scanning Goniophotometer [5], shown in Figure 30, to perform and report absolute BSDF measurements following the ASTM standard. The machine takes a range of measurements in several different spherical patterns around the sample as shown in Figure 30 and can produce varying levels of resolution. The system reports BSDF information for each point in this somewhat random array of data. It can also produce BSDF data via interpolation for standard planes of vertical and horizontal incident angles.

The scatter measurements encompass the entire sphere around the sample allowing the system to measure asymmetric scatter. The scatter measurements and θ_i angle changes are automated for an isotropic sample. For an anisotropic sample, different ϕ_i angles are measured by manually rotating the sample relative to the incoming ray and running the automated scatter measurements. This is a more time consuming and expensive effort as it requires user intervention for every θ_i measured.

While the measurements are absolute values, these values vary due to lamp drift, so it is necessary to calibrate the measurements based on total reflectance and/or transmittance measurements. Total hemispherical reflectance and transmittance measurements were provided by LBNL and used to calibrate the absolute BSDF measurements.

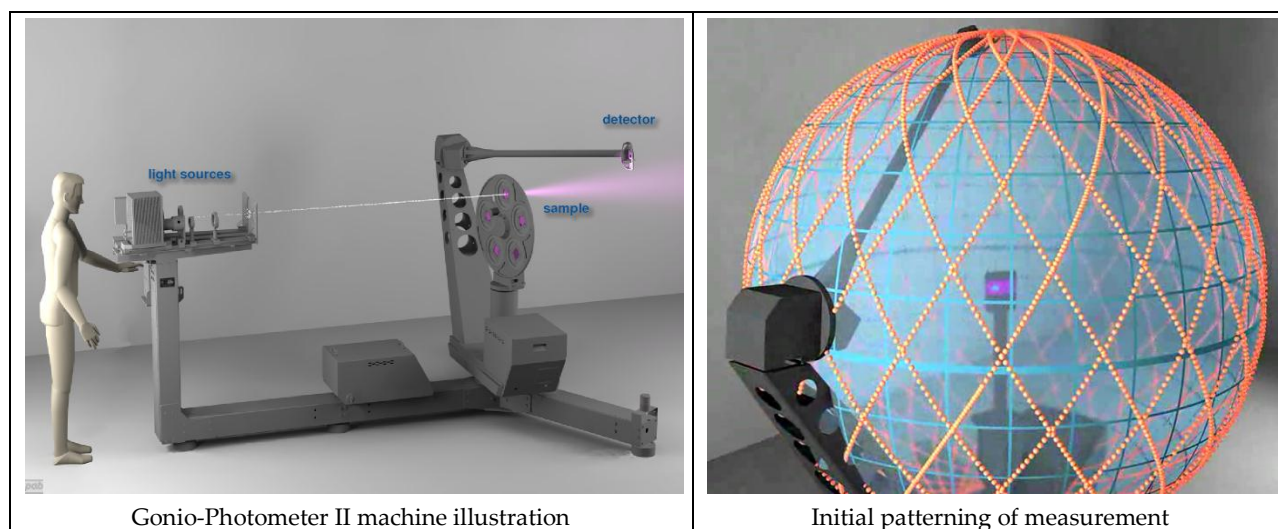


Figure 30: Illustration of the PAB Ltd Gonio-Photometer II used at LBNL

For this project, the BSDF data sets provided by LBNL included hemispherical scatter information for an incident plane defined by $\phi_i=0^\circ$ and for incident angles from 0° to 90° in 10° increments of θ_i . This plane was defined such that XB aligns with the long direction of the

samples and the long diagonal of the prisms. As discussed above, this single plane of incident angles assumes isotropic behavior. This is an acceptable assumption for the specular metal walls and shiny white finishes. However, this isotropic data is limited in accurately describing the prismatic lenses as they exhibit anisotropic behavior given their asymmetric diamond shaped prisms, see Figure 31. The prisms show two planes of symmetry, so a $\frac{1}{4}$, or 90° of the incoming hemisphere needs to be measured, from the short to long diagonal planes, and can then be mirrored to create a full hemisphere.

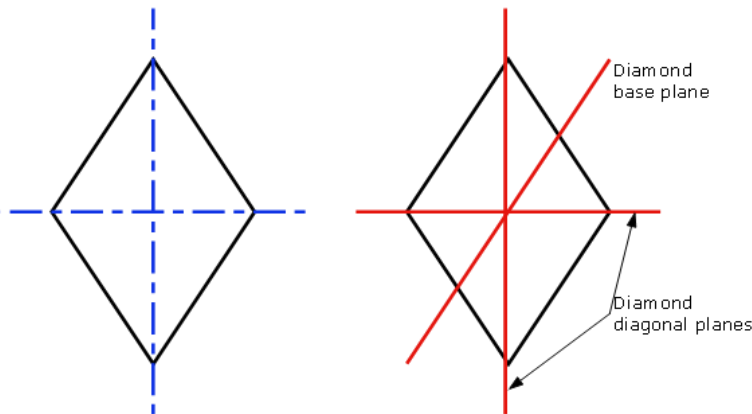


Figure 31: A diamond prism's planes of symmetry (left) and measured planes (right)

The LBNL BSDF measurements were implemented in TracePro, the TracePro sections below discuss the process of getting the data into the software using various BSDF representation models. The LBNL data for the isotropic materials, namely the reflective tube walls, were used to calibrate the Radiance and Photopia definitions as well.

Radiance BSDF Approach

Radiance has several newly implemented tools for creating BSDF definitions and using BSDF materials in simulation. However, a computer model of the material is required. Typically, models of these types of optics assume perfect geometry, perfect pyramids, with perfect curves. However, in reality there are many imperfections due to the manufacturing process. To serve our goal of validating the simulations of real skylight systems, and to align with the physical measurements, a computer model of the actual lens samples was created. This model was then used to simulate BSDF information for the prismatic lenses for use in further Radiance simulations. The following sections describe this process.

Laser Scan Model

A detailed 3d model was created by the QC Group (www.qcgroup.com) from samples of the SunOptics and SunTunnel lenses using laser scan equipment able to capture detailed part contours. The system used had an XY grid resolution of $\sim 0.002''$ and a Z resolution of $0.0001''$. The resulting 3d computer models of these samples used in Radiance are shown in Figure 32. Closer inspection of these models does in fact reveal dimple marks from plastic injection points, rounded peaks, and the rippled back of the SunTunnel lens.

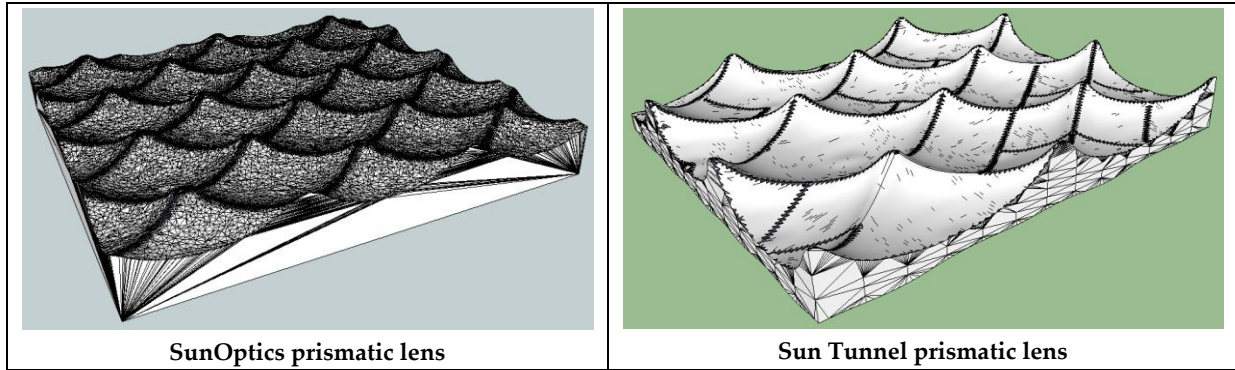


Figure 32: Laser Scan 3D Prismatic Lens Material Models

Radiance accurately models the refraction and reflection that occurs with clear transparent or semi-transparent materials. When using solid geometry models, where each ray will intersect a surface at least twice, the material can be modeled in Radiance using the interface material definition. This defines the reflection and refraction that occurs at the surface between air (or some other transparent medium) and the acrylic transparent plastic. The following radiance definition was used:

```
void interface acrylic
0
0
8 .65 .65 .65 (r,g,b inside transmission coefficients)
1.491 (inside index of refraction)
1 1 1 (r,g,b outside transmission coefficients - air)
1 (outside index of refraction - air)
```

The published index of refraction of clear acrylic ranges from 1.490 and 1.492.[6] The transmission coefficients model the reduction of light traveling through the acrylic medium, or absorption of light, due to the nature of acrylic, manufacturing imperfections and other particulates in the manufactured acrylic. The 0.65 transmission coefficients were determined iteratively by matching up the resulting BSDF simulations with more accurate hemispherical reflectance and transmittance measurements provided by LBNL. A rendering of the lens with the final material definition is shown in Figure 33.

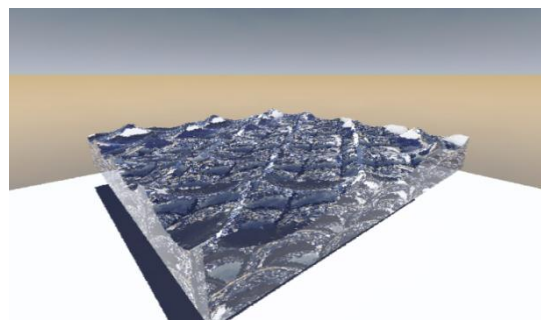


Figure 33: Rendering of the SunOptics lens Radiance model

Window 6 / Radiance BSRF Standard

Both the Window 6 and Radiance software developed by LBNL have implemented a standard BSRF methodology aimed at modeling the effects of fenestration systems, such as venetian blinds. The base functionality is built on Klems hemispherical discretization models that break up a hemisphere into 145 patches. The patches are sized to give approximately the same illuminance at the center given uniform luminance of the dome. [7]

Figure 34 and Figure 35 illustrate the coordinate system used, the patch numbering, horizontal and vertical angle and orientation standards for the Klems model. A circular patch, #1, is located perpendicular to the surface. The positive X axis defines $\phi_s=0^\circ$ and is the center of patch #2 and the first patch in each new ring. The negative X axis defines $\phi_s=0^\circ$ and the next patch number for outgoing (reflected or transmitted) hemispheres. The circular direction of Patch #3 or the following patch number is then determined by right hand rule for both the incoming and outgoing hemispheres. The vertical angles are defined from both Z and Z' and range from 0° to 90° rather than $0-180^\circ$ used in the ASTM standard. Because of the duplicate vertical angles, the resulting data requires information regarding whether it is transmitted or reflected and whether light is incident on the "front" or "back" of the material.

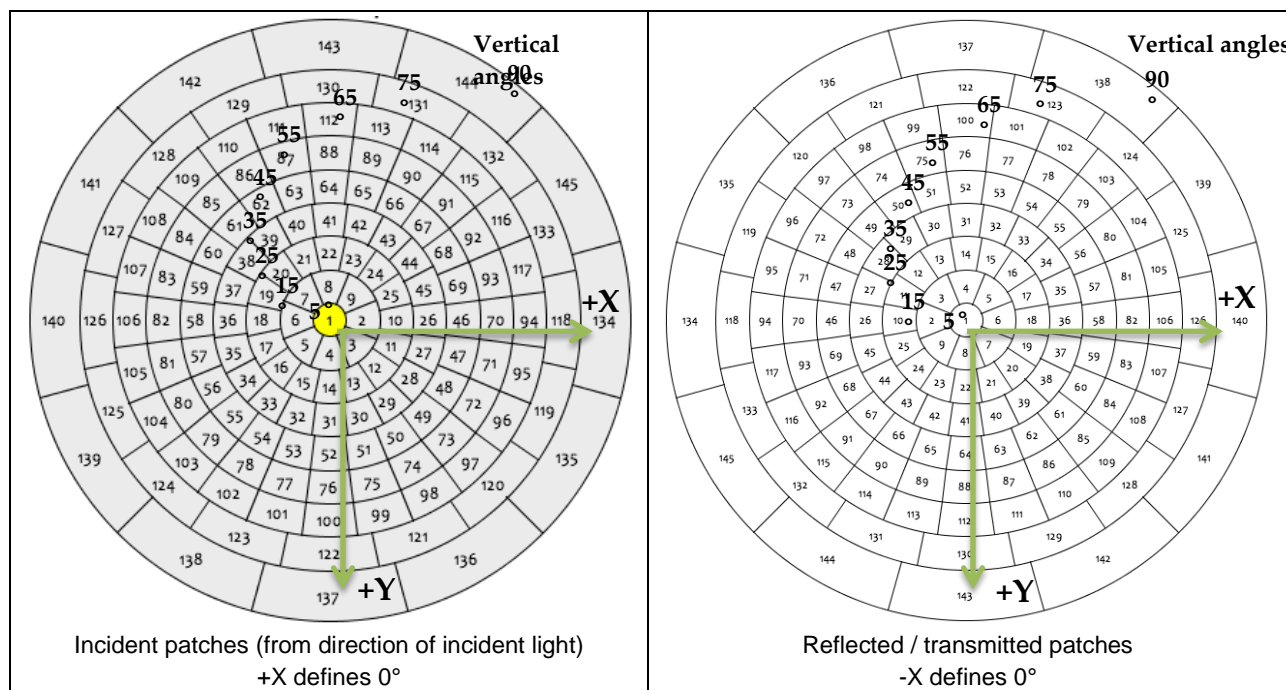


Figure 34: Klems Hemisphere Patches – Standard numbering and orientation

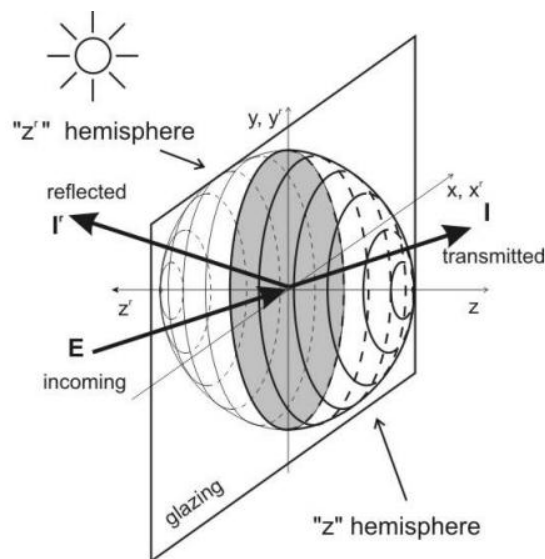


Figure 35: Klems coordinate system for incident, reflected and transmitted light

It has been found that the light distribution in systems that show a high variability in the angular output, i.e. large and steep “peaks” and “valleys” in the angular distribution, are not represented well with the relatively coarse 145 patch discretization. Studies have explored the impact of higher resolution discretization models, such as a 2X Klems or 4X Klems patch models illustrated in Figure 36, and showed that while all the models accurately predict the amount of light being transmitted, the higher resolution models are often necessary for detailed visual analysis of the material or system. [8]

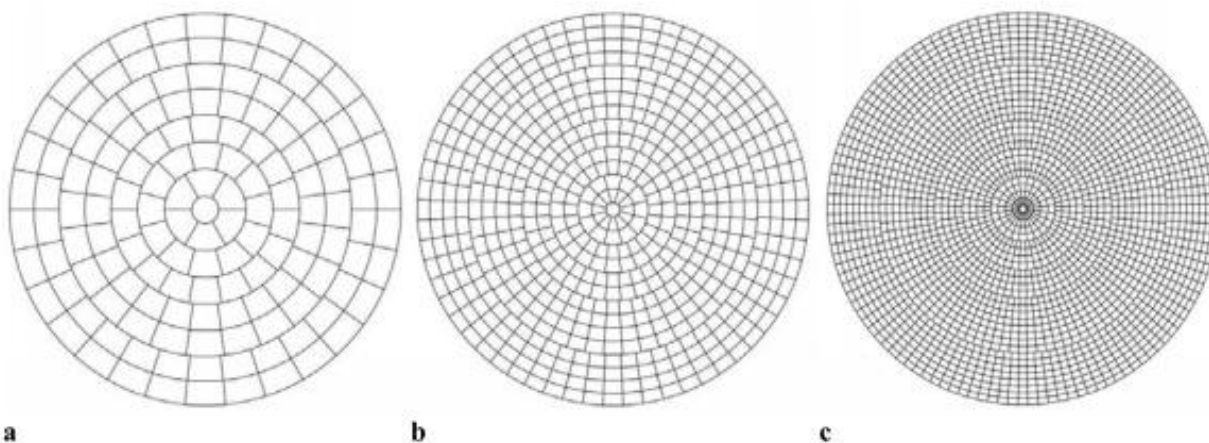


Figure 36: Orthographic projections of BSDF hemispherical division schemes a) full Klems basis – 145 patches b) 2x Klems - 580 patches, and c) 4x Klems – 2320 patches [ref andys paper]

The downside of the higher resolution discretization models is the larger data set and data file that result and the slower read/write times when used in simulation. In addition to sharp peaks and valleys, there are often also large portions of the hemisphere that do not exhibit much change in luminous intensity. To address these concerns, a variable resolution BSDF format has been developed and implemented in the Radiance software that auto-discretizes the

hemisphere based on the gradient of the luminous intensity. Where the gradient is large, multiple patches result and when the gradient is small the patches get larger. These are done via rank 3 (isotropic) or rank 4 (anisotropic) tensor-tree representations. [9] An image illustrating the outgoing scatter of a device using a variable resolution rank 4 tensor-tree representation is shown in Figure 37.

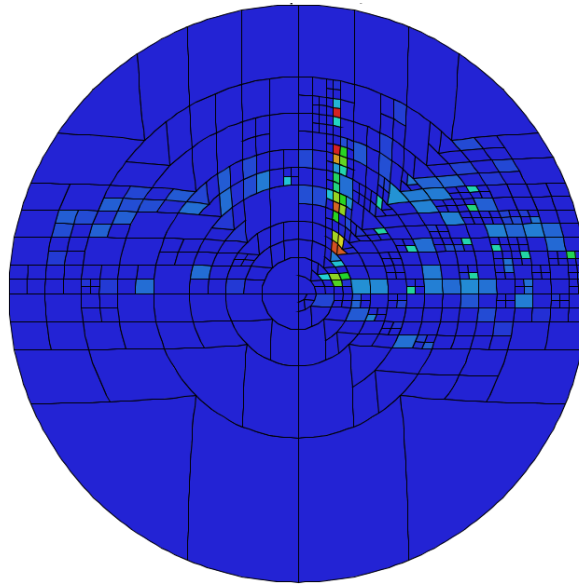


Figure 37: Example of variable resolution BSDF tensor-tree representation

A standard XML based file format has been defined and used by the two software. [10] Window 6 produces XML formatted BSDF files for user defined fenestration system scenarios. However, the software is limited to simpler louver models and produces standard Klems 145 patch resolution files. Radiance has also defined a new variable resolution XML format in addition to the standard Klems resolution. The exact formatting of these XML files is unclear and seems to be under development with current documentation available via e-mail to LBNL.

BSDF Material and genBSDF

Radiance has several utilities to read and use BSDF information in simulation and to create BSDF information from optical models. A BSDF material definition was introduced in Radiance 4.1 that reads in the standardized BSDF XML file format, and accurately simulates the behavior in both the indirect and direct Radiance calculations. The user can define the orientation of the BSDF file and specify an offset that allows the actual geometry to be included and used in the direct calculation. [11]

A new utility in Radiance called “genBSDF” automates the simulation of BSDF information given a valid Radiance model. The utility is intended to be used on relatively thin but large in area optical systems such as a window frame with venetian blinds. It is to be determined whether it can be used on smaller more optically complex and deep daylighting systems such as tubular skylights. Radiance (or backward ray-tracing in general) is great at handling task side

renderings and calculations but is not as accurate with source side lighting simulations, where forward ray-tracing or photon-mapping algorithms excel. [12]

A current limitation to this standard BSDF XML file format is the only currently available ways to produce a file of this format are via the Window 6 and Radiance genBSDF software. At the time of this study, the goniophotometer labs used to measure BSDF information do not produce BSDF information according to the Klems 145 patch discretization standard, variable resolution standards or the Window 6/Radiance xml file format.

Measurement Results

GenBSDF was used to create several different types of BSDF XML files for use in the Radiance simulations. The BSDF file formats created and analyzed were:

- Standard Klems – 145 patches
- Klems 2X – 581 patches
- Klems 4X – 2321 patches
- Rank 4 Tensor-tree $\log 5 - 2^5 * 2^5 = 1024$ maximum patches

A custom genBSDF was created to generate the 2X and 4X Klems versions. However, the resulting Radiance simulations with these BSDF definitions proved to take significantly longer, on the order of 100X, than the tensor-tree and Standard Klems versions. This may be a function of an undefined or improper XML definition or bugs/incompatibility with the Linux and Windows version of Radiance. Since, the tensor-tree versions can provide an equivalent level of resolution with potentially smaller files, these higher resolution Klems BSDF formats are not recommended and were not analyzed further.

The resulting standard Klems and tensor-tree BSDF files were calibrated, via adjusting the transmission coefficient in the acrylic material definition, to closely match total hemispherical transmittance and reflectance measurements provided by LBNL. The following Figure 38 through Figure 45 illustrate the standard Klems and the log 5 Tensor-tree scatter simulation results for perpendicular incoming light. The expected cross pattern to the scattered light can be seen in each, see 0 for a theoretical scatter discussion.

The log 5 tensor-tree image shows areas where the higher resolution is necessary to describe distribution as well as areas where much larger patches suffice, see Figure 39 and Figure 43. The Sun Tunnel lens has been shown to result in a triple-peak distribution using the other BSDF methods and Figure 43 reflects this behavior as well showing an offset ring of brightness around the central peak.

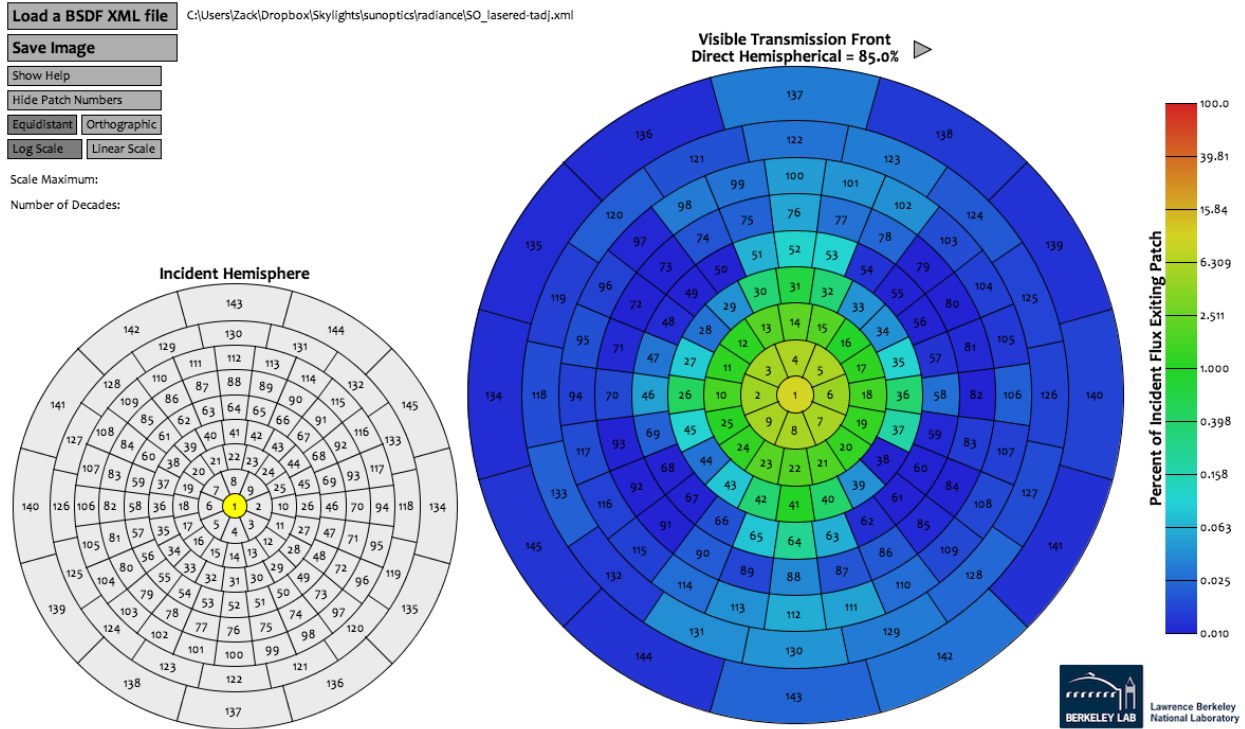


Figure 38: SunOptics Lens: Perpendicular Front Transmission – Klems scatter Plot

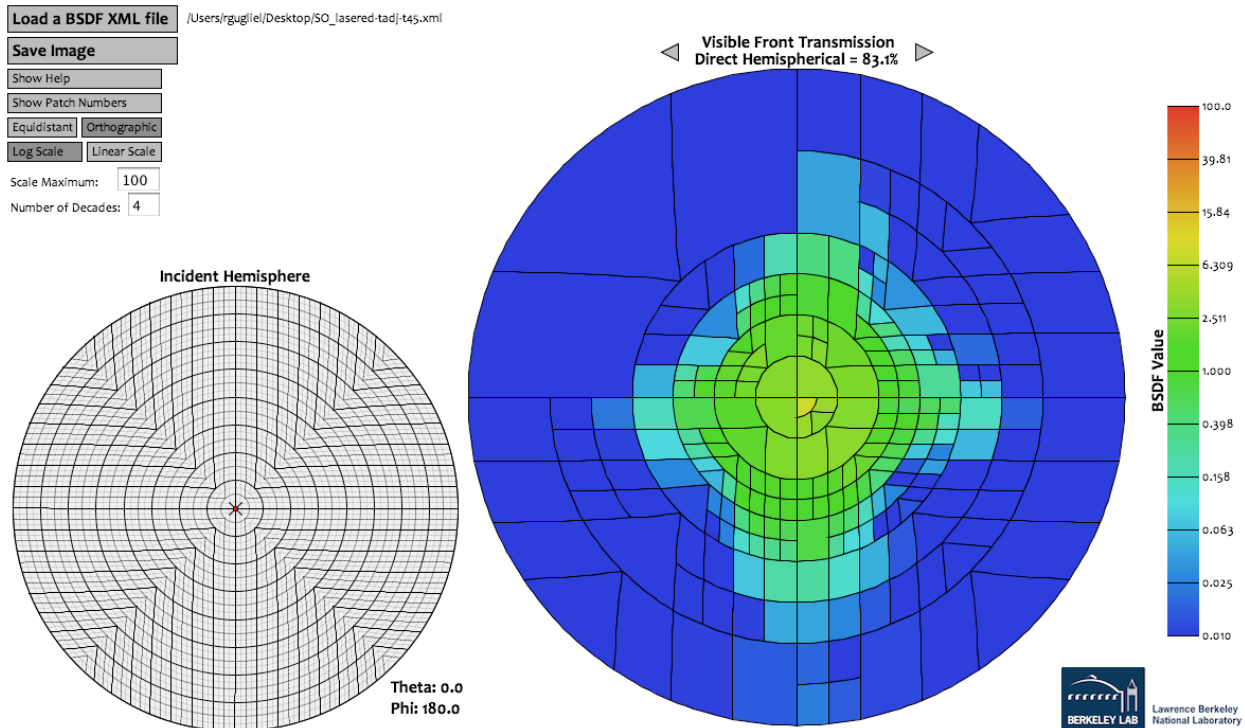


Figure 39: SunOptics Lens: Perpendicular Front Transmission – Variable resolution scatter plot

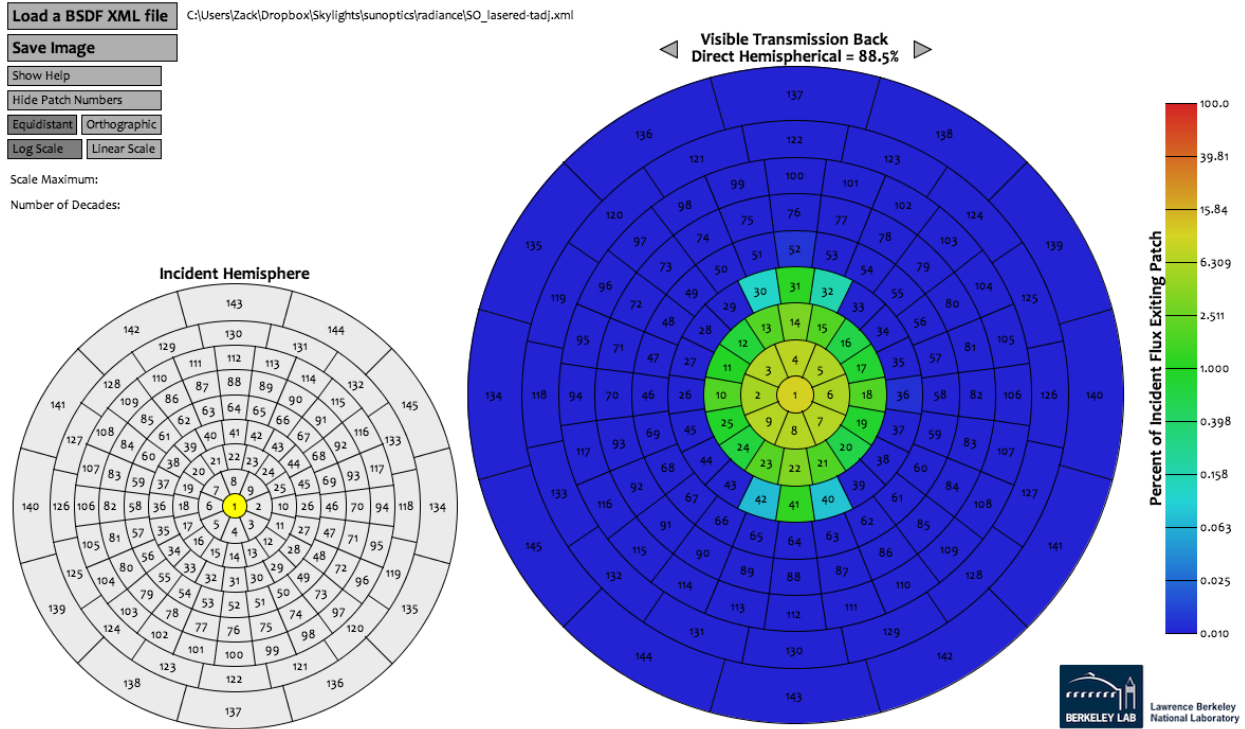


Figure 40: SunOptics Lens: Perpendicular Back Transmission – Klems scatter plot

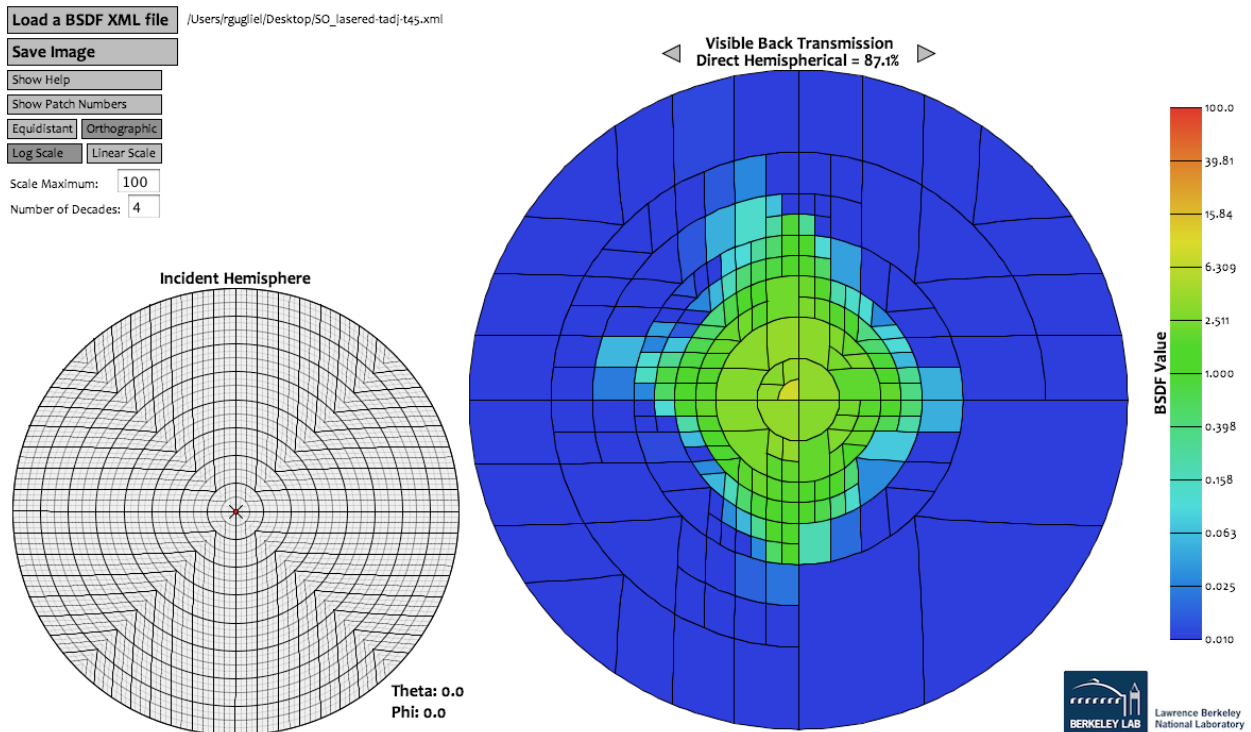


Figure 41: SunOptics Lens: Perpendicular Back Transmission – Variable resolution scatter plot

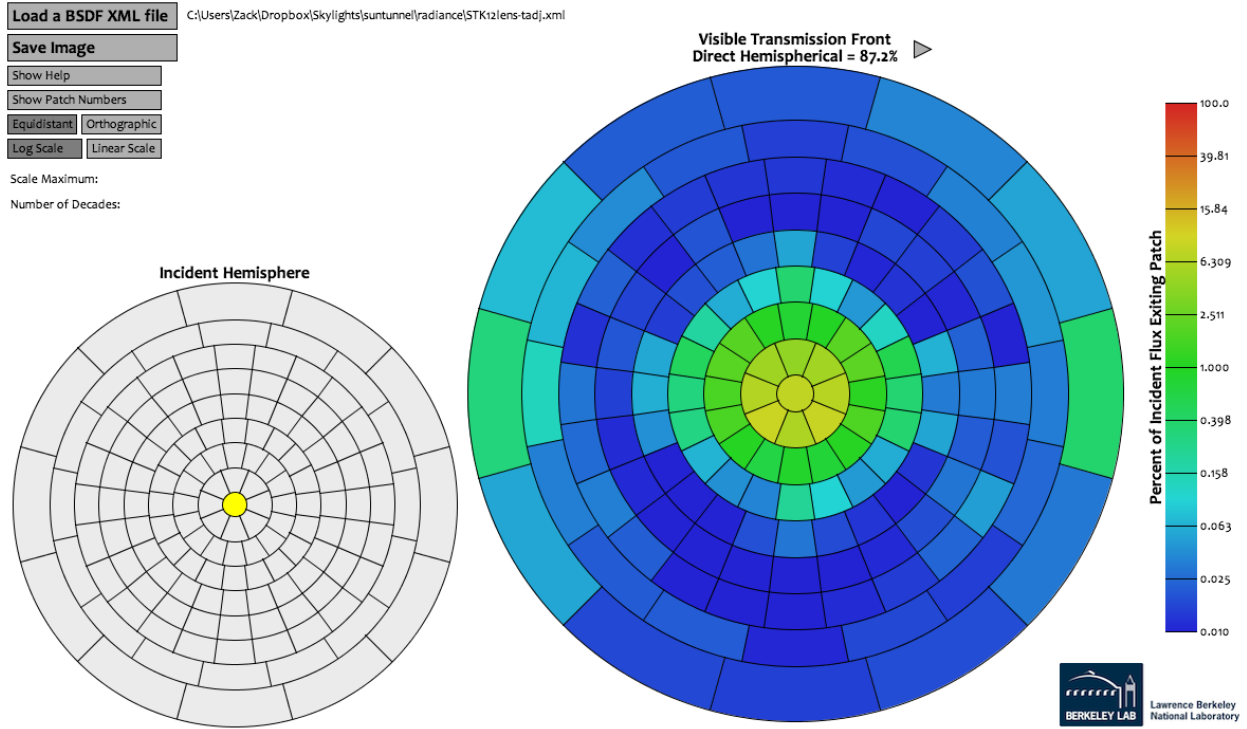


Figure 42: Sun Tunnel Lens: Perpendicular Front Transmission – Klems Scatter Plot

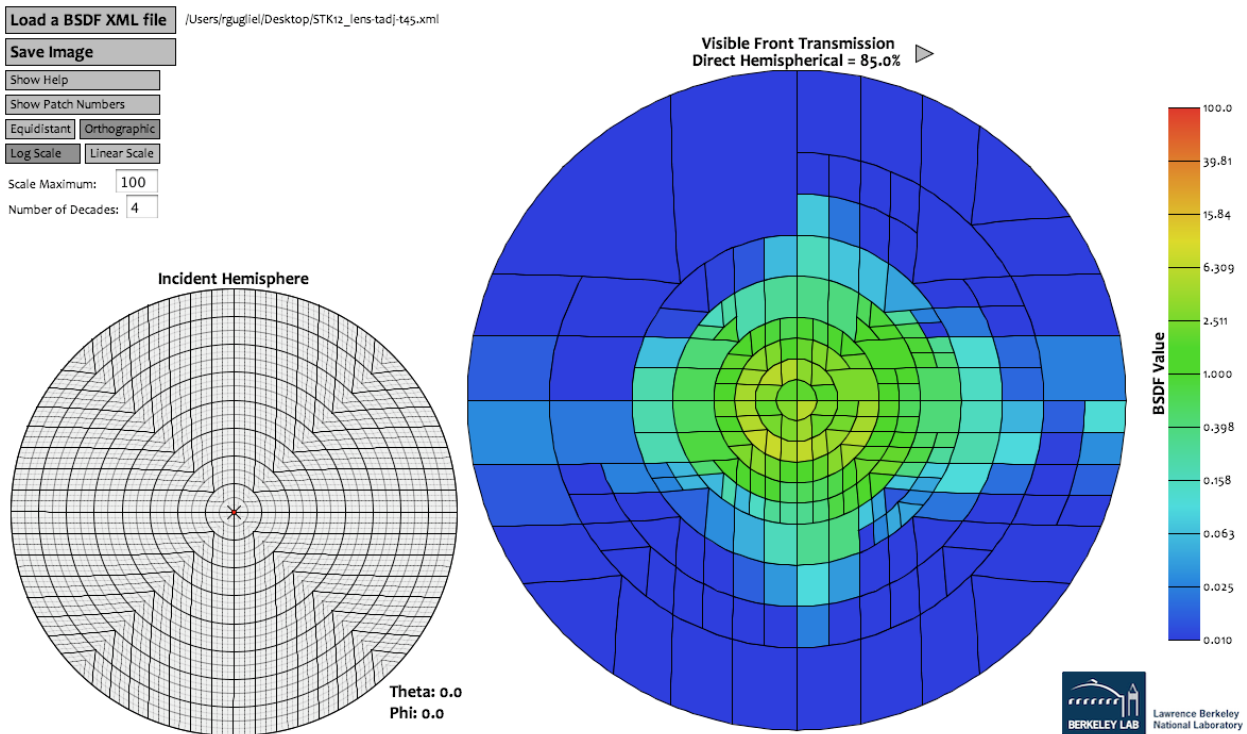


Figure 43: Sun Tunnel Lens: Perpendicular Front Transmission – Variable resolution Scatter plot

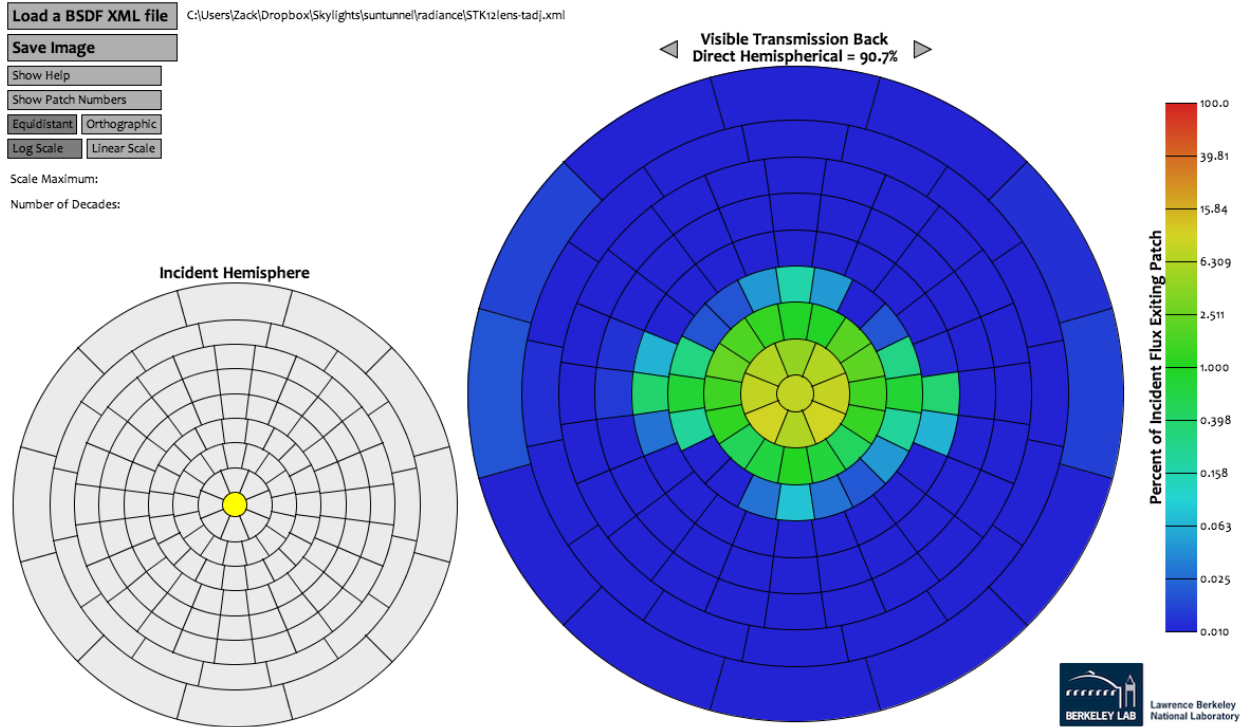


Figure 44: Sun Tunnel Lens: Perpendicular Back Transmission - Klems scatter plot

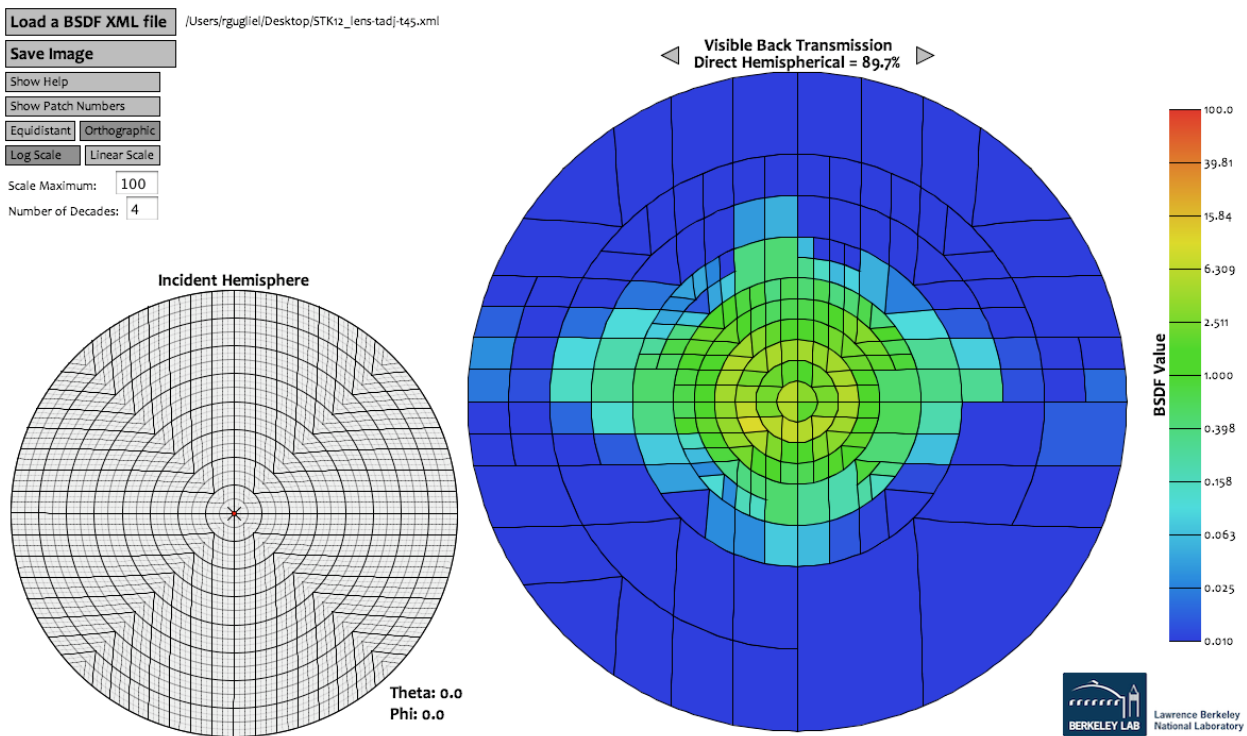


Figure 45: Sun Tunnel Lens: Perpendicular Back Transmission - Variable resolution scatter plot

The following lists the final Radiance simulation parameters used to generate the BSDF files using genBSDF:

- Direct: -dj 1, -ds 0.01 -dt 0.05 -dc 0.95 -dr 12
- Specular: -ss 2, -st .01
- Indirect: -ab 7, -ar 100, -aa 0, -ad 2048, -as 1024
- General: -lr 12, -lw 0.0001
- genBSDF: -c 10000

The simulations took approximately 20 min for the Standard Klems basis and up to 2 hours for the high resolution tensor-tree versions on a modern 6 core CPU. Some sensitivity studies were performed and indicated that the parameters provided adequate accuracy. However, additional study of the exact parameters is in order to determine the minimum parameters acceptable for accurate yet efficient simulation.

TracePro BSDF Approach

TracePro offers several methods for representing BSDF surface behavior. There are several simplified methods for describing BSDF information in either an isotropic or anisotropic but symmetrical form. There are also completely anisotropic methods that rely on brute-force interpolation from large tables of BSDF data. Other methods rely on modeling the geometry of the optical elements in the software and using replication to simulate that behavior across the material surface. In addition to the LBNL data, scatter measurements were performed using techniques common in TracePro for measuring and fitting the data to a native TracePro BSDF definition.

Curve-fit BSDF Representations

It has been shown that many isotropic materials exhibit symmetrical scatter distributions relative to the specular ray. Other materials show a tendency to maintain a strong normal component to the scattered light even at higher incidence angles but while still exhibiting side-to-side symmetry. Some materials will show some characteristics of both resulting in a double peak of output intensity. Many of the more prevalent BSDF representation models have been developed around these two common characteristics.

The standard Harvey-Shack Gaussian BSDF model available in TracePro assumes isotropic behavior and symmetry relative to the specular ray for all incidence angles, see Figure 46. For materials that fit this behavior, a single equation shown below, can be used to describe the scatter of light for any direction of incidence. [ref] Anisotropic “elliptical BSDF” definitions are also available that allow two-axes to be defined in the same manner.

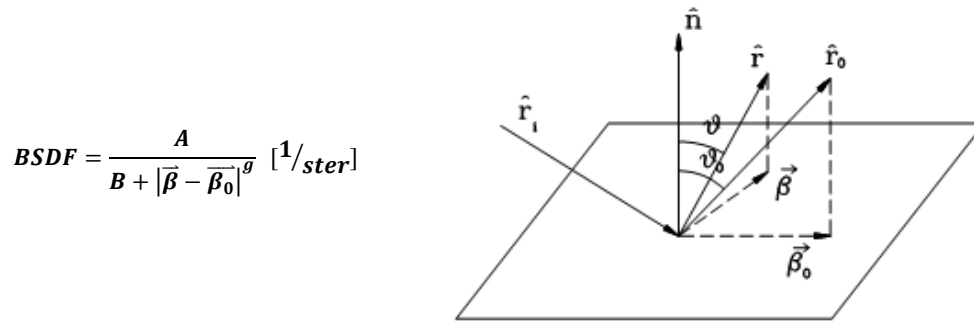


Figure 46: Harvey-Shack BxDF equation and angle definitions used

There are three parameters used in the Harvey-Shack BxDF representation: A, B and g. Each parameter controls a different characteristic of the scatter distribution. The A parameter adjusts the overall magnitude, the B parameter adjusts the overall width of the scattered distribution and the g determines how quickly the distribution falls away.

This approach was used to create material models of all the isotropic and symmetric optical elements in our skylight systems: the reflective tube walls (both metal and foam core) and the reflective white boot. For these materials, the model fits the measured BxDF well for all angles of incidence. Figure 47 shows the LBNL measurements and Harvey-Shack representation for the highly specularly reflective materials used in the SunOptics box system. As expected this material exhibits highly specular behavior at all angles with the dominant exiting angle equal to the mirror direction for all incidence angles. The data does not indicate perfect specularly but a very small spread to the reflected light.

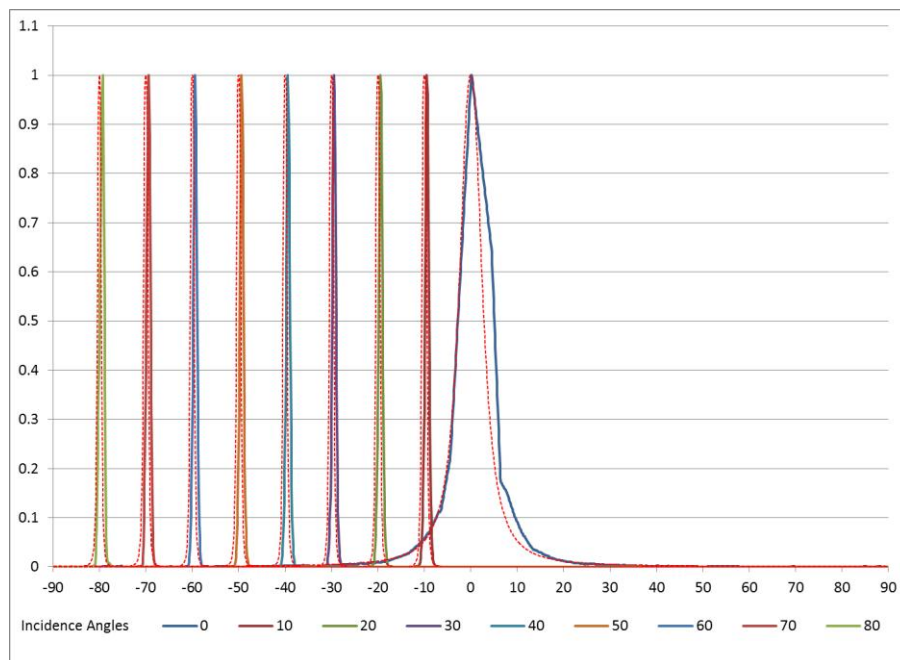


Figure 47: Sunoptics Reflector BRDF Measurements

Figure 48 and Figure 49 presents LBNL data for the reflective Suntunnel tube material and the reflective white transition boot material. Like the reflective SunOptics tube, the Suntunnel tube material exhibits high specularity at all angles. The white boot exhibits more of a diffused specularity with significant light spreading $\pm 10^\circ$ around the mirror ray.

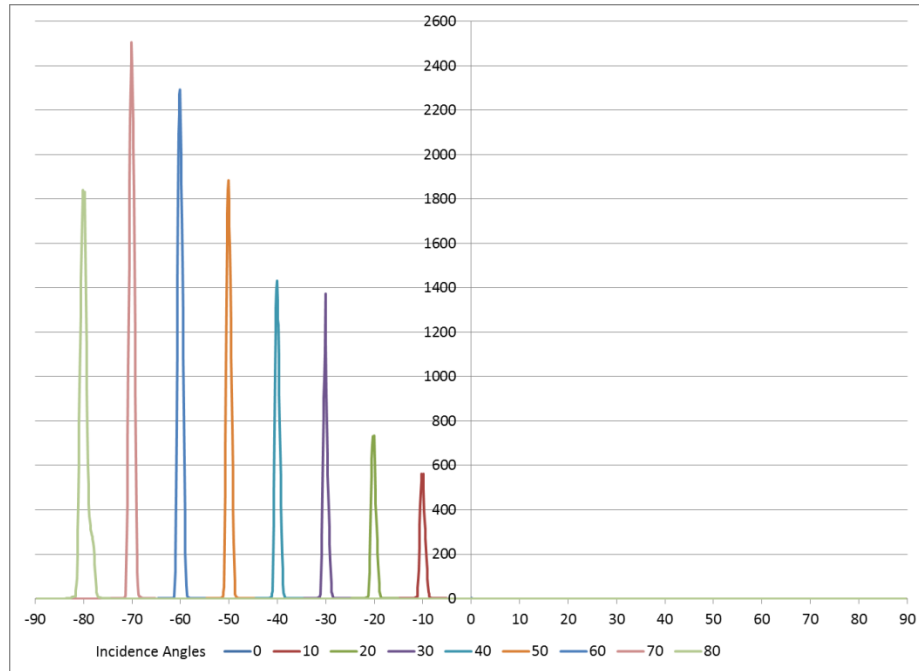


Figure 48: Suntunnel reflective tube wall reflectance by incidence angle

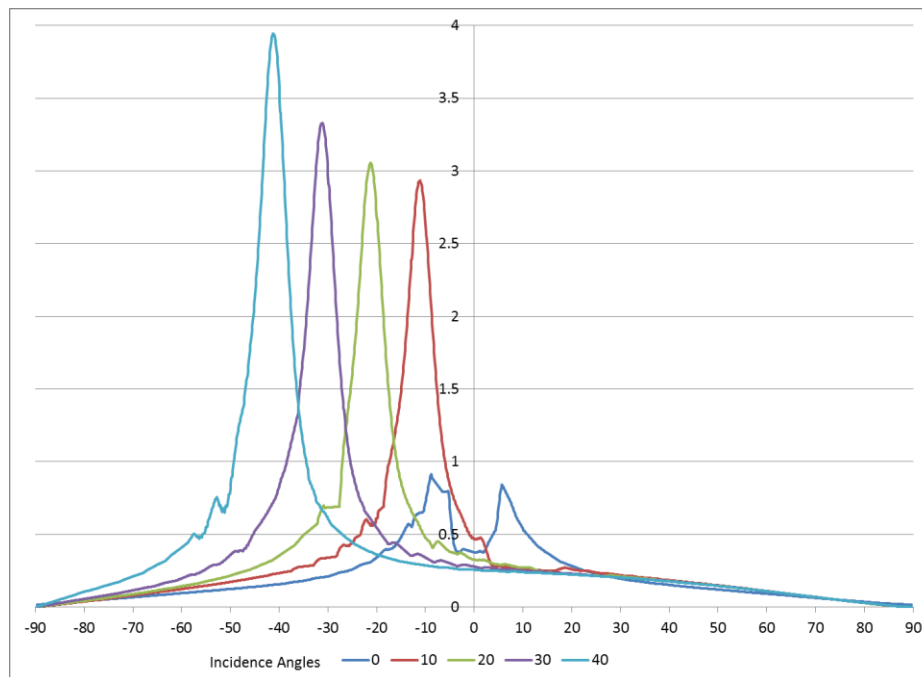


Figure 49: SunTunnel white boot reflectance by incidence angle

These mathematical representations however do not work well for the prismatic lenses. Figure 50 and Figure 51 show attempts to match a Harvey-Shack curve-fit with the measured data for the SunOptics prismatic lens. Each incident angle has a slightly different curve-fit with adjusted B and g parameters. Even with this, it can be seen that the curve-fits do not match the scatter data well for many of the conditions, particularly at the higher incident angles. Often the peaks and slopes can be closely matched, but the scatter around these specular directions is not matched well.

Additional comparisons of these LBNL isotropic measurements and the original LTI Optics averaged isotropic measurements are included in Appendix A. This data was not used in lieu of more accurate anisotropic data from simulation and additional measurements.

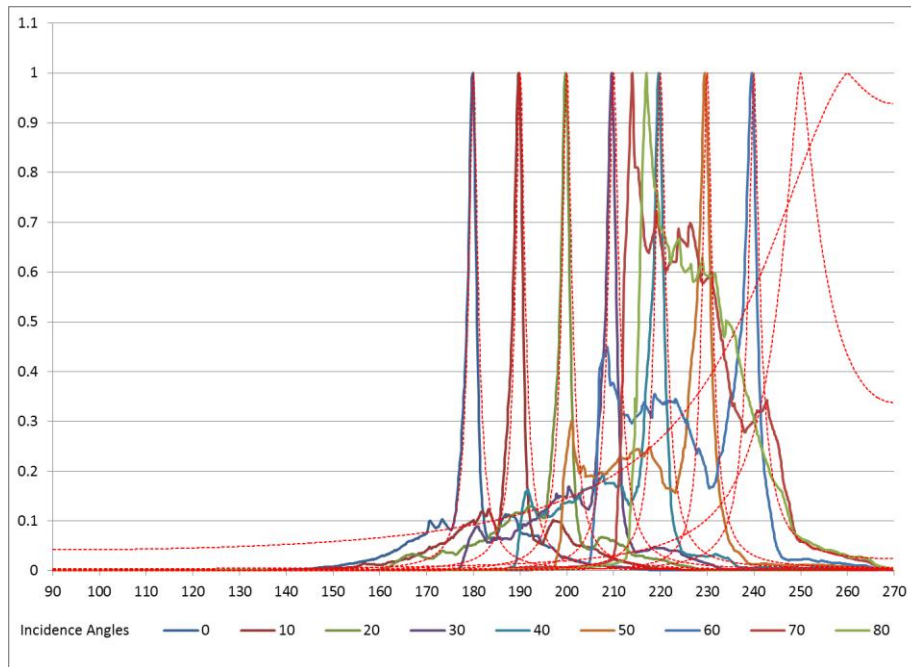


Figure 50: Flat side Harvey Shack transmittance curve-fits

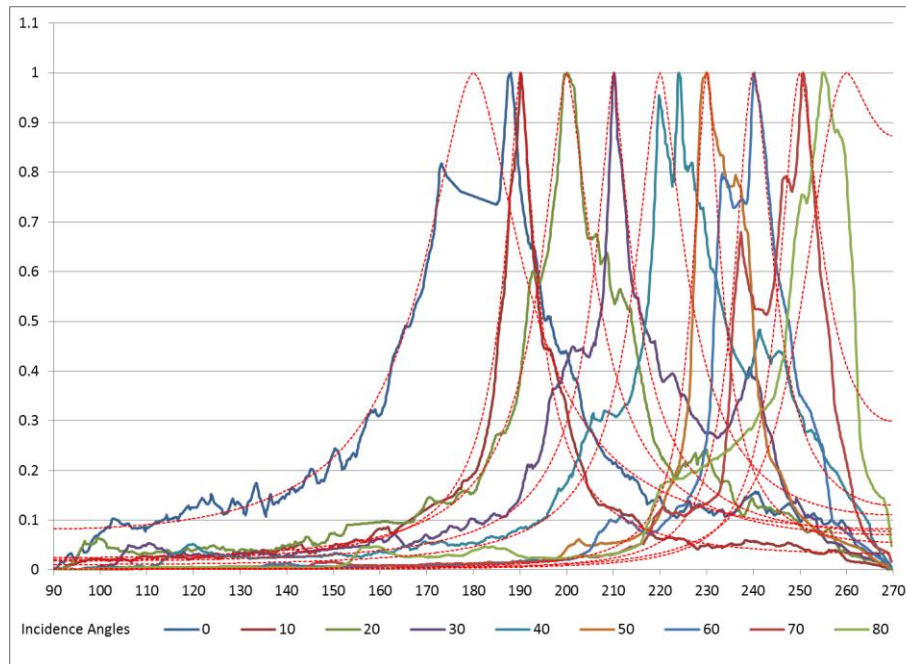


Figure 51: Prism side Harvey Shack transmittance curve-fits

Anisotropic and Asymmetric BSDF Representations

TracePro provides a Table BSDF definition for modeling asymmetric and anisotropic materials. This method requires absolute BSDF numbers and can best match measured data. These can be defined as isotropic or anisotropic and symmetric or now with either single or multiple incoming or outgoing angles. The angles cannot be random, like the raw data provided by the PGII goniophotometer, but need to be fit to an even grid of vertical and horizontal angles.

This lookup table BSDF representation can handle completely anisotropic and asymmetric behavior as well as symmetric materials that just don't conform to the Harvey-Shack mirror ray assumptions. The downside of this method is that it requires a time consuming process, using a separate spreadsheet program, to enter all the data into the interpolation format required, which uses the same $b-b_0$ term seen in the Harvey Shack curve-fits. The method also results in significantly longer simulation times. For example, a simulation of one of the skylight systems using the Harvey Shack curve-fits might took 3 minutes while a simulation using a complete BSDF interpolation table took nearly 2 hours: a 50x increase.

A script was written to convert the dense, but random, PGII goniophotometer data to this table format and definitions were created for both prismatic lenses. However, the data available was still isotropic and test simulations with these table BSDF definitions did not yield better results in many cases.

Physical Geometry Techniques

TracePro Expert includes a feature to model small, repeated optical geometry named "RepTile". RepTile is a module within TracePro that allows small repetitive optical structures to be modeled individually and then arrayed onto applied surfaces. This saves time during the development stage as it requires only a single optic to be modeled and saves time during

simulation as the optical performance is calculated analytically rather than through intersections with geometry.

However, there are limits to what can be modeled for each individual element. TracePro provides multiple options including rounded bumps/protrusions, Fresnel lens elements, and rounded pyramids to name a few. While this is a great method for modeling optically perfect elements, it is not able to take a non-perfect optical element, such as our scanned lens models, to then simulate the imperfections that occur during manufacturing. This is a good approach when the optical elements are well known and consistently manufactured.

Scatter Measurements and Anisotropic Curve-Fits

A common approach used in TracePro for obtaining BSDF scatter information is through the use of two common scatter measurement systems: a Complete Angle Scatter Instrument (CASI) or a ScatterScope3d system. The ScatterScope system works well for predictable scatter around the mirror/direct angles, those that can also be described well with the Harvey-Shack representation, but is limited to about a 40° angle around the mirror/direct beam. The CASI system can capture complete hemispherical transmittance and reflectance data for a given incident angle. The system requires incident angles to be adjusted manually making the generation of complete anisotropic measurements a more timely and expensive endeavor. Both systems use lasers rather than collimated light in their measurements. This appears to cause some inaccuracies for anisotropic materials with varying geometry, such as the prismatic lens, partly due to the small size of the laser and partly due to the polarized nature of the laser.

CASI measurements were performed for the SunOptics lens material for four (4) different vertical incident angles ($\theta_i = 0^\circ, 30^\circ, 45^\circ, \text{ and } 55^\circ$) and for three (3) different horizontal incident planes ($\phi_s = 0^\circ, 45^\circ, 90^\circ$) giving a total of 10 different angles of incident light. As discussed above, due to the optical symmetry of the prisms, the horizontal incoming angles can be mirrored to give a complete hemispherical description. The system was limited to a max of 55° for the vertical angles due to physical constraints with the sample.

The measurements were then processed by a TracePro BSDF converter utility to derive a TracePro material definition. It was reported that more data would be required to generate a complete anisotropic table definition. Hence, the data was matched up with an anisotropic Harvey-Shack BSDF representation for each incoming angle, see Figure 52. These representations match up fairly well for the perpendicular incident angles but are not able to represent the asymmetry due to the split beam behavior of the prismatic lenses, particularly at the higher incident angles.

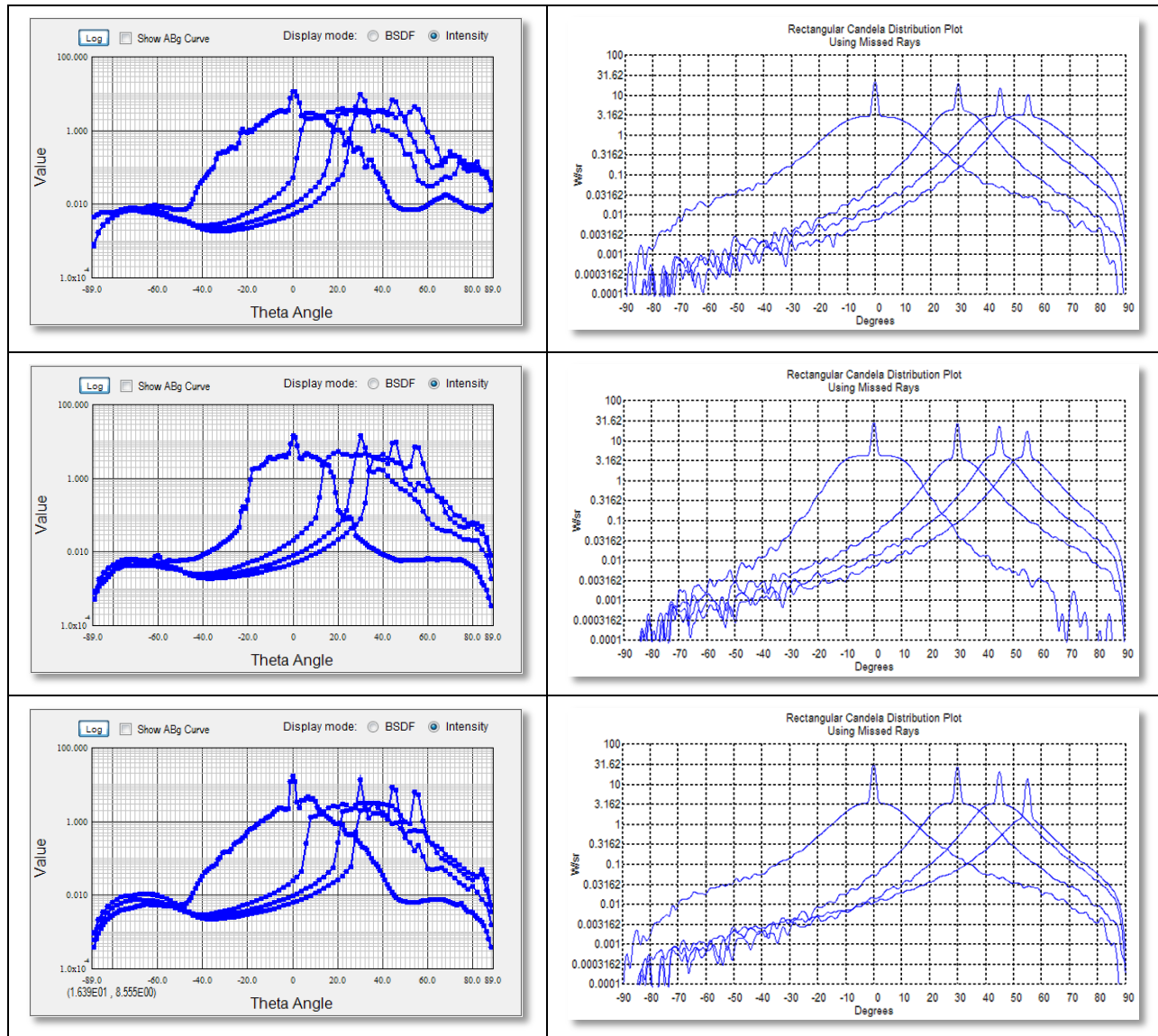


Figure 52: Scatter Works scatter measurements and TracePro ABg Curve Fits

TracePro Measurement Conclusions

For the SunOptics systems, the final TracePro simulations make use of the low-resolution but anisotropic data measured by Scatterworks and represented in TracePro with Harvey-Shack curve fits shown in the previous section. The original LBNL data and curve-fits were used for the Sun Tunnel system as complete scatter measurements of the Sun Tunnel lens were unavailable. All the reflective elements, including the metal highly specular reflective walls, and white boot were simulated using the accurate curve-fits created from the LBNL data. The foam core was modeled with a similar curve-fit derived from LTI optics measurements of a similar white foam core material.

Photopia BSDF Approach

The Photopia approach for creating and defining BSDF files is described in the following sections and includes: values stored and the coordinate system used; physical goniophotometer used to measure isotropic and symmetrical materials; simulation approach to generating these BSDF files using a newly added Material Lab tool; discussion of the validity of the resulting BSDF definitions.

Relative Luminous Intensity and Coordinates

LTI Optics records BSDF data in terms of relative luminous intensity distributions. For a given incident flux (lumens) for each incident light direction, the luminous intensity (lumens/steradian or candela) distribution of the light transmitting and/or reflecting off of the sample is measured. This data is then normalized. In this way, this initial data set accurately describes the distribution of light for the given sample but does not describe the magnitude which can often contain large errors due to missed peaks and valleys. The magnitude is determined separately by highly accurate hemispherical transmittance and reflectance measurements taken with an integrating sphere. This method ensures accurate tracking of all lumens in a simulation.

The data is in terms of a polar coordinate system centered on the mirror/direct ray to describe the direction of the scattered luminous intensity as illustrated in Figure 53. The mirror/direct ray defines $\theta_s = 0^\circ$ which goes to 180° in the opposite direction. This coordinate system is useful for many of our typical BSDF surfaces as it puts a higher density of points around the direction where most rays will tend to go. This is similar to the Harvey-Shack approach in TracePro that assumes a higher density and somewhat symmetrical spread of light around the mirror ray.

For these isotropic and symmetric surfaces, measurements are performed for a “side” hemisphere, $\phi_s = 0^\circ$ to 180° , which encompasses all angles on one side of the incident ray/mirror ray plane. This hemisphere can then be mirrored for symmetric materials to give a full reflected/transmitted relative distribution of light.

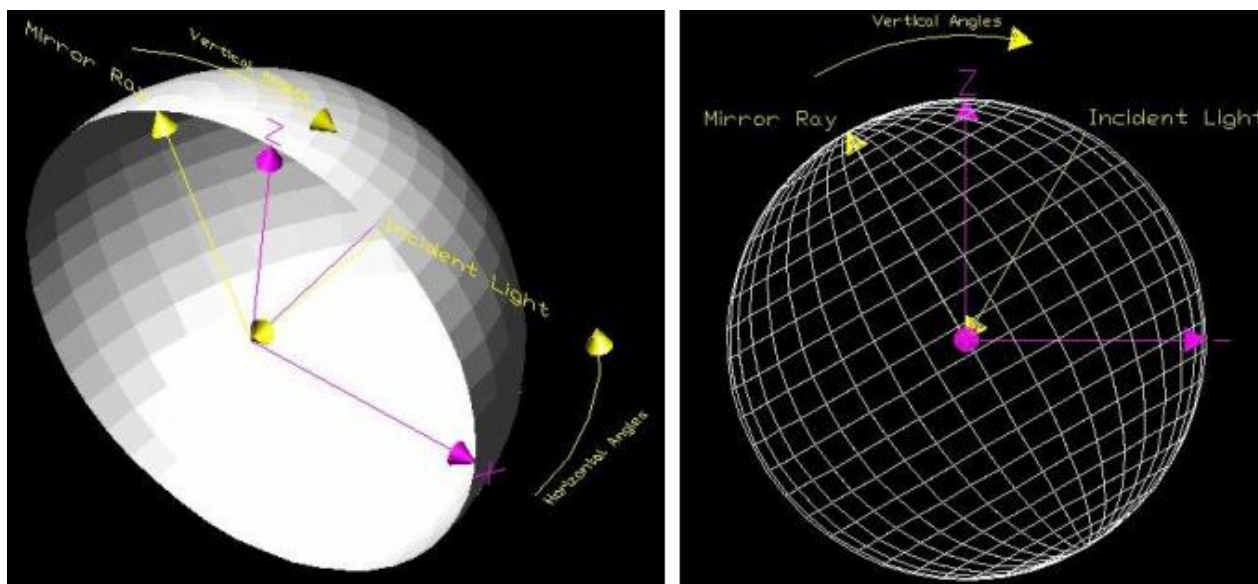


Figure 53: Definition of LTI Optics Relative Photometric Distribution Coordinate System

Goniophotometer Measurements

LTI Optics employs a goniophotometer system that can measure isotropic or anisotropic symmetrical distributions see Figure 54. [13] Isotropic measurements are automated with the lightsource and detectors moving through each set measurement position. For anisotropic materials, different ϕ_i angles are measured by manually rotating the sample. This system measures a side hemisphere of scattered light, as discussed above, which assumes a symmetrical distribution around this ϕ_i plane. A full distribution measurement is possible by requires more manual manipulation of the sample.

The measurement resolution is coarser than the LBNL data with outgoing angles of every 3-4° and incoming rays at 22.5° ϕ increments and 5° θ increments. The coarseness results in a higher risk of missing specific peaks and valleys in the data. However, this leads to distribution errors only as an integrating sphere hemispherical transmittance and/or reflectance measurement is used along with the relative luminous intensity distributions ensures all lumens are accounted for.

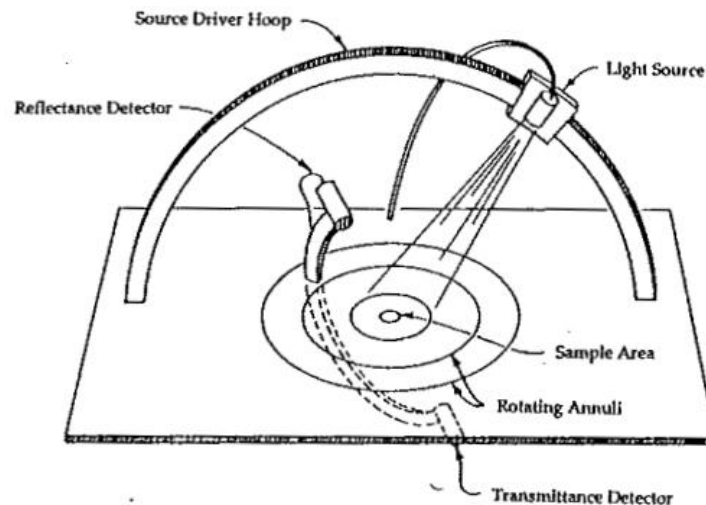


Figure 54: Diagram of LTI Optics goniophotometer

Isotropic material definitions are often created for these anisotropic materials by averaging the two most different distributions for the range of ϕ_i measured. In the case of the diamond prism materials, the most different distributions are for a plane aligned with the base of one of the diamonds and a plane aligned with a diagonal of the diamonds, see Figure 31. The base plane in this case will have errors as it does not align with the planes of symmetry, hence, the outgoing scatter will be asymmetric and not accurately captured.

This approach of averaging anisotropic data to create a single isotropic definition makes a lot of sense for lensed lighting fixtures but may not make sense for skylight system where the performance is largely driven by the direction and intensity of the nearly parallel rays from the solar disc. Parallel rays, or a specific incoming direction of light, being the key difference between the two applications.

Consider a 2'x2' lensed troffer luminaire. Depending on manufacturing procedures, there is no guarantee that the "diamonds" in these prismatic lenses will be aligned with one edge of the fixture or another or even some angle in between. Even if its manufactured one way, there is no guarantee it will be installed the same. Hence, modeling the system with an anisotropic lens definition may or may not result in an accurate representation of the installed fixture. An isotropic definition would give a good average prediction of the light distribution.

Additionally, in a lensed troffer, there are often several fluorescent tubes and a backing white or aluminum reflector providing all the light onto the lens. Hence, the light is coming from many incidence angles, with similar intensity from all directions. Hence, averaging the photometric data to come up with a single averaged distribution for all incident angles is often sufficient to describe the behavior for a typical luminaire. It may not accurately predict all stray light patterns on the fringes, but it will give a good estimate of the average distribution coming out of the fixture, exactly what is needed for the industry.

Photopia Material Lab tool

The goniophotometer does not provide a high enough incident or exitant angular resolution to adequately characterize the scattering properties of the Sun Optics and Velux lens prismatic

materials. In order to generate high enough resolution and fully anisotropic BSDF data for these lens materials, LTI Optics produced a software tool as part of their Material Lab tool to simulate the light scattering properties through 3D CAD models of the materials, similar to genBSDF in Radiance. The tool allows the resolution of both the incident and exitant angles to be specified independently and to be as dense as the computer system will allow (eventually limited by the computer memory).

The CAD models were generated using the same 3D laser scan measurements as Radiance, see Figure 55 through Figure 57. In the case of photopia, these models do not need to be solids but can be a series of faces or surfaces. Care needs to be taken to ensure the model is truly enclosed and that rays don't enter one surface of the acrylic and leave the model without crossing an existing surface.

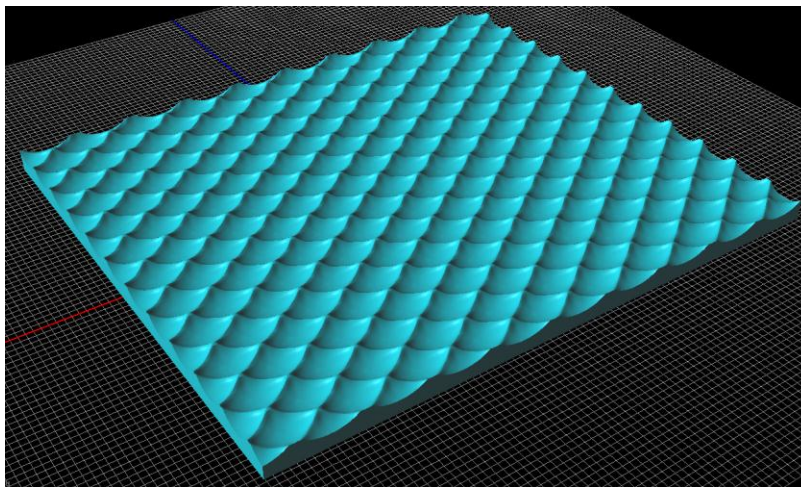


Figure 55: Sunoptics lens CAD model. - other side is flat.

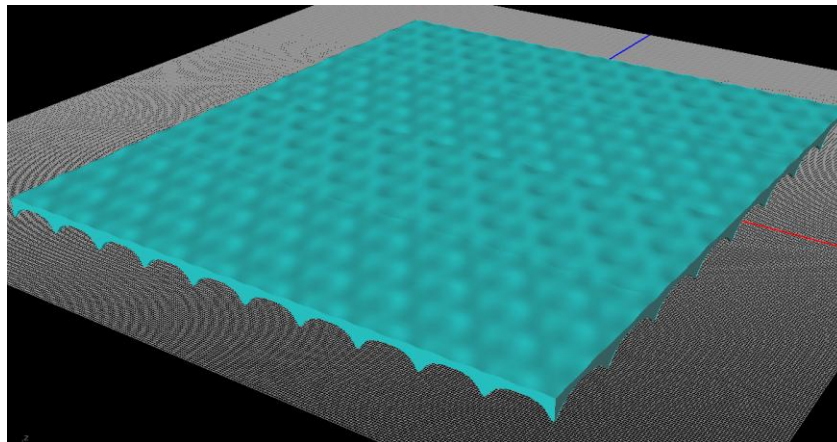


Figure 56: Sun Tunnel lens CAD model - "flat" side

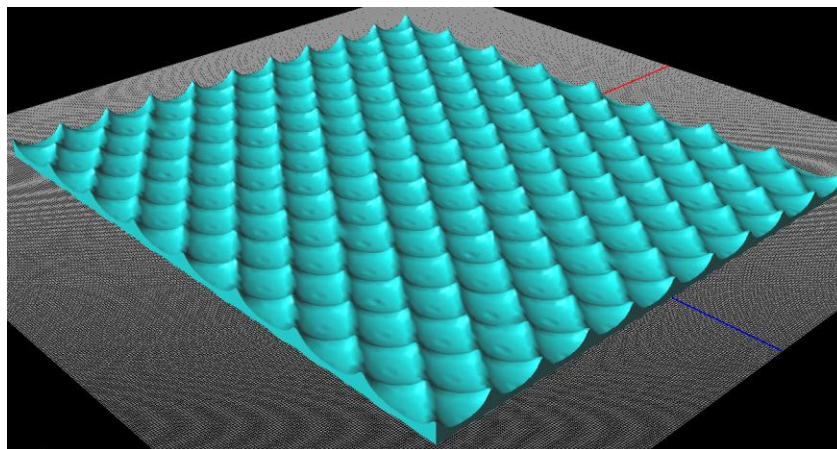


Figure 57: Sun Tunnel lens CAD model - prismatic side

Material Lab Simulation Results

Figure 58 illustrates some of the light scattering behavior of the Sun Optics lens and compares the simulations of the 3d model with a visual inspection of the actual sample. The resolution used for these BSDF definitions was every 15° horizontally and 5° vertically for incident light and every 10° horizontally and 2.5° vertically for exitant light.

The simulated image on the left shows the light pattern of scattered light from a laser that is incident upon the material at a 45° incidence angle. The material is horizontal along the red axis shown in the image, with the flat side facing up. So the top part of the gray scale image shows the reflected light pattern. Since the material is smooth on top, you see a fairly concentrated reflected light pattern. There is some scatter around that spot due to light reflecting off of the prisms on the underside of the material. The light pattern in the lower half shows how the prisms refract the light coming through the material. You can see how the pattern is odd shaped and not simply a central peak with a tapered distribution around it. With this it is clear that it is not possible to accurately model such scattering distributions with the symmetrical equation driven representations, such as the Harvey-Shack model.

The center simulated image shows the light scattering properties from a flat surface to which the simulated BSDF data was assigned with the same laser incidence angle. The goal is for this distribution to closely match the distribution on the left. The lower the angular resolution of the BSDF data, the more you would expect the image of this light scattering distribution to get blurred. As you can see, the details of the distribution are represented quite well so the data resolution looks to be sufficient.

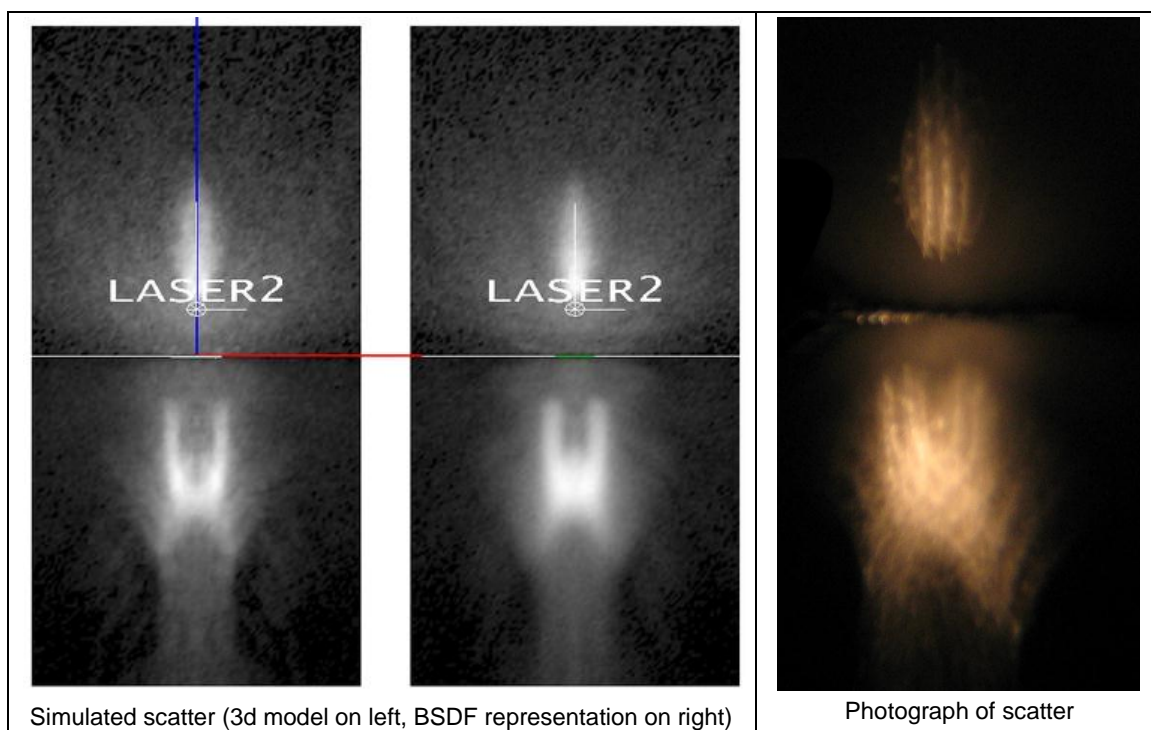


Figure 58: Light scattering patterns from the Sun Optics prismatic lens material.

As another check, the photograph on the right was taken by directing a collimated beam of light through the physical sample of Sun Optics material from a 45° incidence angle just like in the simulations. The size of the spot relative to the size of the prisms was not the same however. The physical spot illuminated much fewer individual prisms, which is why you can see their individual artifacts in the light pattern. Overall however, you can see the same general trends in the light scattering distribution, thus confirming that the simulated BxDF data should be appropriate.

BxDF Measurement Conclusions

All the reflective elements in the skylight systems, the specularly reflective walls of the light-cube and SunTunnel tube and white reflective SunTunnel boot, exhibit highly isotropic and symmetric behavior with no noticeable difference for different directions of incident light. The isotropic planar measurements received from LBNL appear to accurately capture their reflection characteristics and were used directly or to calibrate the model of these materials for all the simulation approaches.

For the anisotropic and asymmetric SunOptics and SunTunnel lens materials, the BxDF approach best suited to the simulation program was used as discussed in the sections above.

It is important to note that even with highly detailed BxDF measurements of real samples and/or simulations of geometrically measured real samples, there is still much manufacturing and installation variability to daylighting systems to be considered. Accurately simulating this variability is exacerbated by the fact that the main source of light on a daylighting system is the very intense solar disc providing nearly parallel beams. Direct sunlight striking a BxDF

material is completely different than light from a diffuse electric light troffer in that it is striking it at a single, very specific incidence angle. If that incidence angle is not measured well there is the potential for large interpolation errors, magnified because of the extremely intense single direction source. Under a cloudy sky where daylight is coming, more or less, from all angles, a detailed BSDF is not as critical and an averaged isotropic definition, as discussed in the Photopia goniophotometer section, could suffice just as it does for electric lighting. However, when direct sunlight is involved it is unlikely specific patterns will be predictable with averaged isotropic BSDF data.

Additional variability and simulation complexity is introduced in forming prismatic skylight “domes”. These are formed by taking a flat sheet of diamond prisms and forming them to the skylight shape. There is no guarantee that this flat sheet is oriented in a specific direction when the dome is formed. Optical complexity is created by the fact that these known and uniform diamond shapes have now been stretched and compressed to create the final three-dimensional dome shape. Consider the standard Signature series domes from SunOptics; they are essentially barrel vaults with ribs across the length, see Figure 59. The diamond shaped prisms will be distorted one way or another on all facets of this final dome and will not exhibit the optical behavior that a flat prism sheet would. BSDF measurements would likely be taken only of a flat sample, as there are numerous technical difficulties in measuring large, curved, three-dimensional samples of this kind.

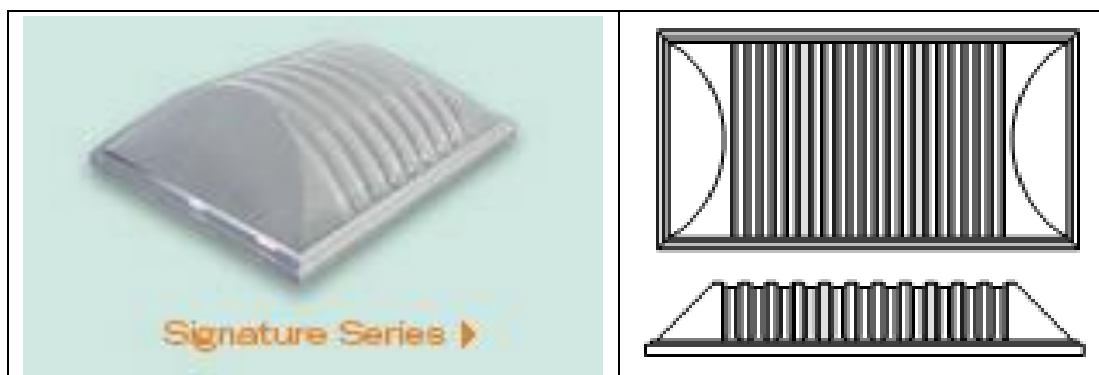


Figure 59: SunOptics Signature Series Barrel Vault Skylight

This page deliberately left blank

CHAPTER 7: Simulation Setup

This section describes the various simulation processes and settings used in creating photometric results using the calibrated sky models and BSDF measurements. The process used in TracePro is discussed first followed by the process used for Radiance and the process used in Photopia.

TracePro

The following sections describe the simulation models created in TracePro and the simulation settings used to generate the system photometry predictions.

Geometry Representation

TracePro expects elements to be modeled as 3d solids and does not allow overlapping solids, essentially requiring the model to be a physically valid model. This helps ensure the validity of the simulation results by ensuring all components are physically feasible. However, it does allow for thin sheets to be inserted as elements and it allows for individual surfaces of solids to participate alone in a simulation. In this way, BSDF material definitions that represent a complex optics of a solid element, such as the prismatic lenses in our systems, can be applied to a single surface in the TracePro model.

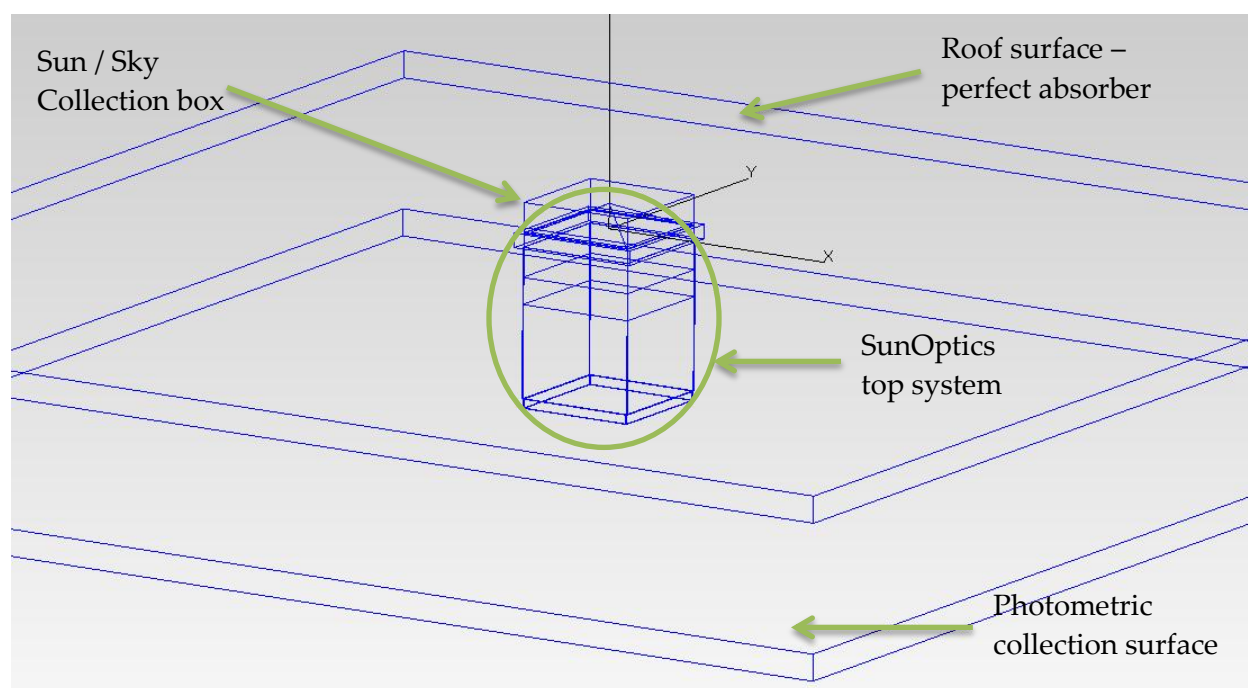


Figure 60: TracePro Sunoptics Top Model

Figure 60 shows an isometric of the SunOptics model in TracePro. The sun/sky source collection box is seen at the top of the model as discussed in Chapter 5. The system geometry starts directly below this. A roof surface is modeled as a perfect absorber to block any stray

sun/sky rays from directly passing through. A plane sitting directly below the exit opening of the system is used to collect all system photometric information. As it captures the angle of every exiting ray, this plane captures nearly all the exiting light and treats it as an absolute far-field measurement. As the near-field and far-field comparisons in Chapter 5 did not show significant differences, these far-field measurements were used for all TracePro simulations.

Raytracing Settings

TracePro has a number of parameters that adjust the overall speed and accuracy of the simulation. A brief impact study of the following parameters was performed to determine satisfactory settings to use for skylight simulations;

- No ray spawning versus ray spawning of 1, 2, 3, and 4
- Minimum flux thresholds
- Total number of initial rays traced
- Importance sampling

Ray-spawning

Ray spawning is the concept of splitting rays at each surface intersection in a forward ray-tracing simulation. When a given ray strikes a surface, rather than purely using probability to determine the direction of that reflected/transmitted ray, ray spawning allows the ray to be split via the same probabilities into two or more “child” rays, each containing accordingly less flux than the incident ray. This technique can help increase the density of rays further into an optical system. However, it can be misleading in that it does not increase the initial sampling from the source and can just exacerbate errors from a poorly sampled source. Depending on the nature of the optical system being simulated, it may or may not improve the speed and accuracy of the simulation.

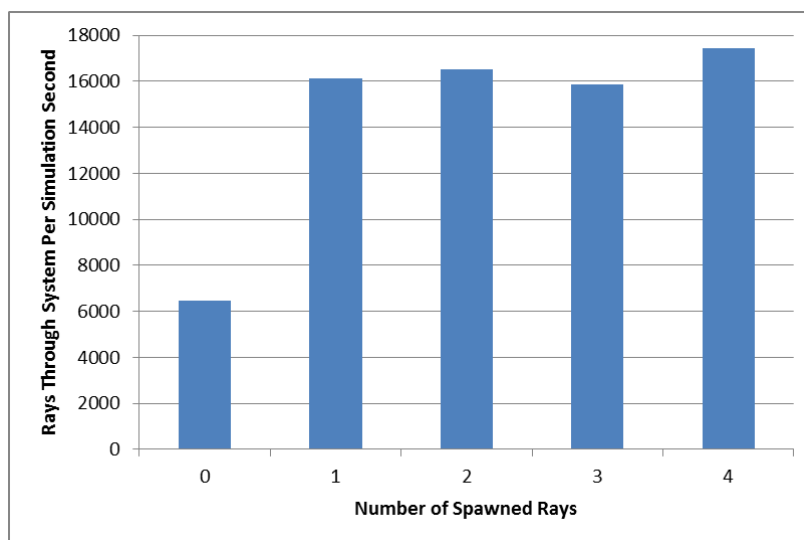


Figure 61: Plot showing performance relative to the number of spawned rays

Figure 61 shows a quick comparison between no ray spawning and spawning either 1, 2, 3, or 4 rays per surface intersection for a similar optical daylight system. The plot shows the number of rays that make it to the final surface of interest, in our case, the plane where we wish to capture luminous intensity data, per simulation time. This shows that beyond 1 additional ray spawn per surface there is little simulation speed benefit to additional ray spawns. If increased ray density is needed, then it is best to just increase the initial ray set rather than to set additional spawning. For all skylight system simulations, 1 ray spawn is used in TracePro.

Flux Thresholds

A similar quick comparison was performed to determine the minimum flux threshold setting which determines at what threshold should the system stop tracing a ray. The default is 0.001 or 0.1% of the initial ray value. Settings of 0.01% and 0.001% were explored and showed little impact on the final predictions with increased simulation time.

Limit Bounces

In addition to the flux thresholds, a limit can be set to the maximum number of bounces to simulate. The default setting of 20 was used for the simulation. Although a higher setting may be appropriate for these long tube reflectors that result in numerous reflections under low angled light.

Size of Ray Sets

Once the ray spawn settings (1 split) and flux thresholds (0.1%) were determined, the size of the initial ray set was explored. Chapter 5 discusses the creation of the sky source and size potential. Different sampling densities were explored that results in ray sets from 750,000 up to 20,000,000. The accuracy of luminous intensity calculations were explored with these different size ray sets and the results showed very little difference once the initial ray set exceeded 1.5 – 2 million rays. However, it is likely that the more optically complex and elaborate the system is the more initial rays would be necessary for adequate accuracy (minimal noise) in the simulation.

Importance Sampling

A final “Importance Sampling” setting was made in TracePro to further boost the number of rays reaching the final plane of interest. A 2’x2’ ‘target’ was placed at the bottom of the skylight systems and tagged as an importance sampling target. This tells TracePro to spawn more rays in this direction which it does while adjusting ray flux values to accurately account for the probability of rays heading in that direction.

Final Simulations

Using the raysets and settings discussed above, the TracePro simulations took between 5 minutes for the SunOptics Top system and a couple hours for the Sun Tunnel system using lookup table BSDF definitions. These were using a modern computer with 6 processor cores available. The candela plots were saved at a resolution of every 5° vertical and horizontal angles.

Near Field vs. Far Field Comparisons

When taking luminous intensity measurements it is important to measure the intensity far enough away from the source such that it acts as a point source for the given direction. Typically, a 5:1 rule is followed where the measurements are taken at least 5x the distance of the maximum dimension of the source. The physical luminous intensity measurements performed for the skylights are right around this 5:1 limit and hence represent more of a “near-field” photometry. The computer simulations have the ability to report absolute “far-field” photometry (measurements are taken at an infinite distance away) as well as near-field photometry.

To determine the difference between near and far-field, a comparison was done in TracePro. Sensors were created that matched the exact sensor locations in the field measurements, see Figure 62. The resulting luminous intensity predictions were quite close between the two methods as seen in Figure 63. The far field simulation results show a bit less spread and more of a peak, but overall the two methods provide fairly similar results indicating that the points were adequately away from the large source to be classified as far-field photometry. As far-field is the less time consuming method in TracePro, all TracePro results are provided in terms of far-field photometry.

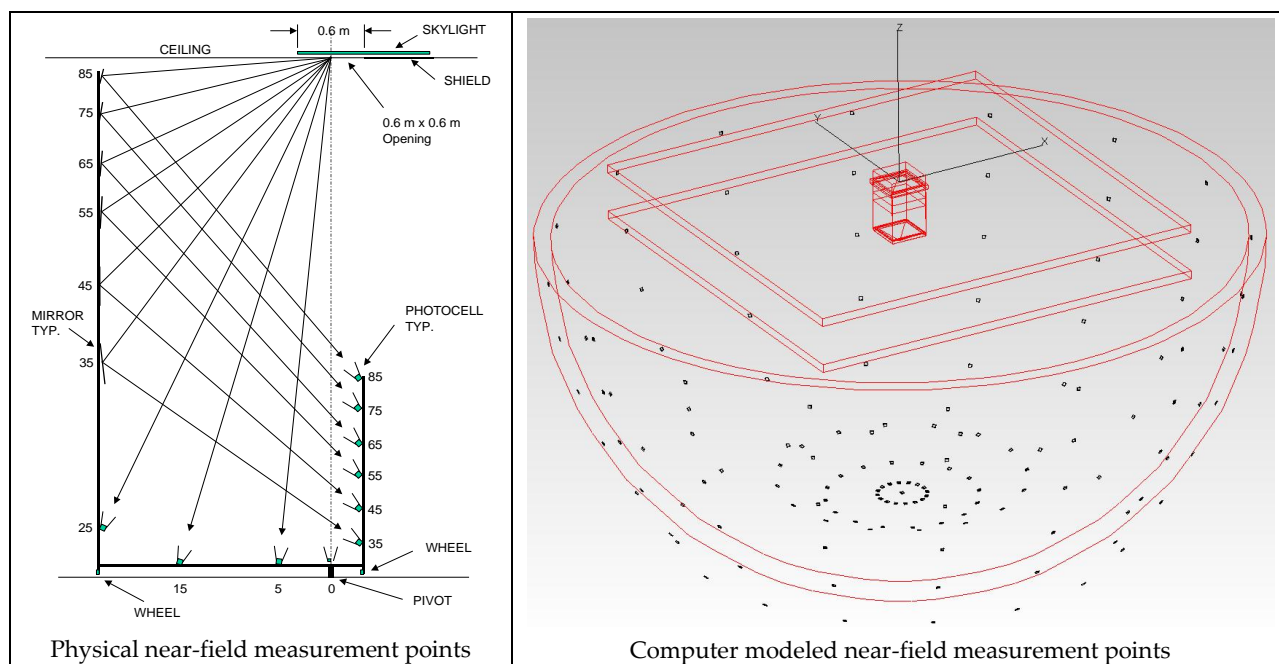


Figure 62: Section of physical measurement points and computer simulated near-field points

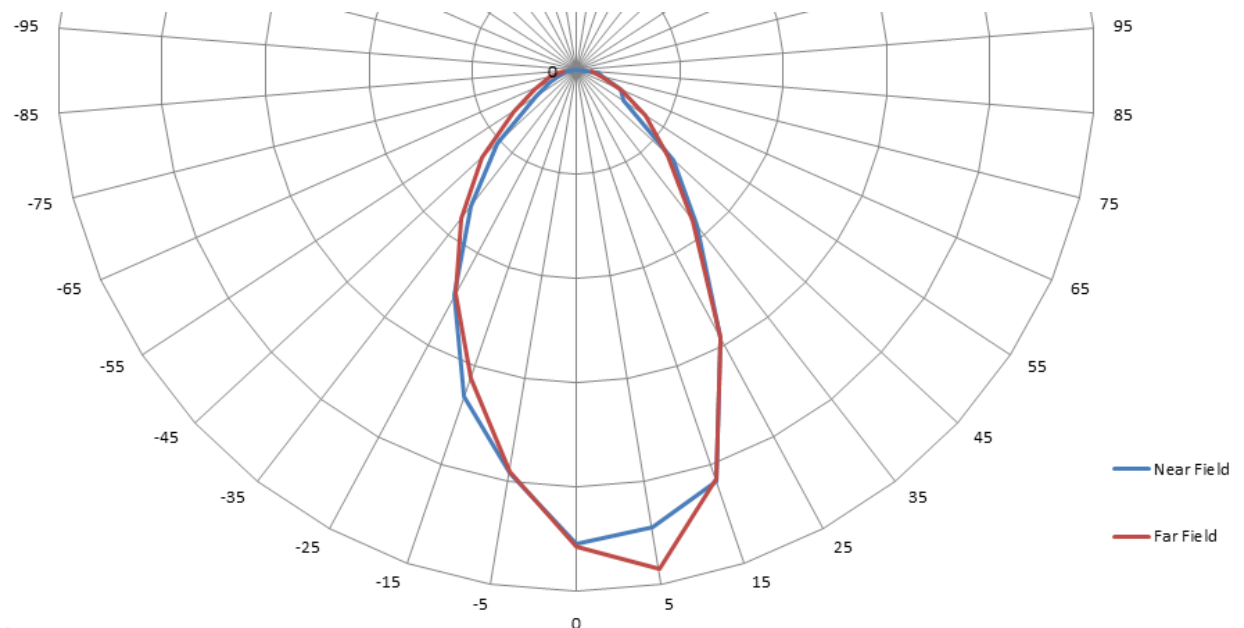


Figure 63: Near field vs. far field photometry comparison

Radiance

The following sections describe the geometric models used to simulate the various systems in Radiance, the different simulation methods explored, and the final method and Radiance settings used to generate system photometric estimates.

Geometry Representation

The Radiance geometry models of the three skylight systems are shown in Figure 64. The prismatic lenses in all models are represented by a single surface with the BSDF information applied. The acrylic dome of the Sun Tunnel system is modeled as a solid and the same interface material that was used for the prismatic lens was applied. Below this, triangular meshes represent the tube and converter boot geometry. This meshed tube and boot results in numerous inter-reflections and poses the greatest challenge for the Radiance simulations. The forward ray-tracers are more adept at these type of optical conditions but also need to ensure adequate bounces are simulated.

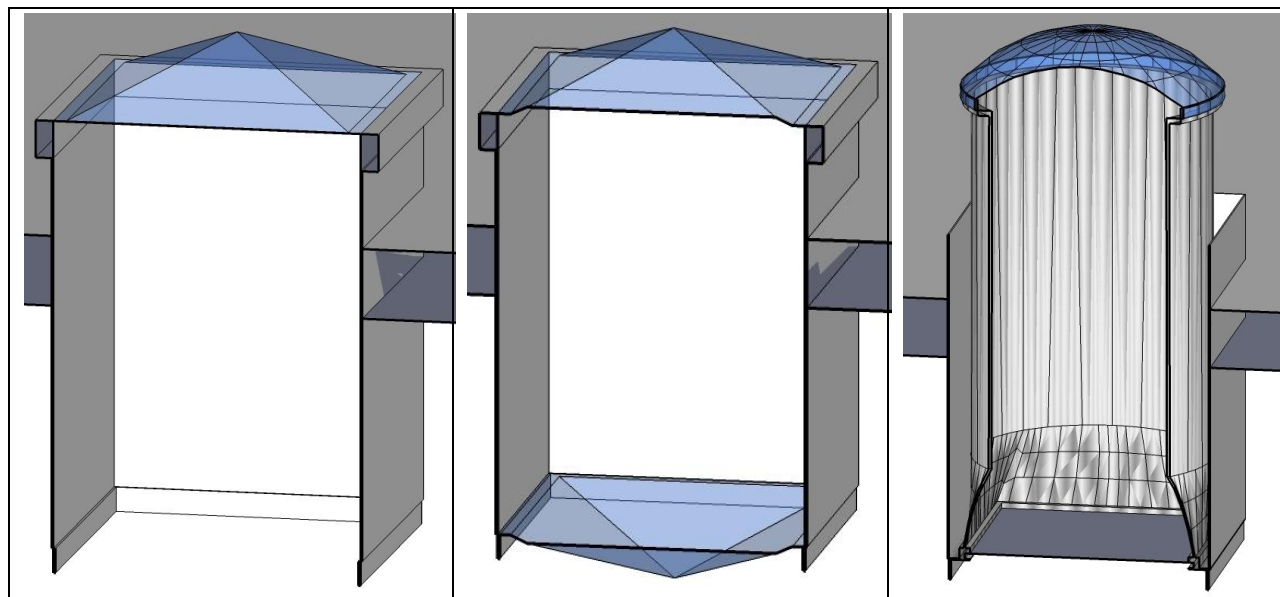


Figure 64: Radiance SunOptics and Sun Tunnel System Models

As a backward ray-tracer, Radiance is not as adept at determining source side distributions as a forward ray-tracer. To determine the photometric distributions, the Radiance model attempts to replicate the test facility by simulating the actual near field sensors locations in a dark room with a low reflectance walls, see Figure 65.

Near Field vs Far Field

There are at least two ways to determine the luminous intensity in the direction of each sensor. One approach is to calculate the illuminance at each sensor and convert to luminous intensity in the same manner as the physical measurements, refer to Figure 10. This near-field approach can then simulate the ambient light that occurs in the physical testing lab that is difficult for the forward ray-tracers. However, the ambient sampling has to be very high for these points to adequately sample the relatively small opening of the skylights, particularly for the points at a steeper angle where the lens has a small apparent area.

Another approach is to calculate the average luminance at each point in the direction of the light source, essentially recording far-field photometry. This requires sampling scattered over the entire exiting surface to obtain an average luminance. This method does not include any ambient lighting in the space and was not pursued further.

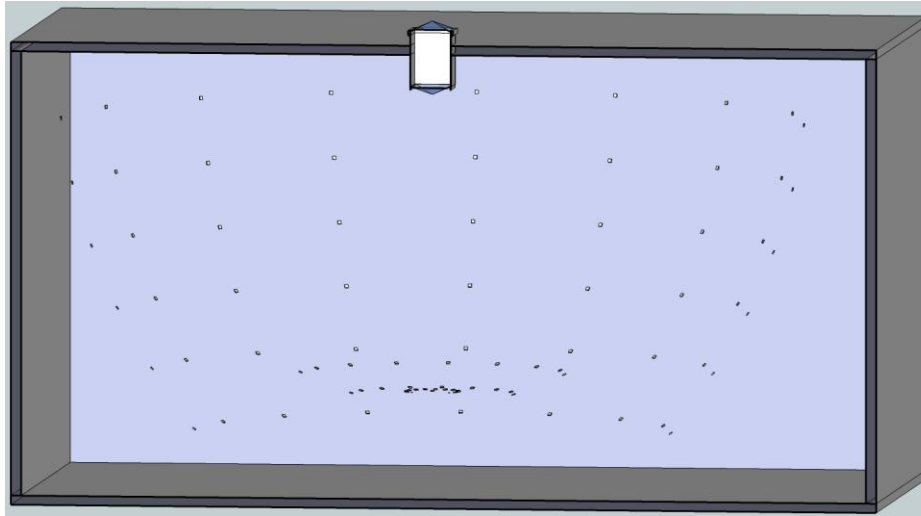


Figure 65: Near Field Sensor points used in Radiance Simulations

Simulation Options

In addition to the sensor locations and calculation method, there are a number of ways to approach this simulation in Radiance. The following sections discuss three different methods that were explored.

Radiance Classic

Straight forward Radiance calculations can be done by directly modeling all the elements seen in Figure 64 and Figure 65, applying the BSDF materials where appropriate, and simulating the illuminance at each point using “rtrace”⁴. Given the pre-calculation already performed for the complex prismatic lenses in the creation of their BSDF definitions, this is not an impossible approach. However, it is definitely challenged by the high ambient sampling required to obtain adequate sampling of the skylight opening itself, as well the multiple reflections that have to be considered to obtain accurate measurements at the higher exitance angles. However, in some cases, the simulations using this method best matched the measured data.

“Mkillum” strategies

The calculations could make use of the Radiance “mkillum” tool. This tool allows for larger, but still significant, sources of light to be used a light source, and therefore accessed in the direct calculation in Radiance. It is applied to surfaces that encompass the light source to be replaced. Windows or skylight openings are often good candidates for this treatment. In our case, the bottom opening of the skylight shaft would be the obvious opening to create an illum surface allowing for a much easier illuminance calculation inside the space. However, the new BSDF material already provides much of the benefit of an illum surface rendering this tool less effective. Additionally, the mkillum resolution standards are not very compatible with the BSDF files. Mkillum resolution can be adjusted using `-d` density parameter, but even with a `-d 1000` setting resulting in 3,140 output directions, this approach appeared to not be as accurate.

⁴ The Radiance module to trace rays in a scene

System BSDF approach

The same genBSDF tool that was used to create the prismatic lens BSDF definitions could be used to create a System BSDF file that describes the exiting scatter of light for each angle of incident light in the exact same manner as the typical BSDF files. The variable resolution Tensor-tree representation can even be used to capture sharper peaks of incoming influence or exiting light. This approach requires the greatest amount of pre-simulation, but results in the quickest end use simulations as all the multiple reflections and complex optics of the system have been taken out of the calculations.

Using this approach, the final simulation model changes slightly. Since the depth of the system no longer needs to be modeled, the model needs only include a single flat surface representing the opening of the skylight system enclosed within the roof of the space. While depth is no longer needed, simulation tools may want to consider allowing an offset between one side of a “BSDF” surface and the other side. This is a feature allowed in Radiance for the ambient calculations, but does not natively include the direct calculation.

The resulting scatter predicted using the system BSDF files are illustrated below using the standard Klems definition. Variable resolution tensor-tree representations were used in all the final simulations. For each system, the scattered distribution is shown for 4 different directions of incident light, 0°, 20°, 40° and 60° as illustrated in Figure 66.

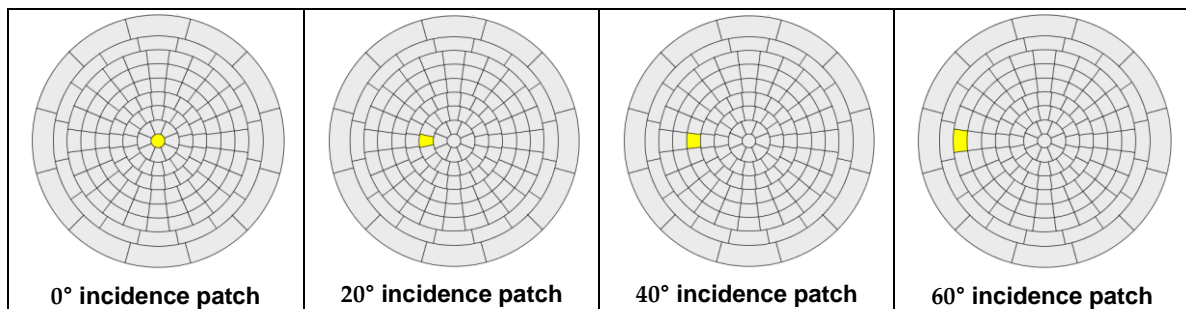


Figure 66: Incoming patches used to illustrate system scatter at different incidence angles

Figure 67 shows the scatter distribution simulated for the SunOptics Top system. There is a faint cross like distribution for perpendicular light, similar to the distribution of the top lens itself. At the higher incidence angles, the impact of the foam core walls becomes apparent. It shows a drastic reduction in overall transmittance, going from 82% transmittance at 0° incidence to just 49% transmittance at a 20° incidence angle. Also, a shift in the direction of the scattered light can be observed due to reflections off the foam core walls. At 40° incidence, the dominant lobe of light exiting the system is heading back in the towards the direction of the sun.

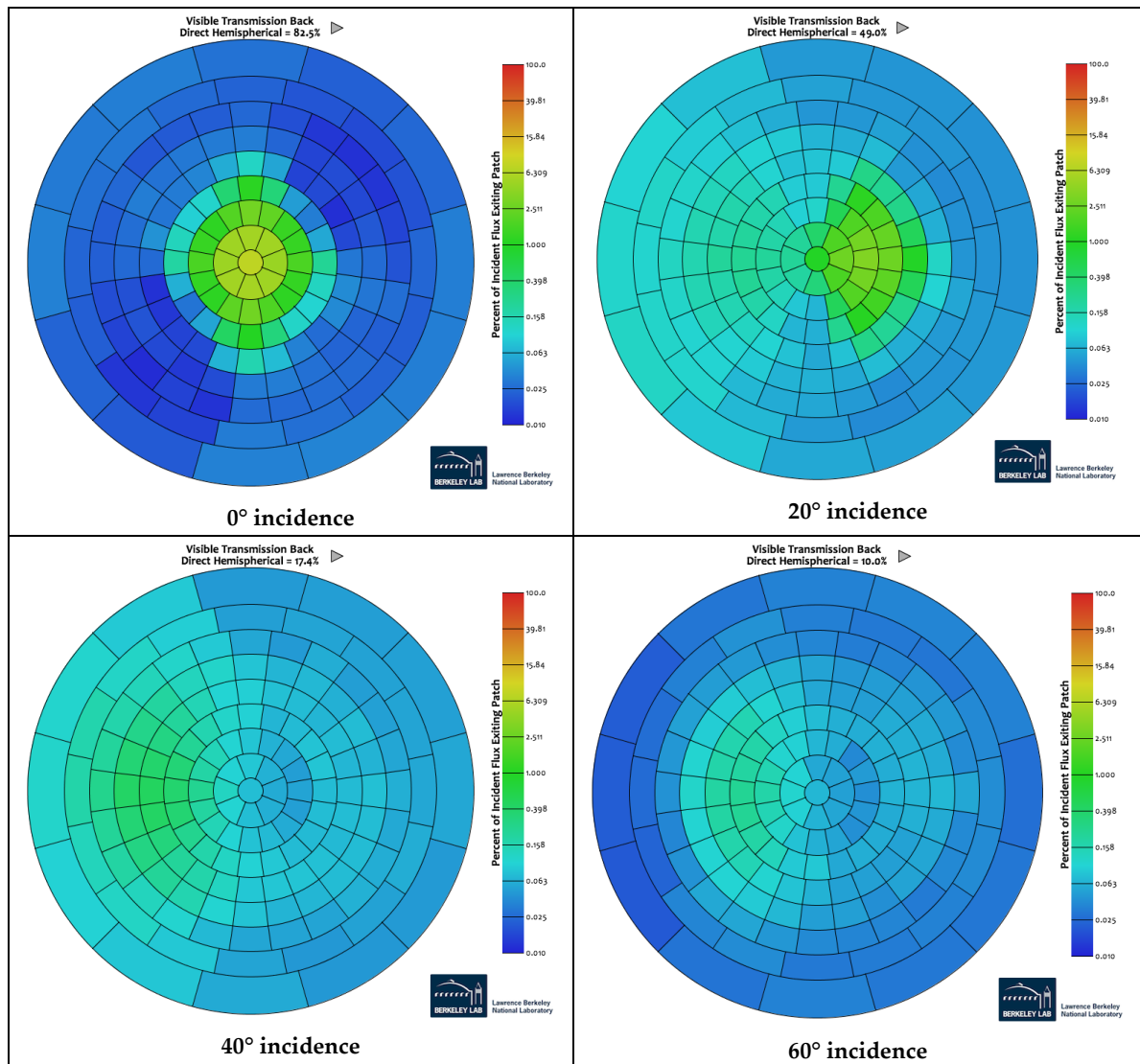


Figure 67: SunOptics Top System – Standard Klems BSDF distribution

Figure 68 shows the scatter distribution simulated for the SunOptics Box system. The perpendicular transmittance is logically lower than the top only system with 63.5% transmittance due to the two prismatic lenses in the system. Also, the transmittance does not drop off nearly as quickly due to the highly reflective and specular walls of the SunOptics box system. It only drops to 55.7% at a 20° incidence angle, already greater than the SunOptics top system.

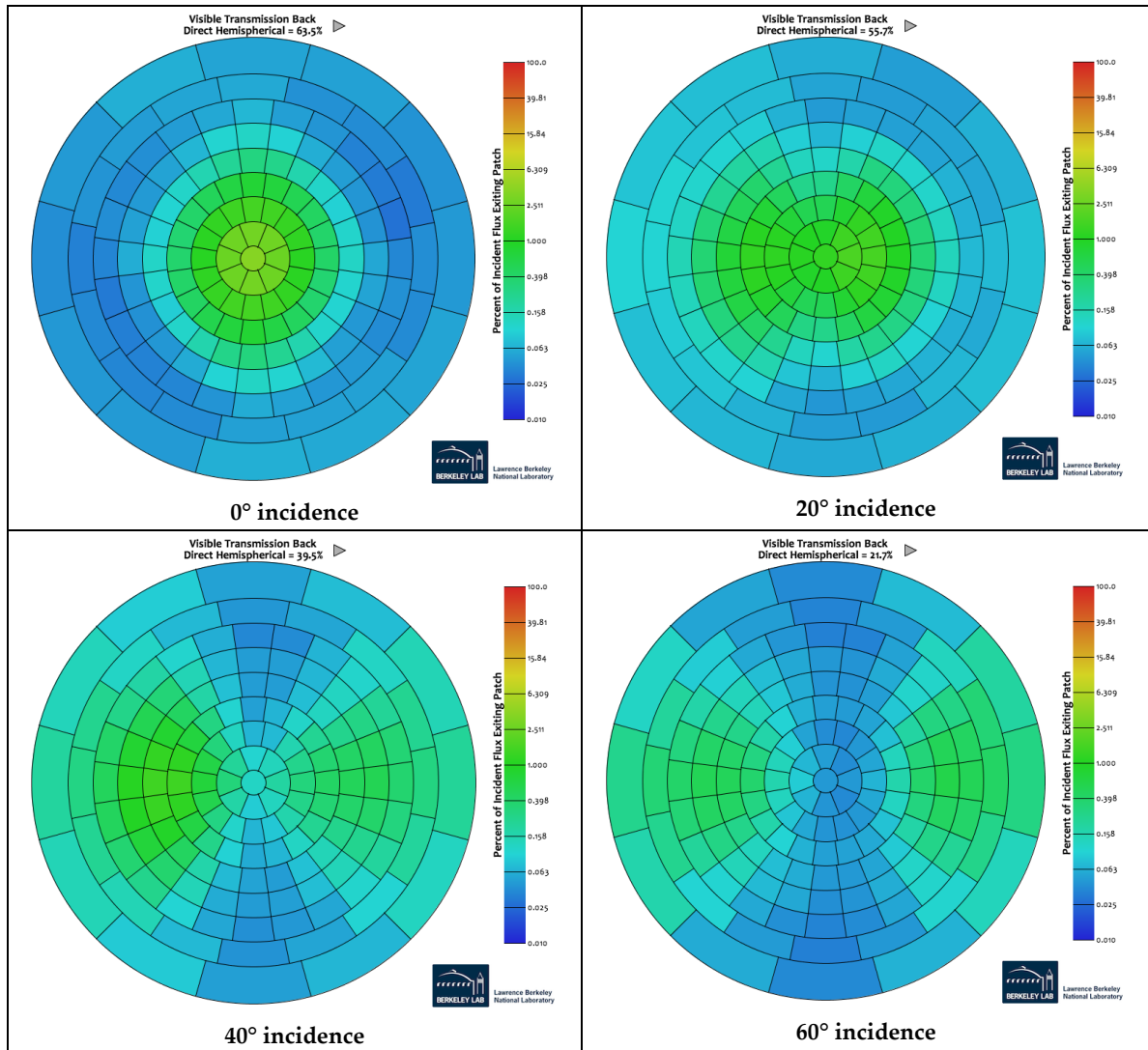


Figure 68: SunOptics Box System – Standard Klems BxDF distribution

Figure 69 shows the scatter distribution simulated for the Sun Tunnel system. This system shows a fairly symmetrical distribution for perpendicular light. At the higher angles, the exiting light shows scatter back towards the direction of the sun with some dual peaks apparent. Interestingly, at the higher incidence angles, a dark area starts to form in a crescent shape in the direction of the incident light.

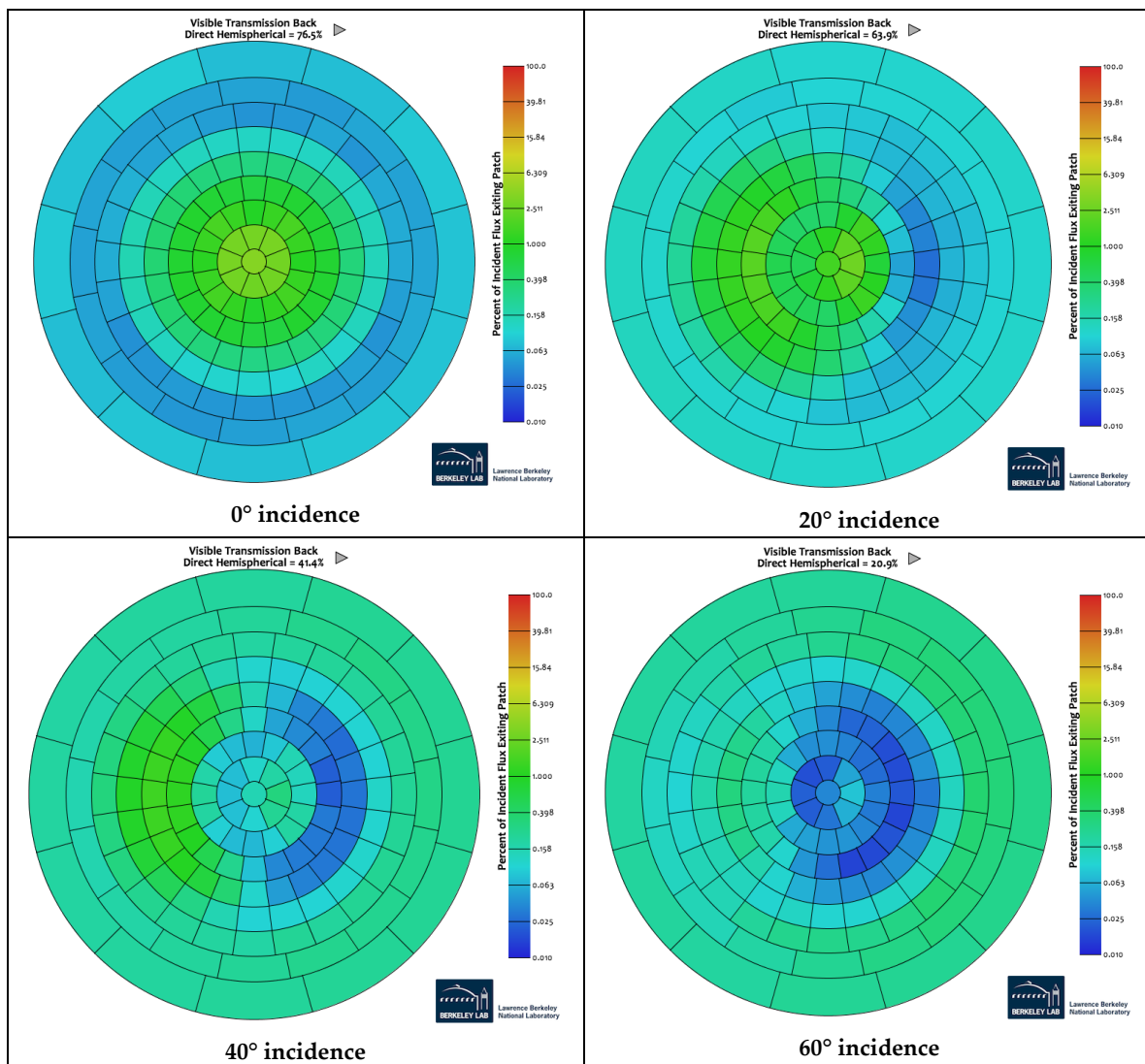


Figure 69: Sun Tunnel System – Standard Klems BSDF distribution

Final Radiance settings

The system BSDF simulation approach proved to be most accurate and efficient to simulate and was used to produce the final photometric calculations. In order to get an adequate ray sampling at each sensor point, extremely high sampling density parameters were required. The following Radiance parameters were used for the System genBSDF simulations and the final sensor illuminance calculations using the system BSDF as a material definition.

genBSDF parameters

- Direct: -dj 1, -ds 0.01 -dt 0.05 -dc 0.99 -dr 6
- Specular: -ss 100, -st .0001
- Indirect: -ab 5, -ar 128, -aa 0, -ad 1
- General: -lr 10, -lw 0.000001
- genBSDF: -c 3000, -t4 5

Illuminance calculation parameters

- Direct: -dj 1, -ds 0.01 -dt 0.05 -dc 0.95 -dr 4
- Specular: -ss 100, -st .00001
- Indirect: -ab 3, -ar 128, -aa 0, -ad 1024000 -as 128000
- General: -lr 6, -lw 0.00000001

Additional studies are warranted to determine the best parameters to use to give accurate results as efficiently as possible. In the genBSDF calculation, the direct relay (-dr), ambient bounces (-ab), and limit relay (-lr) parameters, in particular, may be too low and not letting the simulation accurately capture some of the high angle light that enters and leaves the systems. This is a bigger issue for the systems with highly specular, highly reflective and long shafts. For the illuminance calculations, a very high ambient density (-ad) was necessary to adequately sample the relatively small skylight opening. A high ray weight limit (-lw) was shown to help improve the prediction at the sharper output angles.

Photopia

The following sections describe the sky models and geometric models used to simulate the various systems in Photopia. The ray sets used and simulation settings are also discussed.

Sky Models

The Photopia daylight simulations can be done with standard sun and sky dome source models that come with the software or they can be done with ray sets that are generated independently, like those made for this project. The standard sun and sky dome models are based on the IESNA RP-21 daylight equations that model the absolute illuminance from the sun (solar disk) at various altitude angles and the sky for various sky conditions and solar altitude angles. The sky domes include variable luminance values across the hemisphere as described in RP-21. The sun models include a 0.53 deg. spread in their beam to model the actual angular size of the solar disk, averaged over its elliptical orbit. The combination of both the sun and sky dome models produces a total illuminance onto the daylighting device area that is intended to match real outdoor conditions.

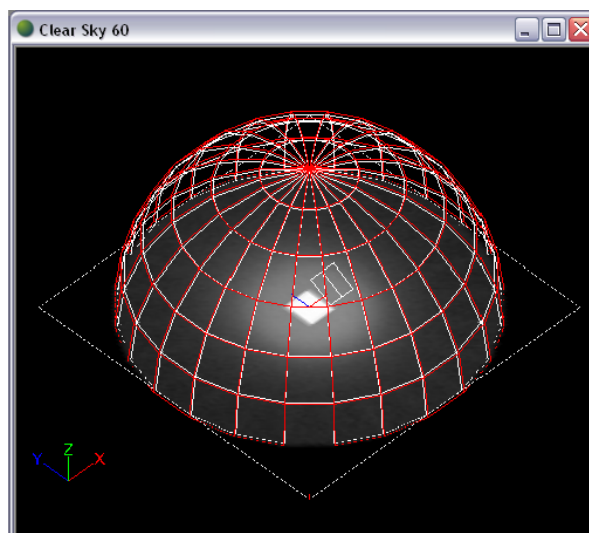


Figure 70: Standard Photopia Sky Dome Model

Figure 70 shows a standard Photopia sky dome model consisting of 144 patches on a hemisphere as well as a model for the sunlight. In this case, the sun model is square to match the shape of the skylight system entrance. Each patch in this sky dome model is assigned a unique luminance based on the solar altitude and sky condition using the sky luminance equations in RP-21.

Since actual daylight conditions can vary widely and the RP-21 equations represent average conditions, the ray set based models were used for this study as they were generated from measured sun and sky dome conditions at the time of the tests. Figure 71 shows the light field produced by the ray set models for Test 18. The image on the left shows the rays from the sky dome and the light pattern they produce onto the daylighting device. The image on the right shows the collimated rays from the sun model, which produces a sharply defined patch of light. Note that the rays in these images just illustrate the general ray directions as their length was limited to make it easier to view the light pattern. The actual rays extend through the illuminance planes.

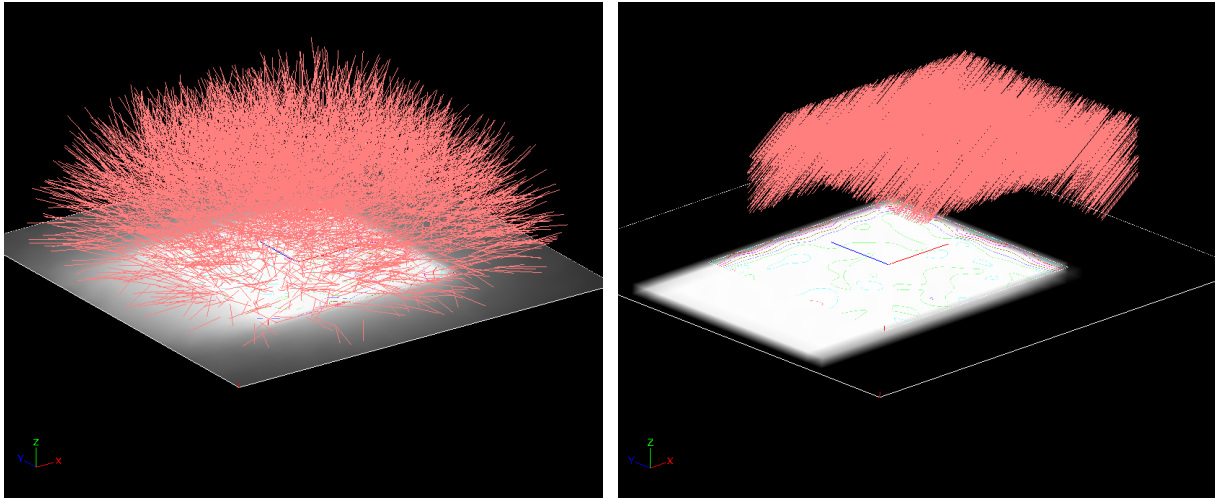


Figure 71: Sky dome and sun ray sets for Test 18

Geometry Representation

Figure 72 illustrates the SunOptics Box geometry as it was imported into Photopia. One modification that was made to the standard model used in the other simulations was the addition of some 1" radius fillets along the ridges of the pyramid. The real lens has rounded transitions between the triangular sections of the pyramid so the fillets were added to better match the physical part. Simulations done with and without the fillets did not change very much, so it was concluded that the fillets are not critical to the final results.

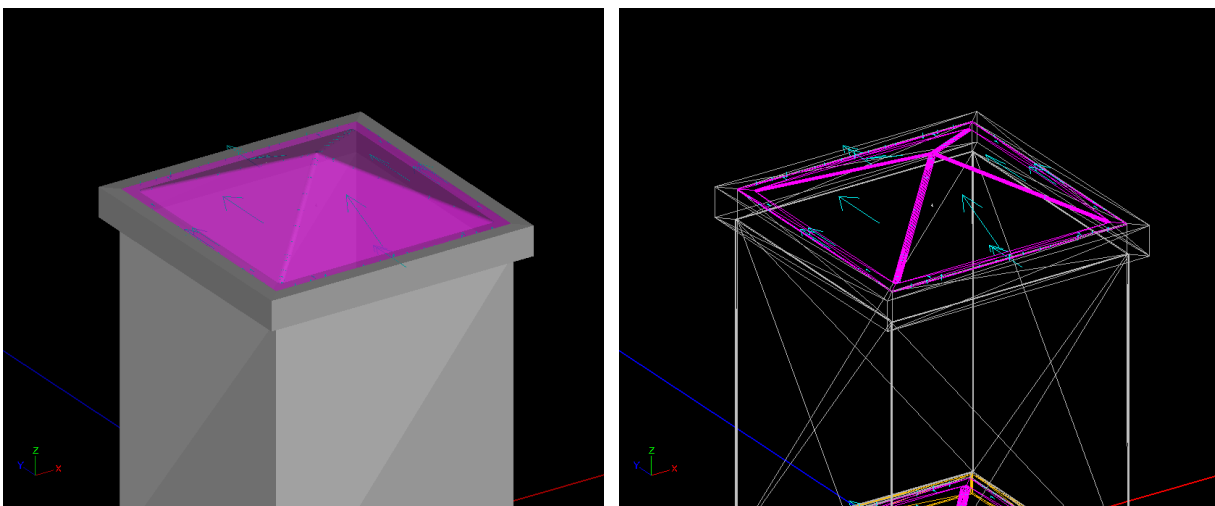


Figure 72: SunOptics Box CAD Model in Photopia

Figure 73a includes vertical and horizontal illuminance planes showing the light field created by the sky and sun ray sets as they illuminate the SunOptics Box pyramid. As seen in this image, since the ray sets were generated to illuminate a box encompassing the pyramid lens and acrylic dome, some rays do stray past the lens and thus need to be blocked so they aren't counted in the output of the device. Similar to the roof element in the other simulation tools, a

shield was constructed around the top pyramid and assigned a perfectly black material to absorb all of the stray rays that don't strike the pyramid as well as block all of the rays that reflect off of the pyramid. Figure 73b shows the shield drawn as the red mesh.

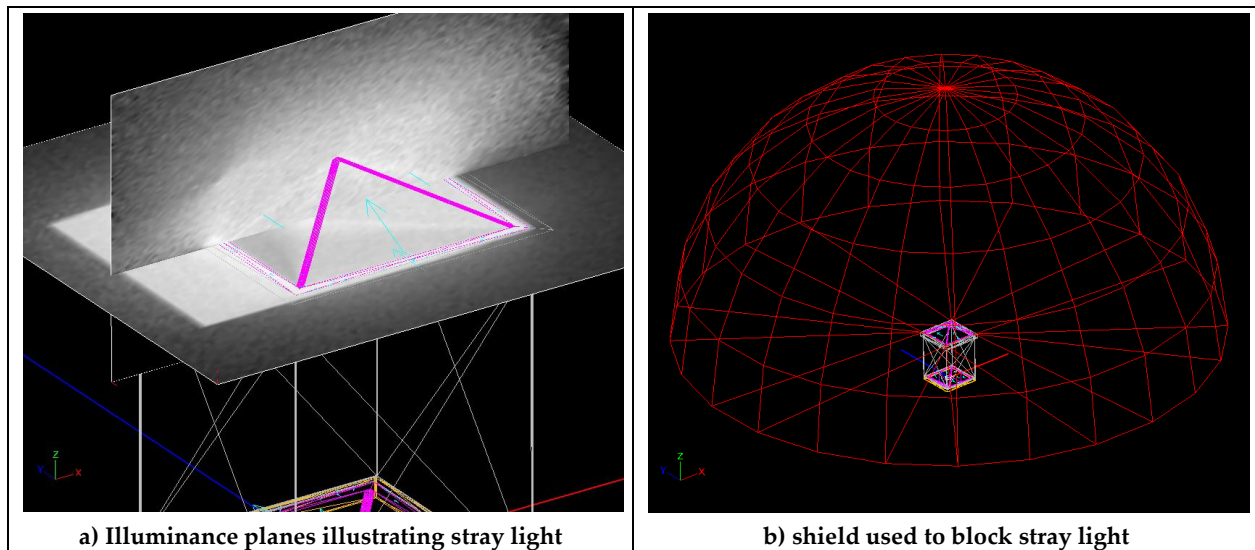


Figure 73: Vertical and horizontal illuminance planes

Ray Sets and Raytracing Settings

As an example of how many of the rays from the ray set actually enter the daylighting device, in Test 18, which had a solar altitude of 31.3° , 54.7% of the light was absorbed by the shield. This includes rays that were reflected off of the outside of the pyramid back upward. Overall this illustrates the importance of using large amount of rays in the ray sets in order to get enough rays through the optical system to create satisfactory results.

In Photopia, ray splitting is a less efficient method for generating more rays versus simply increasing the initial amount of rays in the ray set. For the final simulations, larger ray sets were created and used with the following ray counts:

- 2,268,992 sky rays
- 3,553,271 sun rays

This number of rays produced adequately smooth results for the candela distributions as can be seen in Figure 74. The general trend in ray-tracing software is the more rays you trace, the more accurate your results. When simulations don't have enough rays, candela plots are less smooth, wavier and illuminance planes look more speckled. So while this amount of rays was adequate to produce a smooth candela distribution, it is marginally enough to produce a smooth illuminance pattern on a plane below the device, see Figure 75. This is because the illuminance planes contain a lot more detail, thus requiring even more rays to resolve. Figure 75 shows a shaded illuminance plot for a 40' x 40' floor plane, 8' below the device. The shaded image on the plane would look smoother with more rays, but is still enough to see the general shape of the light pattern. This is an example of a task-side application that backwards ray-tracers are

more adept at simulating since they start the ray tracing from the specific illuminance points in question.

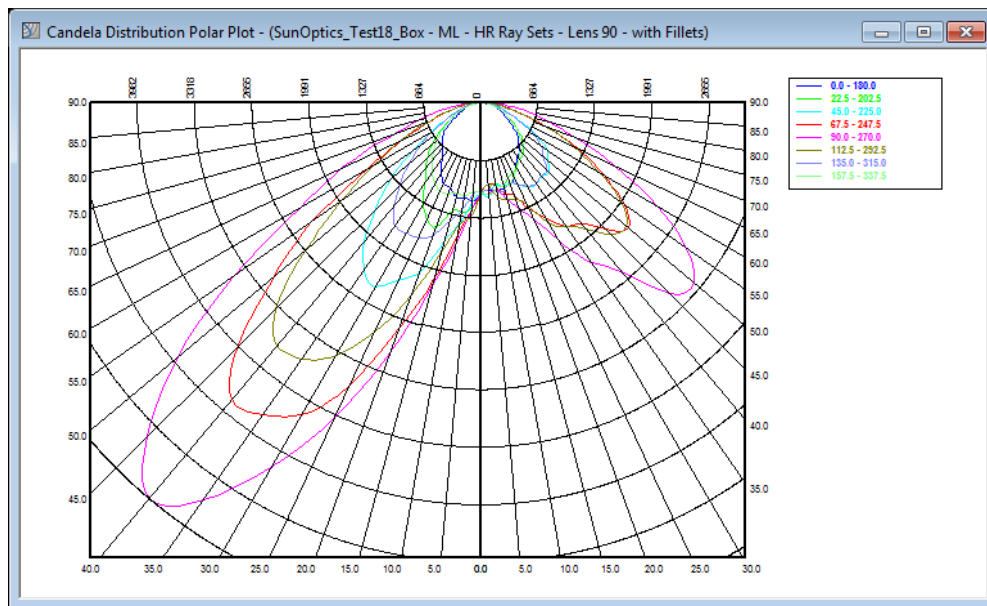


Figure 74: Polar candela plot for the Sunoptics Box Test 18

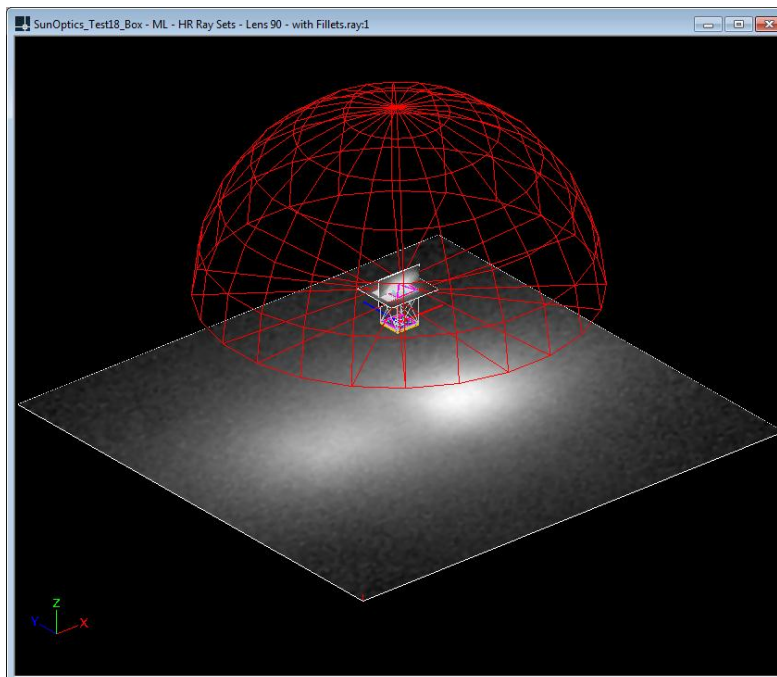


Figure 75: Simulated illuminance on a plane below the skylight

As a reference, the following candela plot shows the distribution produced using Photopia’s standard RP-21 based sun and sky dome models using sky patches illustrated in Figure 70. The overall trends in the distribution are quite similar, with the main differences being the ray set models based on actual conditions showing more light in the center of the distribution. The

amount of light around the center of the beam is largely determined by the ratio of the sky illuminance to the solar illuminance, so that differs in the RP-21 equations from these actual conditions. The angles at which the peak intensities on either side of the beam center are also higher by about 5° when the standard models were used. This distribution was created using 100,000,000 rays, however since Photopia's sun and sky dome models emits light onto a larger area than the input pyramid of this device, 93% of those rays were absorbed in the shield. So this means that about 7,000,000 rays were traced through the device.

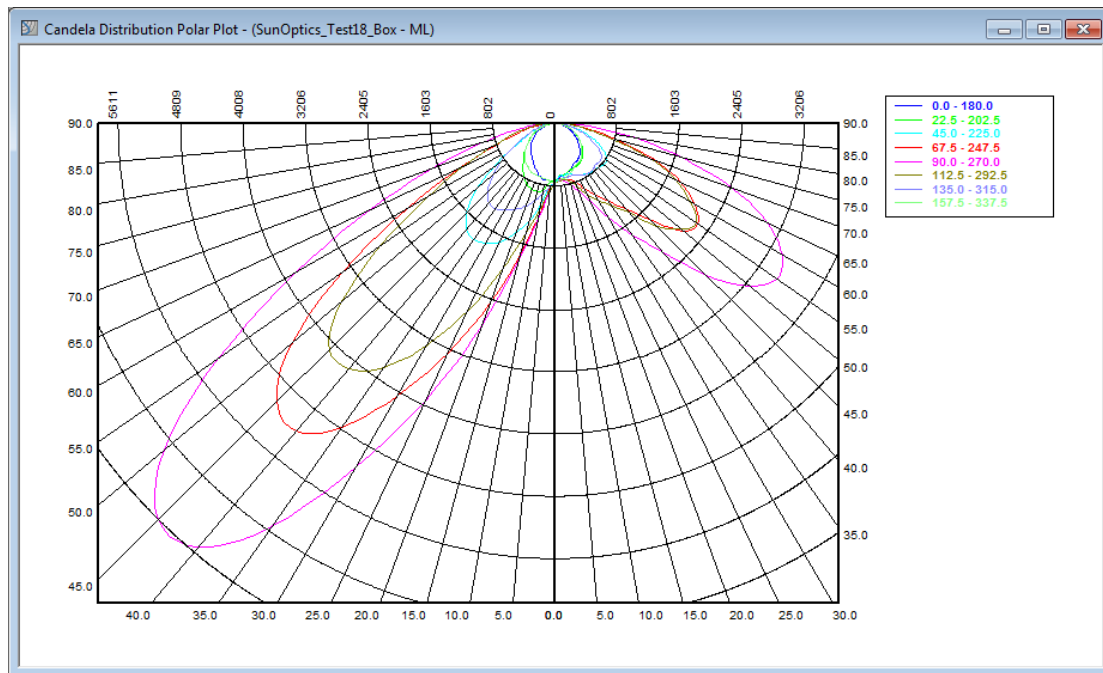


Figure 76: Polar candela plot for Test 18 using standard RP-21 sun and sky models

Due to the potential for a lot of inter-reflected light down the shafts of these devices, 50 ray reactions were specified for the simulations. This means that the light can reflect or refract up to 50 times before the ray is dropped from the results. It was found that after 50 ray reactions, only a fraction of a percent of light was left in the device, so the results were representative of the full output of the device. This is quite a bit higher than the relay limits specified in Radiance (12) and TracePro (20).

The daylight simulations in Photopia are setup so that the major axis of the horizontal angles of the candela distribution are in line with the north-south and east-west directions. In particular, the 0° horizontal angle is aligned with due north, 90° is due west, 180° is due south and 270° is due east, as illustrated in Figure 77. Horizontal angle sets of 0° to 360° in 22.5° increments were used to fully represent the asymmetric output of these devices as the sun was incident from a wide range of azimuthal angles.

This page deliberately left blank

CHAPTER 8: Simulation Results

The final results are presented in the following sections comparing the field measured photometric plots with several simulated photometric plots. The following simulation results are included:

- TracePro simulations using the anisotropic Harvey Shack representations of the scatter data measured by the Scatter Works and processed by TracePro staff.
- Photopia simulations using the simulated anisotropic BSDF definitions generated from the 3d laser scan models of the lens and using Photopia’s Material Lab tool.
- Radiance simulations using the simulated anisotropic BSDF definitions generated from the 3d laser scan and using the genBSDF tool. Additionally, the System BSDF approach was used.

The Sunoptics Top Lens measurements and simulated results, the Sunoptics Lightbox results, and the Sun Tunnel results are shown below. For each skylight system, results are shown for a partly cloudy sky, a low-angle sun, a mid-angle sun, and a high-angle sun.

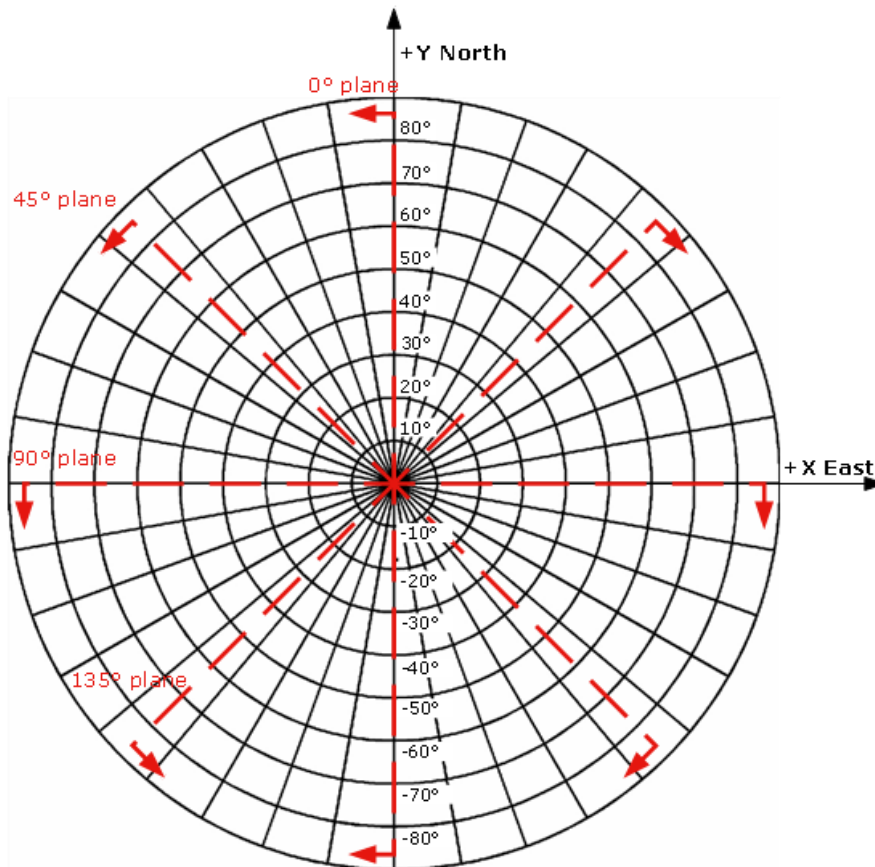


Figure 77: Photometric Coordinate System

All the photometric charts are plotted according the coordinate system shown in Figure 77. This matches the measured results and those natively reported by Photopia and TracePro. Nadir defines $\theta = 0^\circ$ and +Y or north defines $\phi = 0^\circ$. ϕ then proceeds in a right-hand rule direction. While 22.5° ϕ angle increments were measured and simulated, only the 4 planes indicated at 45° increments are plotted for easier visual comparison. Additionally, only θ angles of $0^\circ, 5^\circ, 15^\circ, 25^\circ, 35^\circ, 45^\circ, 55^\circ, 65^\circ, 75^\circ$ and 85° are included in the plots to match the exact angles that were measured. Both TracePro and Photopia will natively provide results for every 5° increment. Note that the sky images included are looking upwards with north at the top.

SunOptics Top Lens

The SunOptics Top Lens only setup represents the simplest optical system measured, basically containing the prismatic top lens, and semi-specular white foam core walls. The foam core walls may represent the biggest unknown in this system as the original foam core was never measured. LTI Optics provided BRDF measurements of a similar white foam core measurement that was matched in TracePro and Radiance.

Figure 78 shows the results for test 11: a high sun angle and partly cloudy sky. All simulation approaches match up fairly well with the measured photometrics. All show a peak candela angle at -15° from Nadir, however the Photopia and TracePro results show this peak in the 90° plane while the others show it in the 135° plane. In reality and considering the angle of the sun, the peak is right in between very near a 115° plane. The Trace and Photopia results also show a smaller contribution in the 0° and 45° planes. Increasing the sky component and decreasing the solar component improves the match indicating that perhaps the modeled sun and sky source had too low of a sky component.

Figure 79 shows the results for test 15: a low sun angle. The measurement data for this test appears to have an error at the nadir point. Ignoring this spike, all the results vaguely match the shape: a wide distribution with broad peaks at 35° and -45° . However, they all seem to mirror the measured data with the peak on the opposite side. Lower sun angles require many more specular bounces to be simulated and it appears that all approaches lose some accuracy under these conditions.

Figure 80 shows the results for test 25: a mid sun angle. These results show a fairly direct transmission of daylight with the peak candela at a 25° from Nadir in the 90° plane: nearly opposite of the position for the sun. All simulation approaches show this similar peak angle and similar intensities in the other planes. The exception is that both TracePro and Photopia predict a small counter peak in the surrounding 45° and 135° planes. It appears that something may be amiss with either the simulated source or surface but it is not clear where an increase in diffusion or specularity would improve the match.

Figure 81 shows the results for test 28: a high sun angle. These also show a fairly direct transmission of daylight with a strong peak at 15° from Nadir. All simulations match fairly well with a similar relative intensity to all four planes of data. They all indicate a 15° peak angle in the 45° plane and the least flux in the 135° plane.

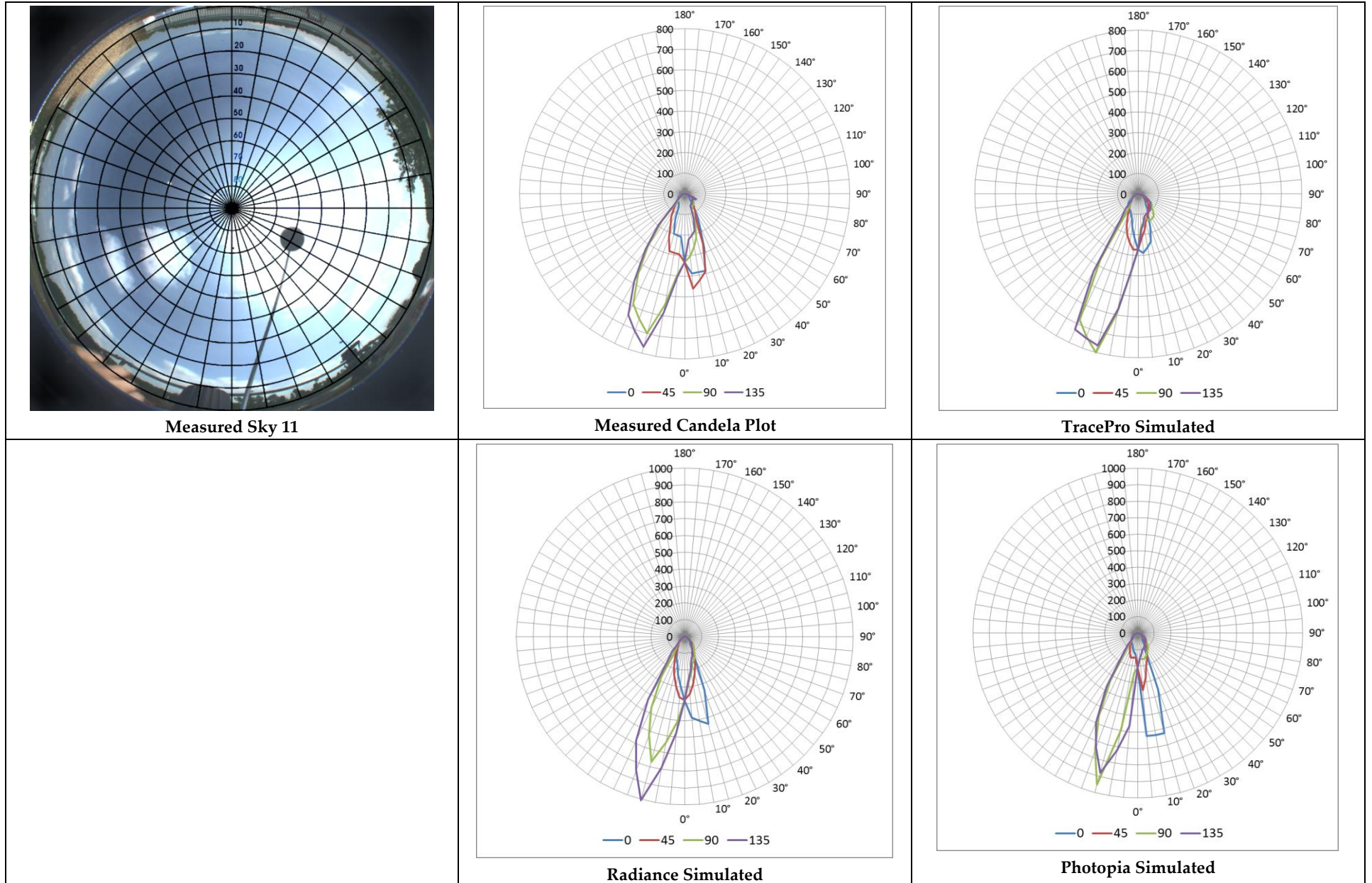


Figure 78: Sunoptics Top photometric comparison, partly cloudy sky (Test 11)

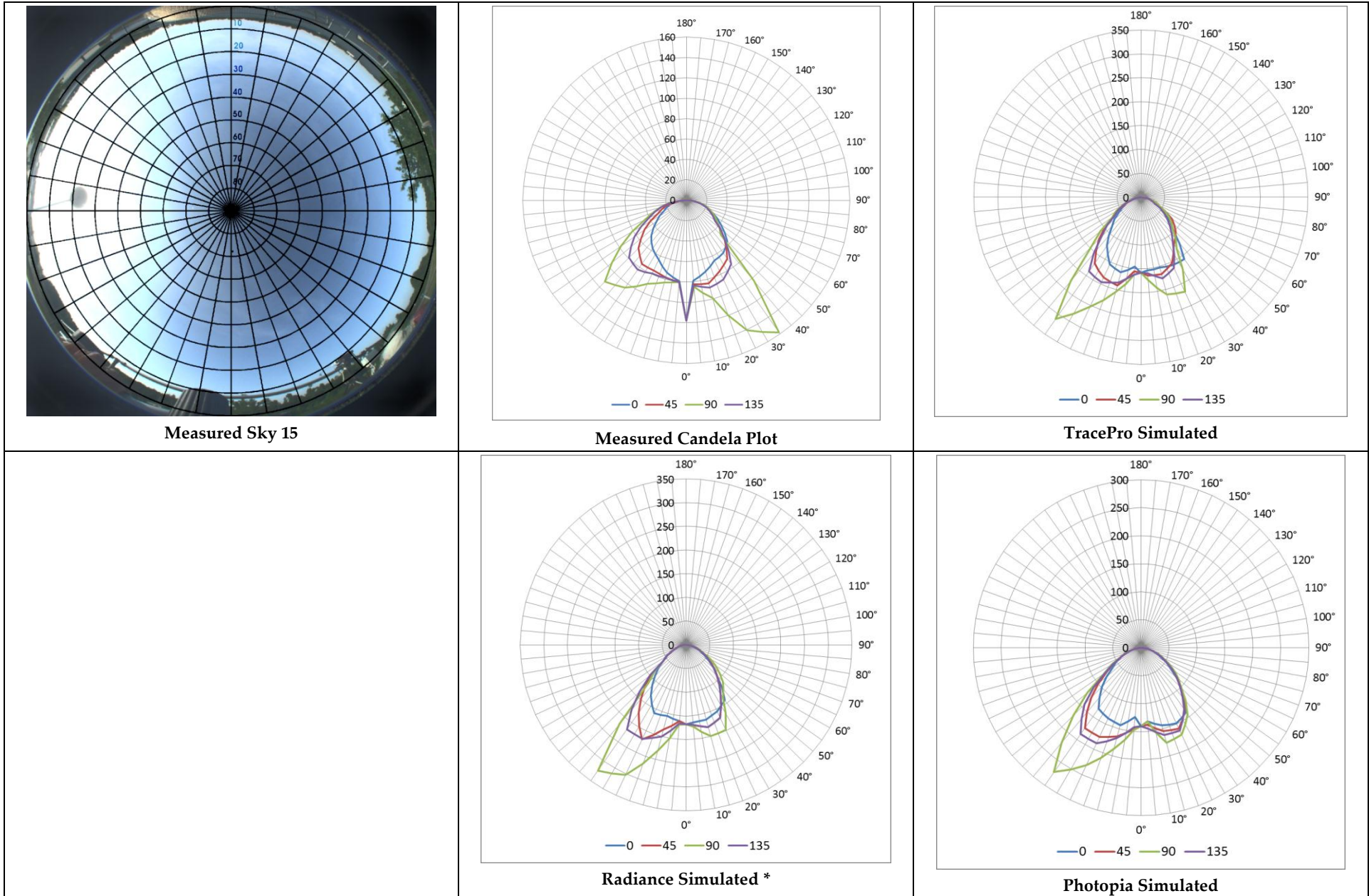


Figure 79: Sunoptics Top photometric comparison, low sun angle sky (Test 15)

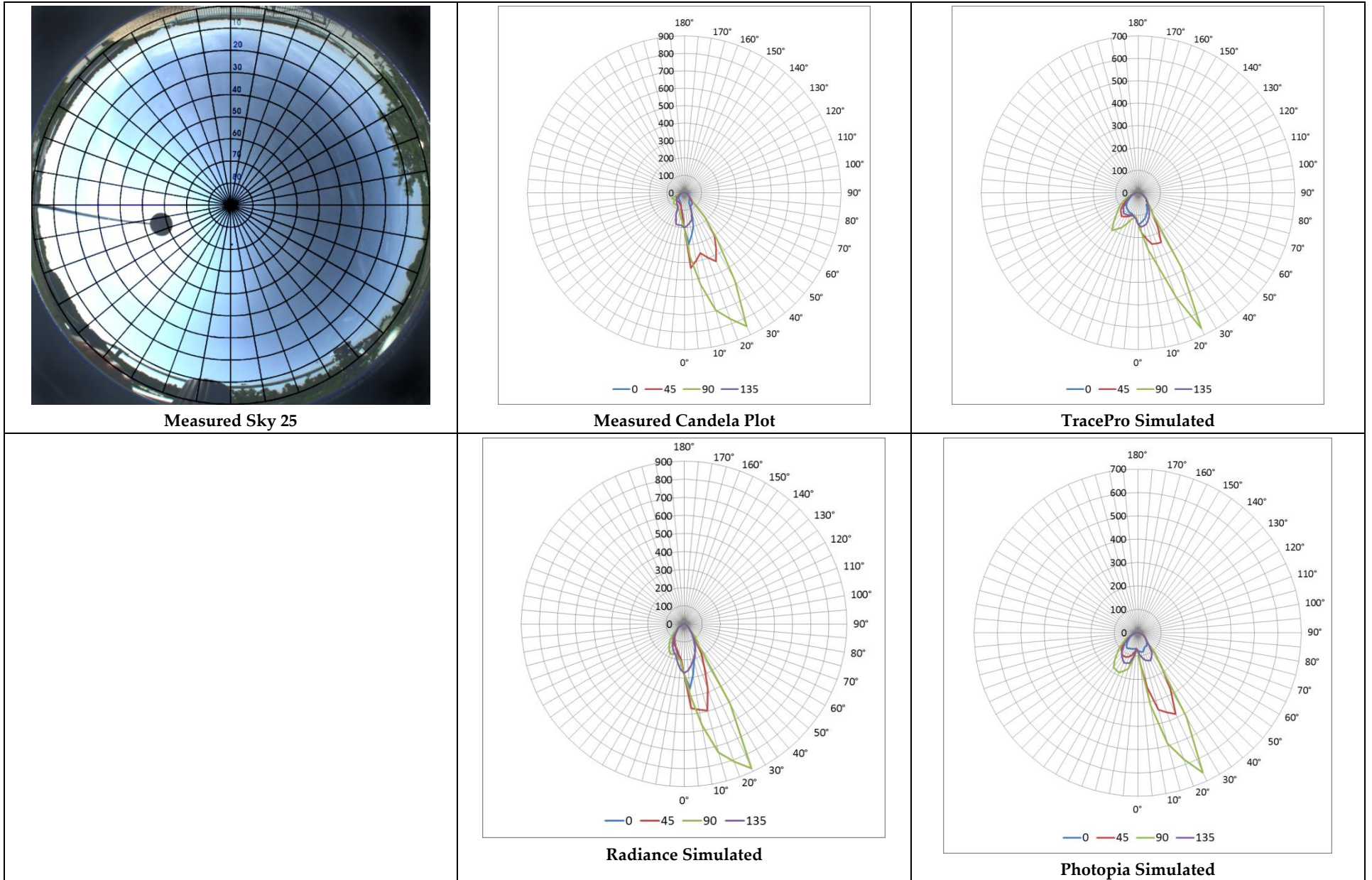


Figure 80: Sunoptics Top photometric comparison, mid sun angle sky (Test 25)

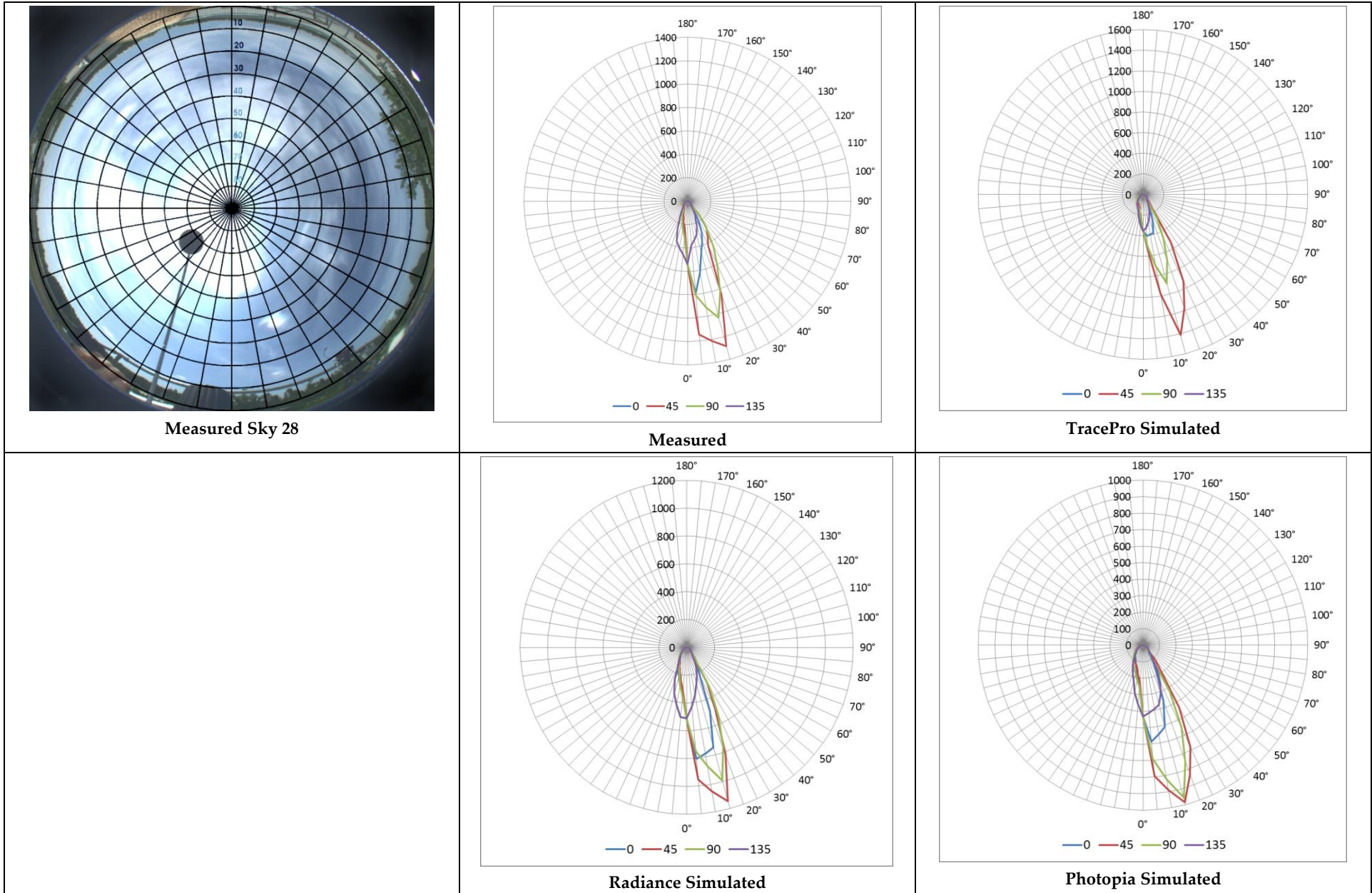


Figure 81: Sunoptics Top photometric comparison, high sun angle sky (Test 28)

SunOptics Box

The SunOptics Box setup represents a more complex optical system with two prismatic lenses at the entrance and exit of the system, and highly specular metal walls. LBNL isotropic BRDF measurements were used to calibrate the surface models in all simulation approaches.

Fortunately, this material showed highly specular, symmetric, and isotropic behavior and is simulated fairly easily in all approaches.

Figure 82 shows the results for test 9: a high sun angle and partly cloudy sky. All simulation approaches match each other very well with a larger peak at -15° in the 135° plane. The measured results indicate more of a balance with an equal 0° and 135° plane. It is interesting to see all measurements match so well and perhaps indicates a systematic error in either the measurements or in something common to all simulations.

Figure 79 shows the results for test 18: a low sun angle. The measurement data shows one significant spike at 45° and a much bigger one at -35° in the 90° plane. Given the sun's 90° azimuth angle at this time, this makes sense as perhaps a single reflection peak and a double reflection peak. None of the simulated results match this shape extremely well but they all show a similar dual peak distribution. They all have the right peak at 55° , instead of 45° , and a broader left peak closer to -40° . While Photopia and Radiance match the measured data with a stronger peak on the right, TracePro shows the opposite. This may be due to lacking BSDF data in the TracePro simulation that missed or misinterpreted a peak in the scattered data. Radiance indicates a much more diffused distribution than the others indicating possible issues with the specular reflection model and/or with the specular bounces included in the simulation. Overall, it appears that the simulations did not exactly capture the initial scatter at the top lens and the multiple reflections that occur in this system given the lower sun angle.

Figure 80 shows the results for test 22: a mid sun angle. Like the previous sky, the measurements show split peaks in the 90° plane, however not as pronounced with more diffusion in general. All the simulations correctly matched this peak at -35° but all seemed to over predict the magnitude of it as the other planes are smaller in comparison. This could be another systematic issue in the simulations, perhaps due to the sky source being too small relative to the solar source.

Figure 81 shows the results for test 32: a high sun angle. The measurements show a fairly symmetric lobe of distribution centered around 5° from Nadir. With the high sun angle, this indicates minimal direct solar reflections within the SunOptics box. The Radiance simulations match the best with very close magnitudes in all planes. The TracePro and Photopia results indicate a slightly stronger peak at 15° in the 45° plane. This matches the location of the solar disc a bit more which is roughly 15° from zenith and could indicate too much specularity in the SunOptics prism models.

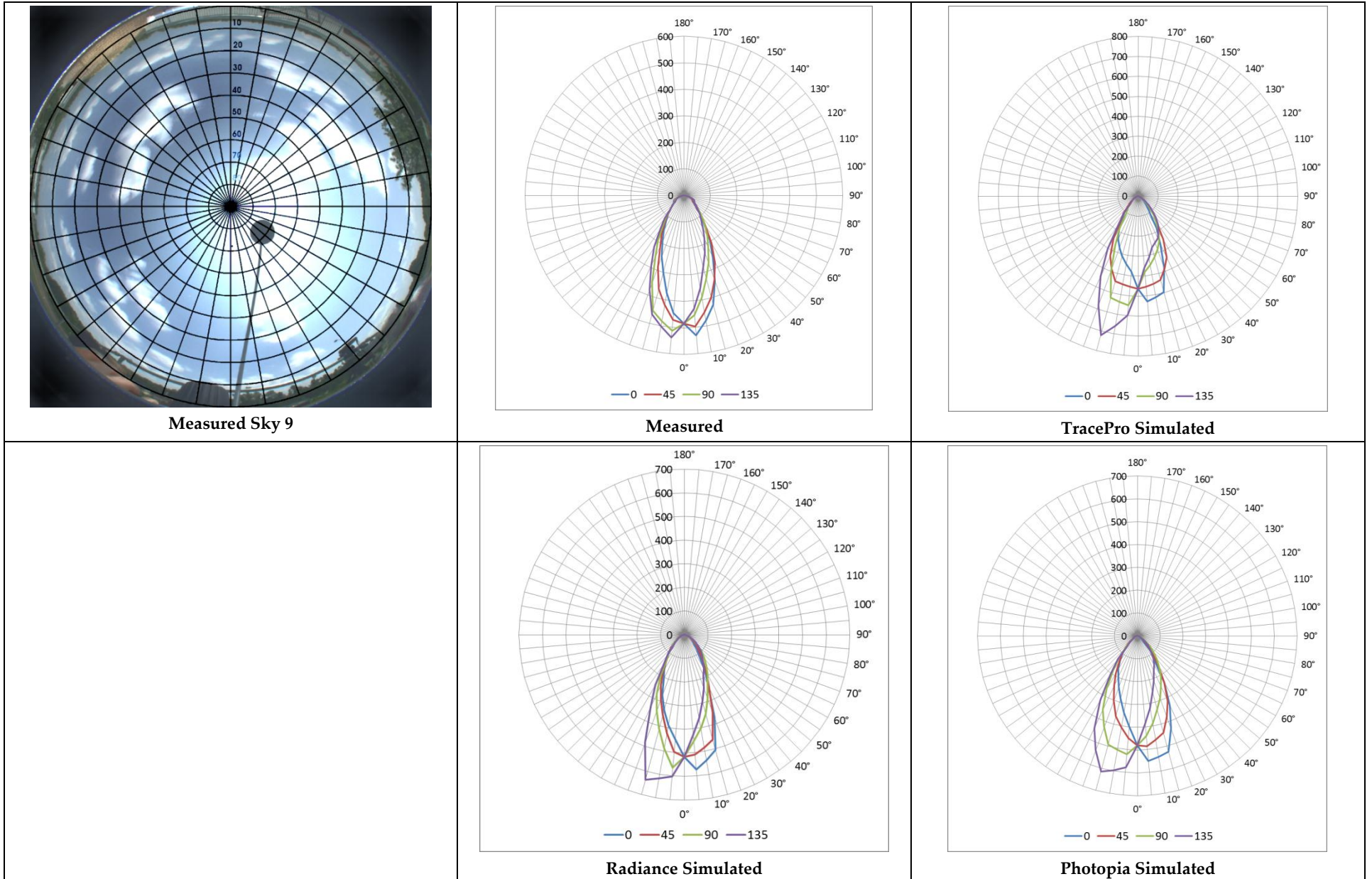


Figure 82: Sunoptics Box photometric comparison, partly cloudy sky (Test 9)

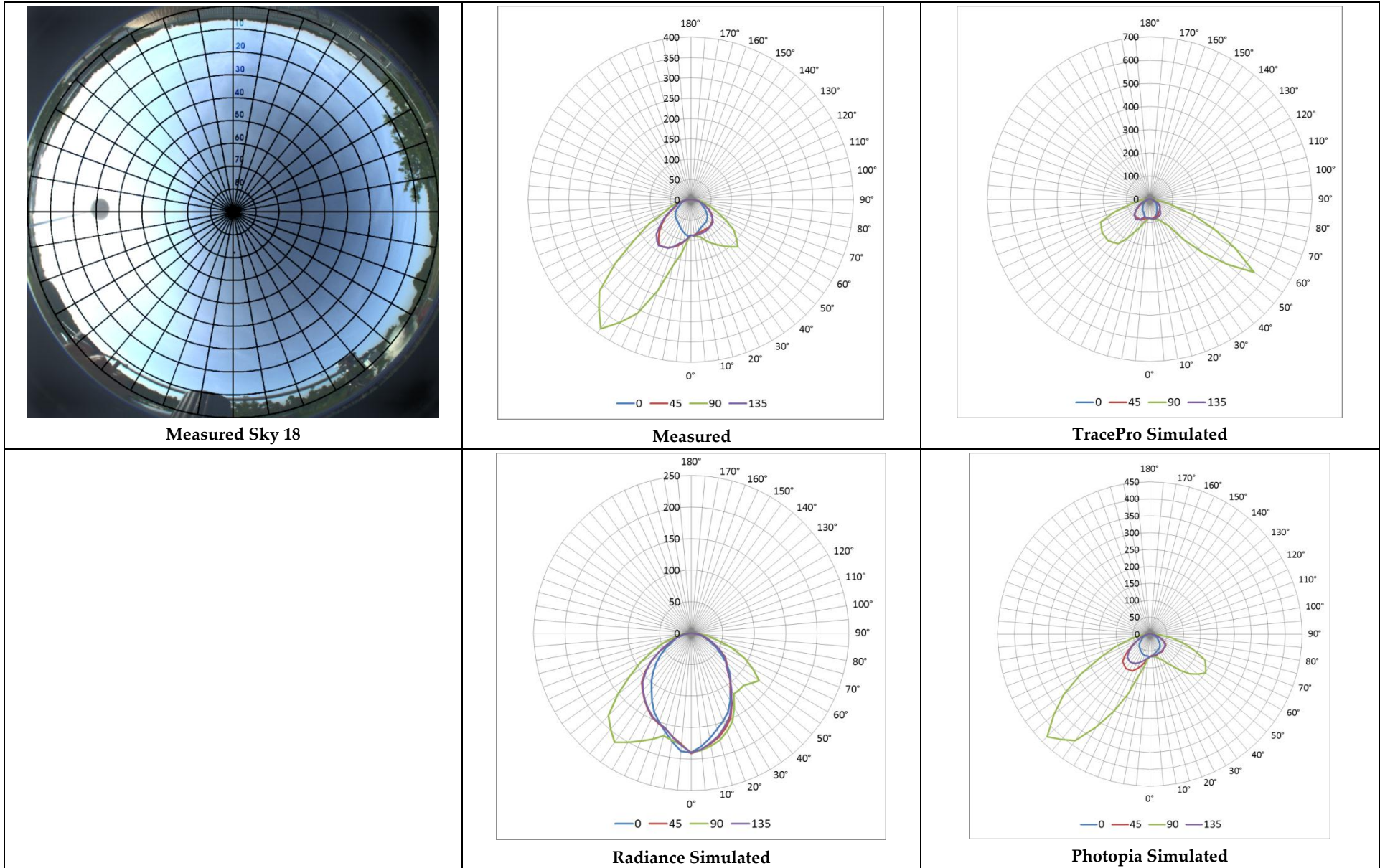


Figure 83: Sunoptics Box photometric comparison, low sun angle sky (Test 18)

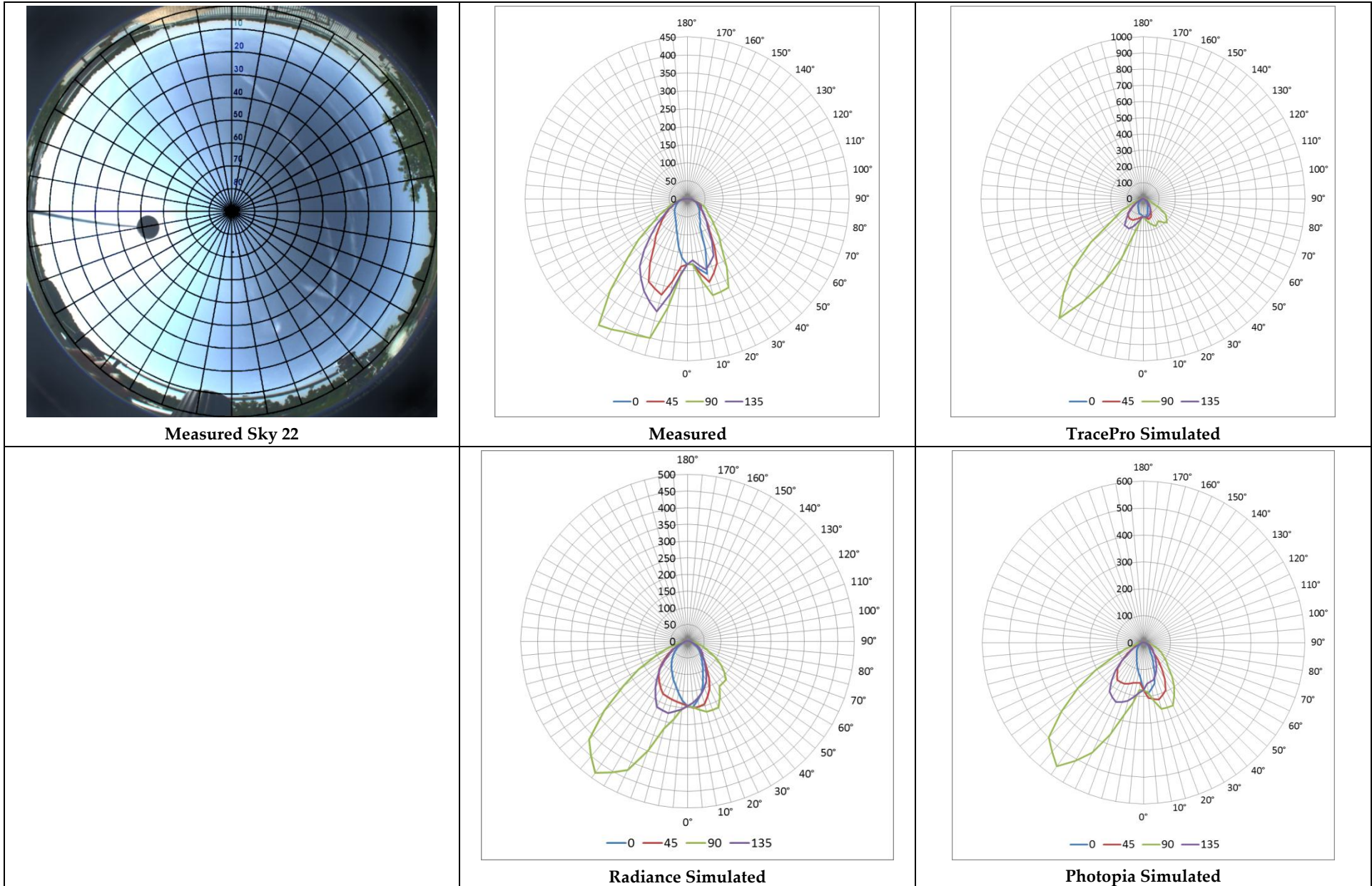


Figure 84: Sunoptics Box photometric comparison, mid sun angle sky (Test 22)

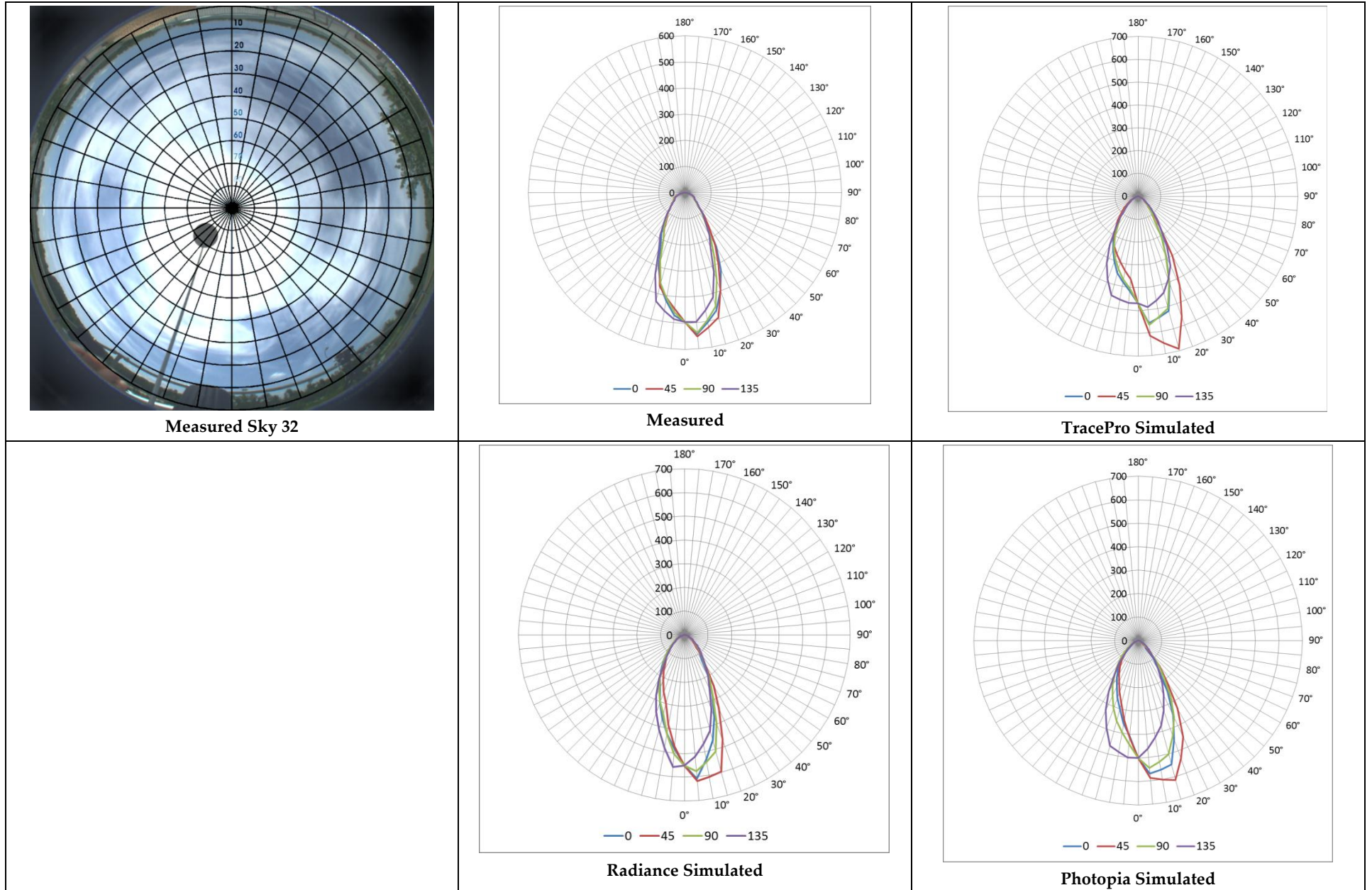


Figure 85: Sunoptics Box photometric comparison, high sun angle sky (Test 32)

Sun Tunnel

The Sun Tunnel system represents the most complex optical system measured. Optical elements include the clear acrylic top dome, a highly reflective metal tube, and a bottom prismatic top lens.

Figure 86 shows the results for test 6: a high sun angle and partly cloudy skies. The measured results indicate a sharper peak somewhere between 15-25° from Nadir and between the 0° and 135° planes. The TracePro results show similar sharp peak while the Radiance and Photopia results show wider lobes in the same direction. The Radiance results seem to favor the Nadir direction.

Figure 87 shows the results for test 16: a low sun angle. The measured results show a very wide and symmetrical distribution which is also seen in all the simulation results. However, the Radiance results again seem to favor the Nadir direction.

Figure 88 shows the results for test 25: a mid sun angle. The measured results show a sharp peak at 45° in the 90° plane, slightly sharper than the incoming sun angle of 35°. At these angles, there are at least two direct bounces in the tube. The Photopia results match this sharp distribution the best with a peak at 45°. Both the Radiance and TracePro results show a much broader distribution than the measured results or Photopia, with a lower peak angle. This perhaps indicates an inadequate sampling of the high angle, multiple bounce rays or poor BSDF descriptions at the higher angles. The Radiance results again seem to favor the Nadir direction.

Figure 89 shows the results for test 28: a high sun angle. The measured results are similar to test 6, which had a similar sun angle, but indicate a tri-peak in the 45° plane which is the same plane as the sun. The BSDF measurements for the Sun Tunnel lens show a triple split beam behavior reminiscent of these results. The Photopia results best match this behavior with equal split peaks. Both TracePro and Radiance results show some level of split peaks but not nearly as pronounced or balanced as the measurements.

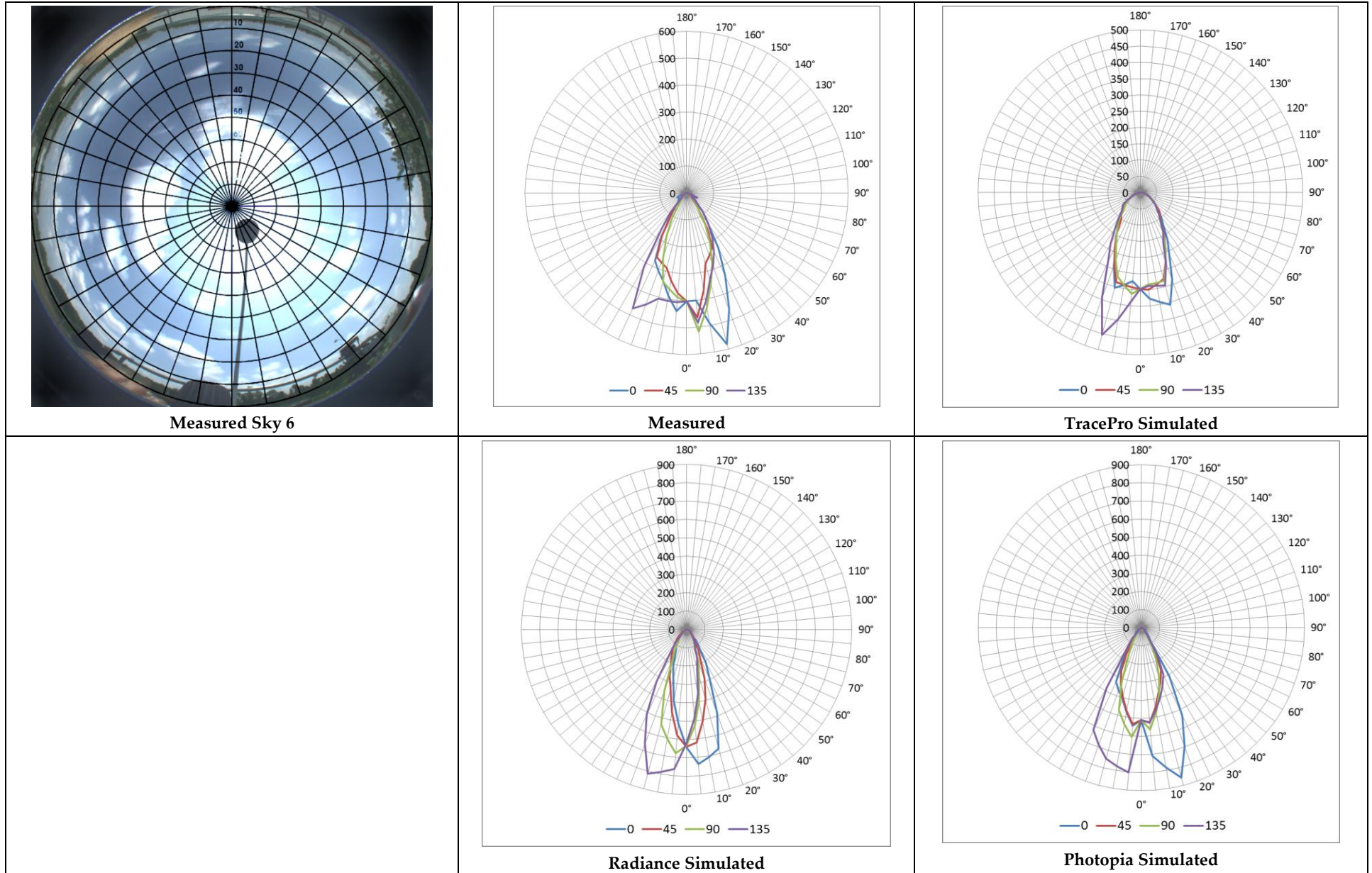


Figure 86: Sun Tunnel photometric comparison, partly cloudy sky (Test 6)

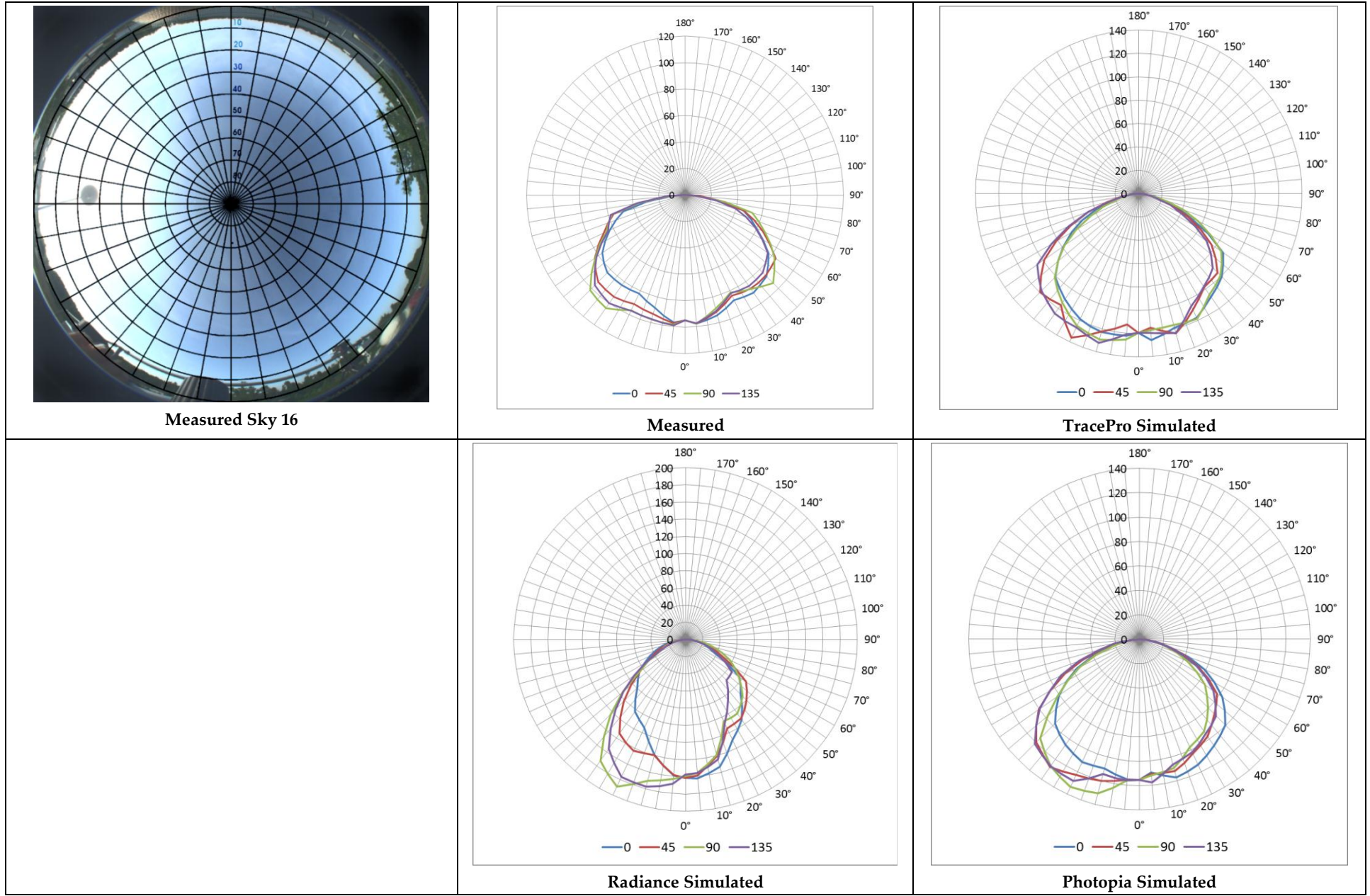


Figure 87: Sun Tunnel photometric comparison, low sun angle sky (Test 16)

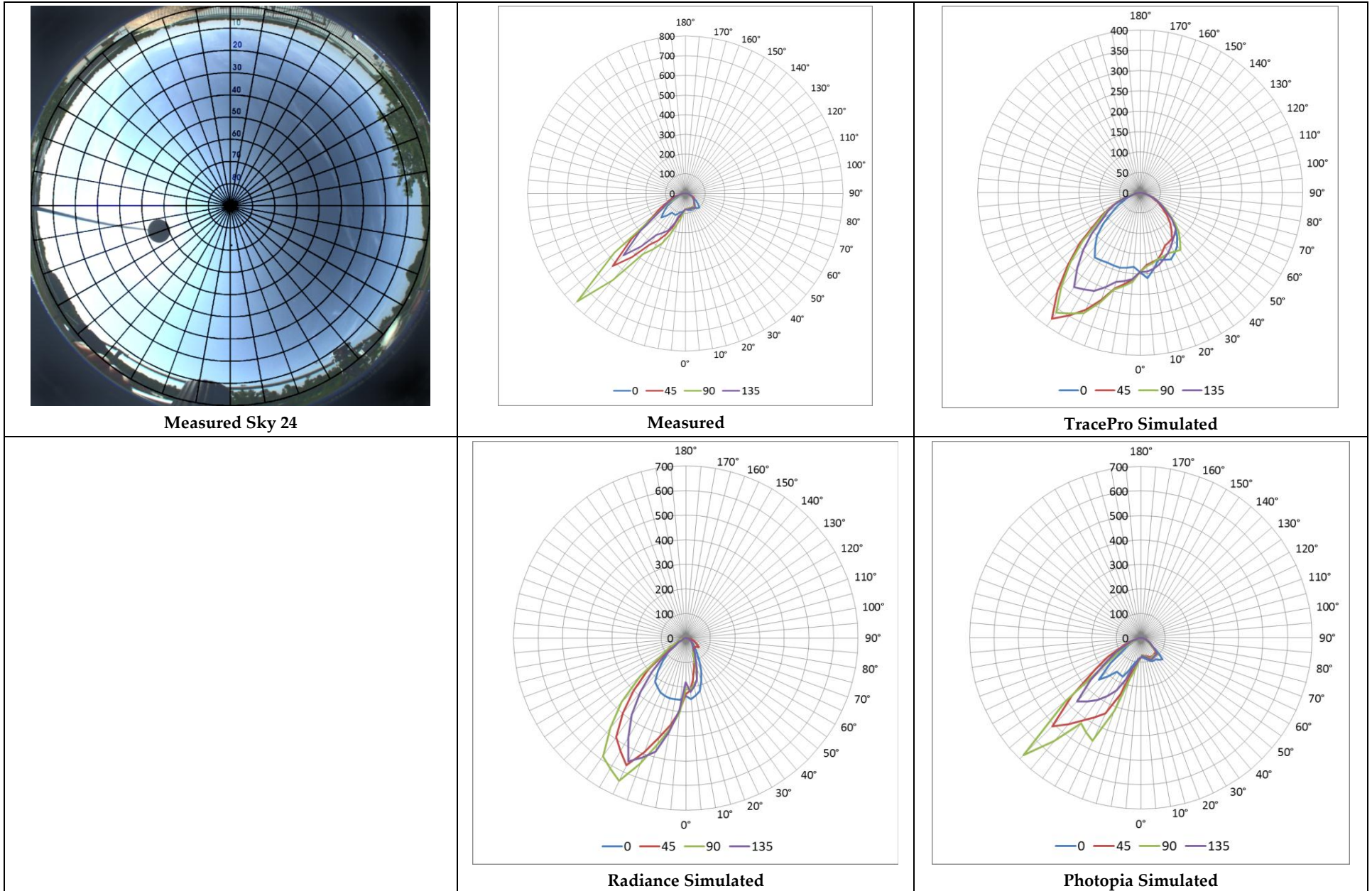


Figure 88: Sun Tunnel photometric comparison, mid sun angle sky (Test 24)

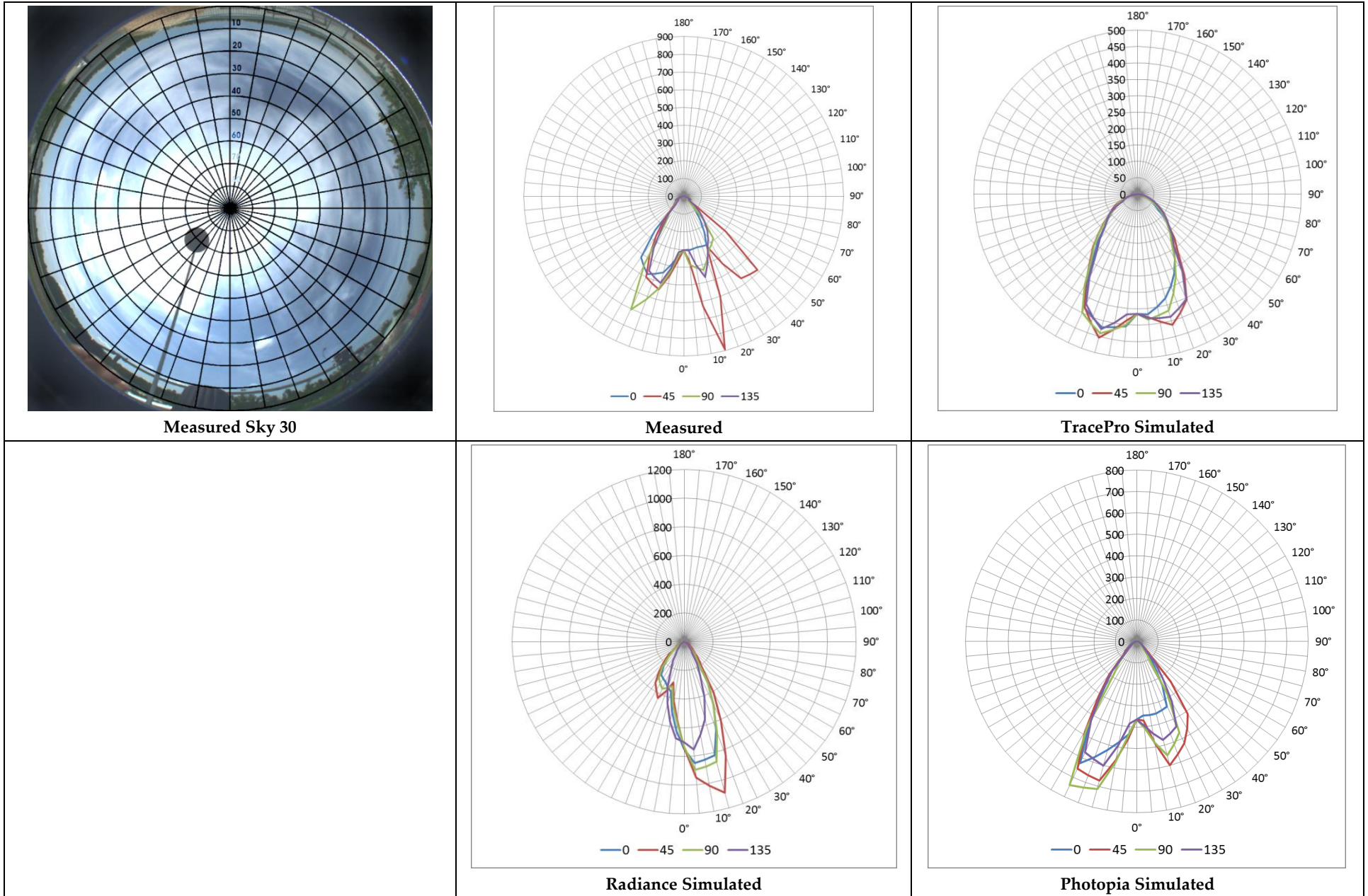


Figure 89: Sun Tunnel photometric comparison, high sun angle sky (Test 30)

CHAPTER 9: Conclusions and Recommendations

The following conclusions and recommendations can be drawn from the results of the various activities performed in this research project.

Sky Measurement and Processing

- The described method for capturing hemispherical sky images resulted in a valid and useable sky luminance description.
 - The method involves a digital camera with a hemispherical lens capable of equi-angular mapping and exposure bracketing and a shading disc to obscure the solar disc.
 - Simultaneous global horizontal and diffuse illuminance measurements were taken to calibrate the resulting HDR image.
 - It is important that the shading disc for the camera and for the illuminance meter (for the diffuse measurement) block an equivalent solid angle of the sky. It is also helpful for this shading disc be as close to the 0.53° angular diameter of the solar disc as possible, while preventing any view of any part of the solar disc by any part of the detector.
 - The illuminance measurements proved to be more useful for calibration than the zenith illuminance measurements that were more variable.
- The method presented for cropping, masking, filling in, and calibrating the obtained HDR sky image resulted in a valid equi-angular hemispherical luminance map useable in lighting software.
 - Given equivalent shading discs, the digital camera skydome image, with the shading disc element present, permits camera absolute luminance calibration from the independently measured diffuse illuminance.
 - Use of a Perez sky patch was found to be most effective at filling in the missing sky patch (blocked by the shading disk) versus other CIE standard sky types.
 - A solar disc source created and located according to solar position algorithms. The filled-in sky source was calibrated to provide the measured diffuse illuminance +10% and the solar disc intensity was calibrated to match the global illuminance measurements.
- The method for using the calibrated sky luminance map to generate a set of sky and sun rays useable in forward ray-tracing software resulted in valid sets of sky and sun source rays, adjustable by desired spatial density and angular resolution.
 - A sky resolution of 128×128 (a sampling of 12,867 sky patches covering the hemispherical solid angle of the sky) was found to provide adequate resolution of the sky source without overloading the ray-tracing software with too many rays (or to be exact, the computer's ram with too much data).
 - An equi-angular mapping appears to be the best hemispherical mapping algorithm as it samples overhead patches, where daylight has the greatest impact on skylights, as well as low patches, where the sun is often found over the course of a year, equally.

- Random sampling of both the ray location and direction gave the best results, avoiding any errors due to any regular or repeated patterning in the sampling.
- The approach of generating rays such that they fall onto 5 surfaces of a defined box to encompass all receiving surfaces of the desired skylight system worked well. The method minimized the amount of rays needed to get good sampling through the system.
- A total ray count of around 1 – 5 million rays appears to give adequate accuracy without overloading today's computer processing capabilities. Using ray-splitting algorithms was determined to be an accurate way of increasing the ray sampling at the exit of a system without requiring larger ray sets.
- We learned to pay careful attention as to the orientation of any anisotropic and/or asymmetric optics as this greatly impacts the exact optical performance of the system.

BSDF Measurement and Processing

- **Anisotropic** and **asymmetric** BSDF measurements are **necessary** for any materials that exhibit such behavior in order to accurately predict a skylight systems **exact** photometric performance for a specific condition.
 - This is primarily due to the large impact that the direct solar beam (nearly parallel rays from a specific direction) has on the skylight system performance. Electric lighting system optics typically have a much more diffuse source of light that justify the use of an averaged, isotropic definition.
 - While not accurate at predicting specific conditions, averaged isotropic and symmetric BSDF representations may still be a good method for predicting annual average performance or performance of systems where the manufacturing and installation orientations are unknown. The LTI Optics goniophotometer method offered us a good approach to creating this type of averaged isotropic representation.
- A maximum BSDF measurement density of 1° - 2° appears to provide adequate resolution to capture the skylight lens optical characteristics and the skylight system characteristics. Horizontal angle (ϕ) increments of 22.5° , a common increment in electric lighting photometrics, are likely too large to capture some of the unique optical/geometric effects that can occur with prismatic lens materials.
 - The standard Klems resolution of 145 patches resulted in a low density of sampling, roughly every 12° , and can miss significant spikes in the distribution for anisotropic and asymmetric BSDF materials. This resolution is likely adequate, however, for many homogenous, isotropic and symmetrical BSDF materials.
 - Variable resolution BSDF definitions offer a good solution in that they provide adequate density when required. Tensor-tree log 5 representations (1000+ sample directions) appear to describe the prismatic lens optics and system optics adequately, though results will likely improve using a log6 tensor-tree representation giving over 3,000 sample directions.
 - Centering spherical coordinates around the mirror/direct ray appears to be a good way of getting a higher sampling density in the mirror/direct ray direction, which is often the

- peak candela direction for many BSDF materials. However, it does not adequately address peaks that occur due to more complex optical elements such as the prism lenses.
- An approach of combining the centered spherical coordinate approach used by Photopia and the tensor-tree variable resolution approach implemented in Radiance could provide the most efficient and effective definitions. The coordinate system would naturally provide a greater density around the mirror/direct ray, while the auto-discretization algorithms would determine when this maximum resolution is needed.
 - Computer simulation of 3d solid models of optical elements using the Radiance tool “genBSDF” appears to be a valid approach to generating BSDF definitions. Caution should be taken to ensure:
 - The solid model is completely enclosed so that any ray that enters also exits the medium.
 - The solid model has adequate density to capture the necessary optics and any manufacturing defects. Ray trace modeling of ideal (perfect) optics does not provide a useful BSDF result as there are too many manufacturing imperfections that are not properly traced with such models.
 - Shielding is used to prevent any stray rays that miss the system from being included in the results.
 - Settings are high enough to accurately capture the multiple reflections and refractions that can occur in more complex optical systems.
 - TracePro BSDF definitions provide acceptable accuracy but care needs to be taken in the creation so that all important optical characteristics are captured.
 - The Harvey Shack BSDF model appears to provide good results for materials that exhibit isotropic and symmetrical distributions but is not able to handle more complex anisotropic and asymmetric materials.
 - A lookup table BSDF definition approach can adequately describe anisotropic and asymmetric materials but seems to drastically increase simulation time, taking nearly 10x the time of a simpler equation based definition.
 - The Photopia Material Lab tool appears to produce accurate BSDF definitions that match those measured and simulated in Radiance. The resulting definition can only be used natively in Photopia simulations.
 - The XML BSDF file format defined by LBNL represents a good start towards a standardized BSDF format. More effort is recommended to determine a common format, similar to an IES photometric file that can be written and read by any lighting simulation engine.
 - The BSDF file formats native to TracePro appear to adequately address scatter from isotropic and symmetric materials but are difficult to obtain for more complex anisotropic materials.

Simulation and Modeling

- For the tested skylight products, far-field simulation did not vary much from near-field simulation using TracePro. In forward ray-tracers, far field simulations and near-field emulators used by Photopia appear to be acceptable alternatives for collecting photometric information.

- An adequate amount of rays is necessary for obtaining smooth and accurate exiting luminous intensity distributions, particularly when using forward ray-tracers.
 - In TracePro, this can be adequately done using ray-splitting algorithms which cause multiple rays to be spawned at each transmitting or reflecting interface. Smaller initial ray sets are recommended, as they load and simulate quicker, along with a 1 to 2 ray spawns per bounce. More spawning per bounce increases simulation time.
 - In Photopia, initial ray sets of 5 to 10 million provide an adequate amount of rays to enter the system for smooth photometric results.
- For highly specular and reflective systems that exhibit potential for multiple bounces within the system, it is important to simulate adequate bounces. The 50 bounces used in the Photopia simulations captured all but a fraction of a percentage of peak candela at sharp exiting angles, and appeared to be the realistic option. The 20 bounces used in TracePro seems to be adequate for most situations but possibly misses some high angle light in certain situations, -such as Sky 24 (Figure 88). The 12 bounces used in the Radiance simulations does not appear to capture this high angle flux, particularly in the optically complex SunTunnel system where many of the results had a strong bias towards Nadir.
- Along with a high maximum reflection setting, a low flux threshold setting is recommended to help capture the flux at sharp incoming and exiting angles.
- Using Radiance, adequately high simulation parameters during the generation of both the lens BSDF definitions and system BSDF definitions is critical for accurate tail end simulations. While these simulations are time consuming, the simulation time is reduced drastically for subsequent application simulations.
 - A system BSDF approach proved to be more accurate than running a classic Radiance simulation or one creating “illum” surfaces with mkillum.
 - A system BSDF approach has an added benefit of being compatible with newly developed 3-phase and 5-phase annual daylighting simulation approaches.

Photometric Validation

Overall, the simulated luminous intensity emanating from the skylight products matched the general shape of those measured quite well. However, while the general shape matches, there is lower reliability in simulating an exact luminous intensity in a given direction. The following conclusions can be made.

- The accuracy and detail of any BSDF measurements used to describe optical materials in the system is critical. Isotropic and low resolution representations appear to miss critical optical characteristics of both a single material and an optical system.
- The accuracy of the small system geometric details does not appear to be as critical. There was minimal impact on the results when fillets were added to the lens in the Photopia SunOptics simulations. This at first seems in contradiction with the statements about not modeling ideal lens optics. However, these fillets represent a very small portion of the overall area of the skylight whereas the little pock marks left by the injection molding process occur at every pyramid and end up representing more of the skylight area. The

tested skylights likely had other imperfections such as scratches and marks on the lenses and dents and marks on the reflective tubes. However, there were no noticeable quirks in the simulated data that would indicate any major imperfections in the manufactured geometry.

- All simulation engines appear to struggle at capturing high angle light leaving the systems. Figure 90 plots the % difference between the simulation engines and the measured data for Sky 9. This was a sky condition in which all simulation results matched each other fairly well. It can be observed that while they were all off from the measured data, they were all off in a very similar way. They tend to underestimate the high angle luminous intensity, while matching the distribution below 50° fairly well. This is likely due to two effects:
 - Even though the goniophotometer room was painted black and the illuminance sensors had black painted shields directed at the skylight opening, there is still significant ambient light that will bounce around the room, more so for the higher sensors that get a more direct bounce of the ambient light off of the floor. The Radiance simulations shown were for perfect absorbing walls, simulating this ambient reflection would likely improve the match with the measured data. While this helps explain the discrepancy between the simulated and measured, it should be noted that perhaps the simulated results are the more accurate as they don't include this erroneous ambient lighting.
 - The higher exiting angles require more bounces and lower ray limits to adequately simulate. These higher points would see a reduction in flux if these parameters are not set high enough.

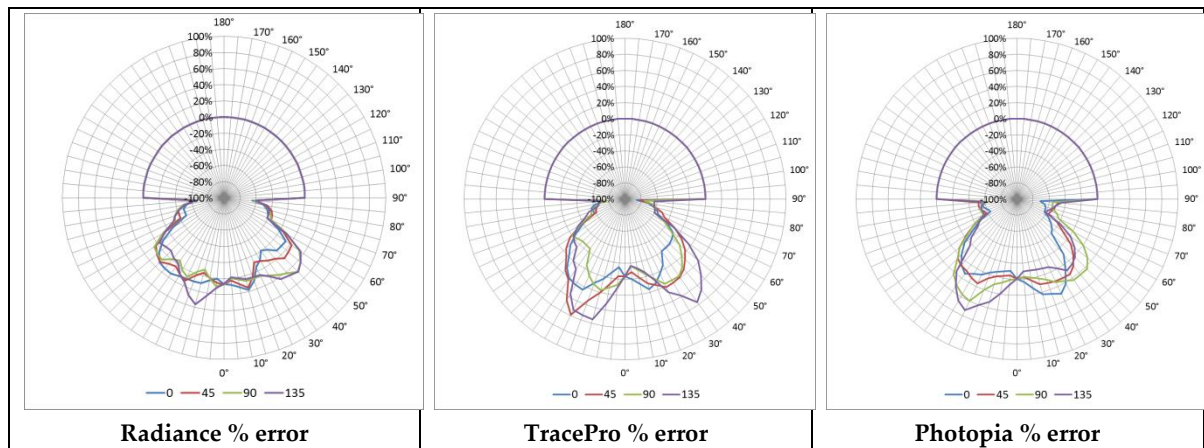


Figure 90: Error Comparison for Sky 9

- All the simulation approaches appear to be adequate in describing the general shape of daylight distribution for simple to complex optical skylight systems under a range of sky conditions.
 - They do not appear to be able to predict very sharp and specific optical effects that may come from an imperfectly manufactured system. However, they do seem to predict performance accurately enough for design work, comparisons, and general skylight layout and analysis.

- The resulting photometrics seem to lack the accuracy and resolution to perform very detailed glare analysis of a skylight system.
- For TracePro, using higher resolution more accurate BSDF definitions of the prismatic lens materials and increasing the total ray bounces and weight limits would improve the overall accuracy of the TracePro simulations. BSDF resolutions similar to the variable resolution used in Radiance (1024 maximum output regions) or Photopia (2.5 – 5° spacing) is recommended. Total ray bounces of 50 are recommended to better capture the high angle light.
- For Radiance, increasing the total ray bounces when generating the system BSDF file definitions and modeling the ambient light in the space would improve the accuracy of the simulations.
- Overall, a computer simulation approach avoids the hurdles facing physical photometric measurements of skylight systems, namely:
 - Size constraints – the simulation methods developed using the three different systems have no size constraints. The daylighting systems could be 1' to 100' wide and the software would deal with the simulation equally. Unless optical elements are added to the system, these larger sizes will not impact the simulation time significantly.
 - Sky constraints – the simulation methods can use any sky/sun source desired, at any time of day or day of the year, at any latitude or for any sky weather condition. Captured sky images can be fed into the simulations or standard algorithmic definitions such as the CIE or Perez standards can be used.
 - Photometric resolution constraints – the simulation methods can produce high resolution photometrics, but not with unlimited resolution. The ultimate resolution is dependent on the resolution used in defining all BSDF materials in the systems and on the simulation parameters used, particularly the number of rays traced. In Radiance, the number of sensors simulated is nearly directly proportional to the simulation time. In Photopia and TracePro, higher resolution photometrics can be produced to the point where the data becomes erratic so that many more rays are required to maintain accuracy.
 - Time constraints – the simulations can be carried out at any time and on any number of computers drastically improving the accessibility to detailed skylight performance data.

Next Steps

The following next steps are recommended based on the conclusions of this report.

1. Organize a daylighting sub-committee within the IESNA to develop and publish a companion document to the IES LM-81-10 document⁵ that outlines an approved method for creating optical daylighting system photometric distributions using computer simulation.

⁵ "Photometric Testing of Skylight and Tubular Daylighting Devices under Hemispherical Sky Conditions"

Part of this effort would be to define some standard formats for the resulting daylighting system photometric information to then be used back in lighting calculations and lighting simulations. This is likely some form of a standard “system BSDF” file format that describes the entire system performance at once. A concise yet flexible format is recommended that can handle the simple Klems 145 patch basis as well as the more complex variable resolution definitions. It may also be in the form of a standard set of photometric data for key representative “design days” throughout the year using the approved IESNA sky models.

2. The National Fenestration Rating Council (NFRC) has shown interest in expanding their rating, certification and labeling efforts to include additional daylighting metrics. Coordinate with the NFRC in implementing system photometric information in future Daylighting Product metric and rating efforts. This is likely an expansion of the simple Visible Transmittance (VT) metric currently used for fenestration which is a simple measurement of light transmittance at a single perpendicular angle.
3. Create an openly available benchmark database with the measured sky and photometry sets for future validation of simulation engines or to validate further refinement of the methods explored in this report. More daylighting benchmarks in general are needed in the daylighting simulation industry to ensure reliable data is being produced and reported to the design industry and this data set could be part of these efforts.
4. Organize a daylighting sub-committee within the IESNA to develop approved annual daylight simulation methods that can take into account optical daylighting systems. Such a committee’s focus would be on **all** annual simulation methods and protocols but would need to coordinate with any standard daylighting photometric file formats coming out of activity 1 above. Such a sub-committee may already be needed as there are other important annual simulation issues to standardize; including shade control algorithms, daylight coefficient standards relative to patch resolution and the number of “phases” implemented, weather data use, and standard annual performance file formats.
5. Engage and inform daylighting software developers of any daylighting system photometric standard developments (activity 1) and any annual simulation standard developments (activity 4). Encourage the adoption and development of software to include daylighting system photometric data and validated annual calculations. Several daylight software developers are already involved in related IESNA daylighting committees.
6. Engage and inform the architectural daylighting design community as to the relevance of having more detailed photometric available when reviewing products and simulating performance. Likely, their main exposure to these advances will be through new labels that reports new daylight metrics on daylighting products and new advances in their lighting software that simply correctly simulates these devices.

This page deliberately left blank

Appendix A: BSDF Measurements

A.1 Theoretical Simulated BSDF Predictions

Diamond shaped, pyramidal prism structures exist for both the Sunoptics and Suntunnel lens products. To get a feel for the type of distribution to be expected with this material, several pyramid prism models were created, see Figure 91. A model with perfect angular pyramids was created to represent one optical performance extreme and a model with rounded peaks and valleys was created to better represent the manufactured materials. For incidence angles parallel, perpendicular, or at a 45° (this prism structure is square rather than diamond shaped) to the prism structure, the material will likely exhibit isotropic behavior. However, for in between incidence angles there is likely anisotropic behavior due to the optical effect of the prisms themselves.

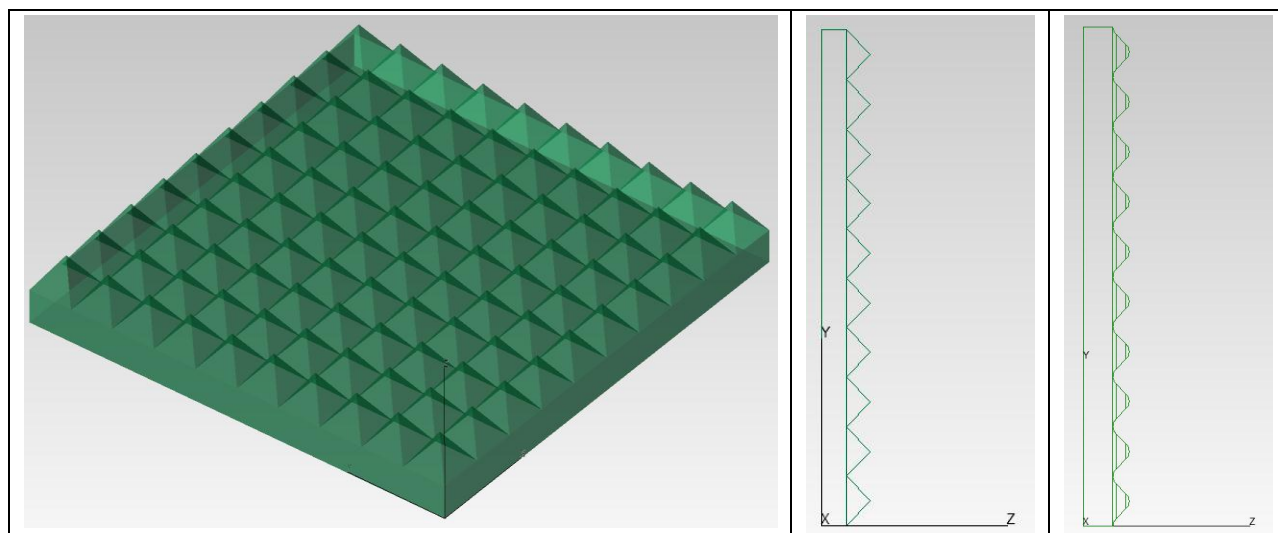


Figure 91: Geometrical models of the prism skylight lens materials (angular and rounded prisms)

As expected, the diamond prism optics creates a split-beam effect, see Figure 92. These are ray trace plots of rays passing through the prism material: they originate on the left and pass through the material from left to right. For a perfect angular prism, there is never an undeviated (“straight”) ray that passes through the system as one would have with transparent (image preserving) materials. Instead, the direct beam is often seen split into two or three dominant directions due to the multiple internal refraction and reflections that occur. In fact, a perfect 45° pyramid will create total internal reflection for rays striking the material perpendicularly (0° incidence angle) and there would be zero transmittance.

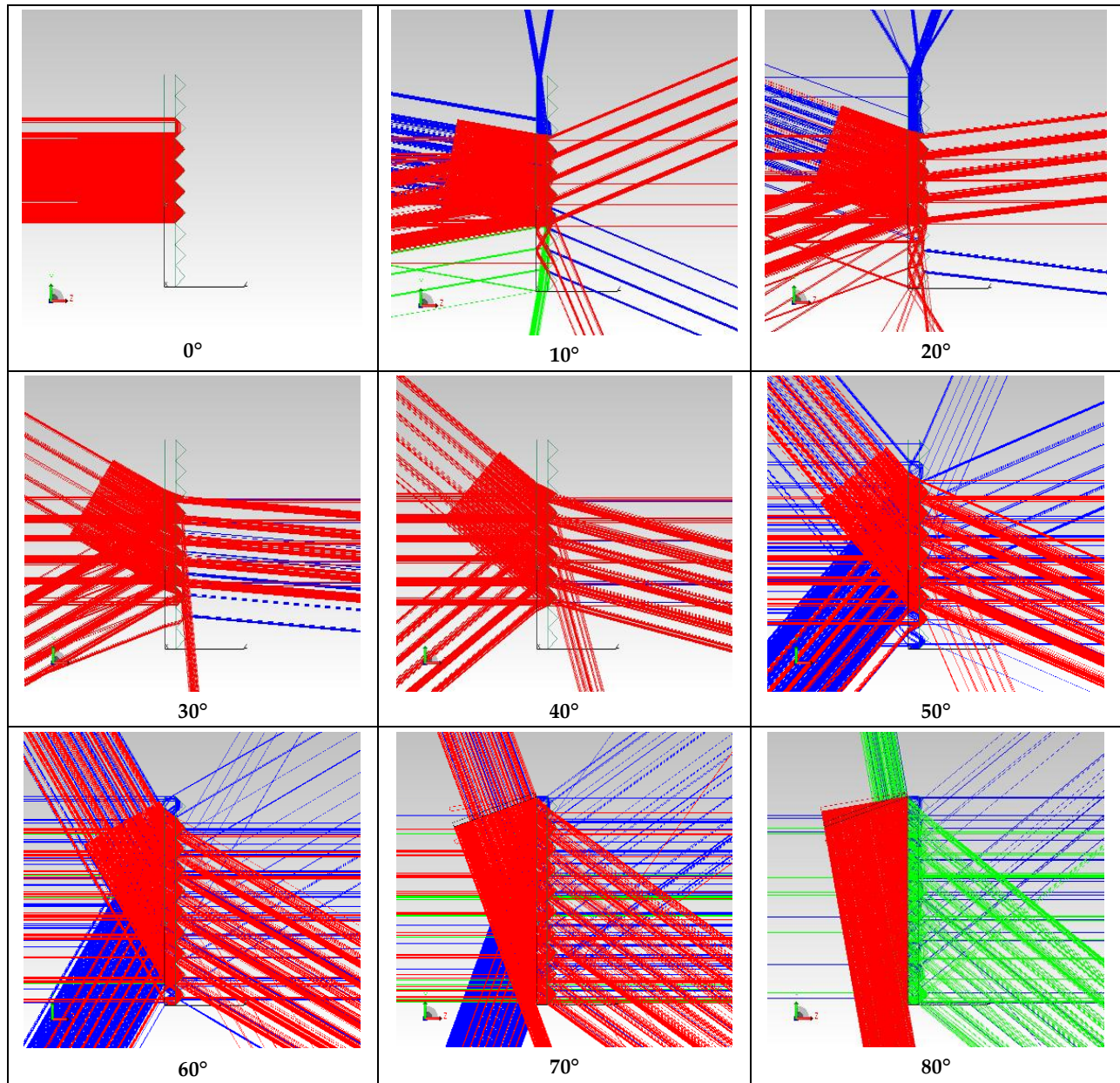


Figure 92: Examples of transmitted scatter for a perfect acrylic prism

In reality, the prisms are far from perfect having rounded peaks, rounded valleys, dimple marks, and other slight imperfections. Because of this, the materials do have some undeviated transmitted/reflected light and a more uniform spread of light than the angular example above showed. Figure 93 illustrates this spreading behavior of the rounded prism model. The light tends to be spread in a “cross” pattern that is relative to the orientation of the prisms. Essentially, light is spread into four directions dictated by the orientation of each side of the square pyramids. This cross pattern is often centered on the undeviated ray direction. However, at higher incidence angles, the side-to-side spread starts to diminish leaving a spread only in the direction of the incident ray.

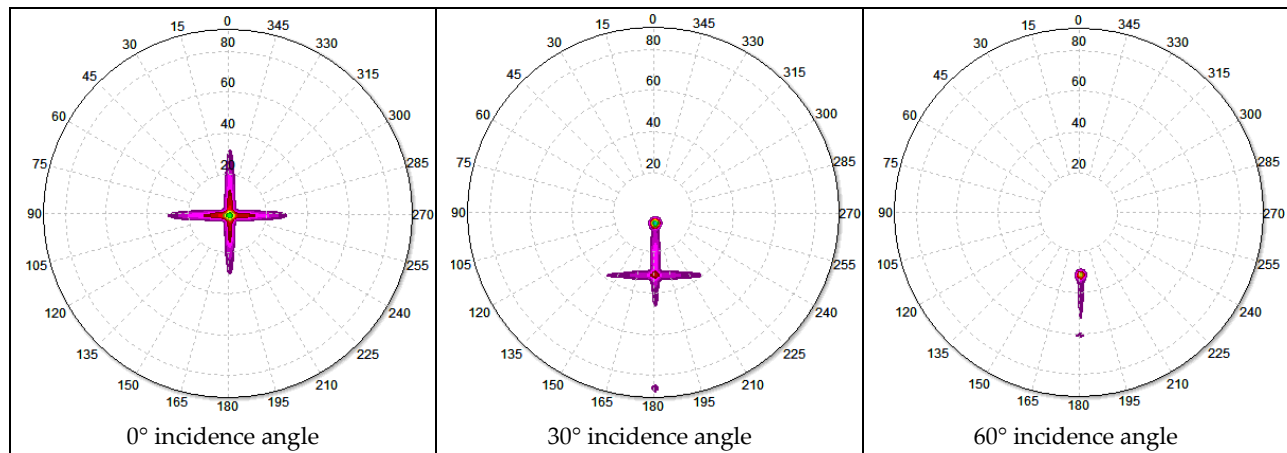


Figure 93: Example of “Cross” distribution pattern common of all square prism materials

When the pyramids are aligned with the direction of incident light, as is the case in Figure 93, the spread is directly up and down, left and right and is symmetrical around the incident ray plane. This is a case where the LTI Optics measurement approach, assuming a plane of symmetry, is sufficient. However, if the diamonds were rotated away from the incident beam, the cross pattern would also rotate accordingly and there would no longer be a symmetry plane.

This study of the theoretical spread of light informs our expectations of the BSDF measurements:

- The materials exhibit some level of beam splitting behavior where there is no longer a single central peak in the specular/transparent direction but often two or three distinct peaks.
- The materials exhibit a cross pattern of diffusion where light is spread in four distinct directions corresponding with the sides of the diamond shaped prisms.

A.2 SunOptics Pyramid Measurement Comparison

A comparison of the LBNL isotropic prismatic lens data and LTI Optics average isotropic measurement data using their goniophotometer system is presented below. This data was not used in the final simulations as more accurate anisotropic data was obtained.

The measurements from both laboratories were normalized to a peak output of 1 (LTI Optics data comes in this form given their relative luminous intensity distribution approach) and the planes of these relative distributions were compared. The results show a discrepancy between the two measurement techniques consistent with the data collection procedures discussed above. Samples of the measurements for a 0 and 180° ϕ_s outgoing plane and for $\phi_i = 0^\circ$ and $\theta_i = 0^\circ, 40^\circ,$ and 70° incoming angles are shown in the sections that follow.

Figure 94 compares the BSDF data for the transmittance of the SunOptics prism material with light incident on the **flat** side of the material. It is readily apparent they do not match up very well except at the higher incidence angles.

LBNL data shows a very significant spike at the directly transmitted angle, indicating a significant portion of light passing directly through the material, and a couple of much smaller peaks indicating more spread to the beam. This somewhat matches our expectations for split beam behavior except for the directly transmitted component which is significantly more intense than any of the split-beam components. At 70° it resembles the theoretical distribution better (refer to the Figure 93 60° example) with a small directly transmitted component and a more intense spread towards the surface normal.

LTI Optics data shows a much broader distribution for all incident angles and exhibits some double and triple peaks indicating some split-beam behavior. Because the data is an average of two incoming horizontal directions, and at a lower resolution it is smoother in general, it does not exhibit the same sharp peaks and valleys indicated by the LBNL data.

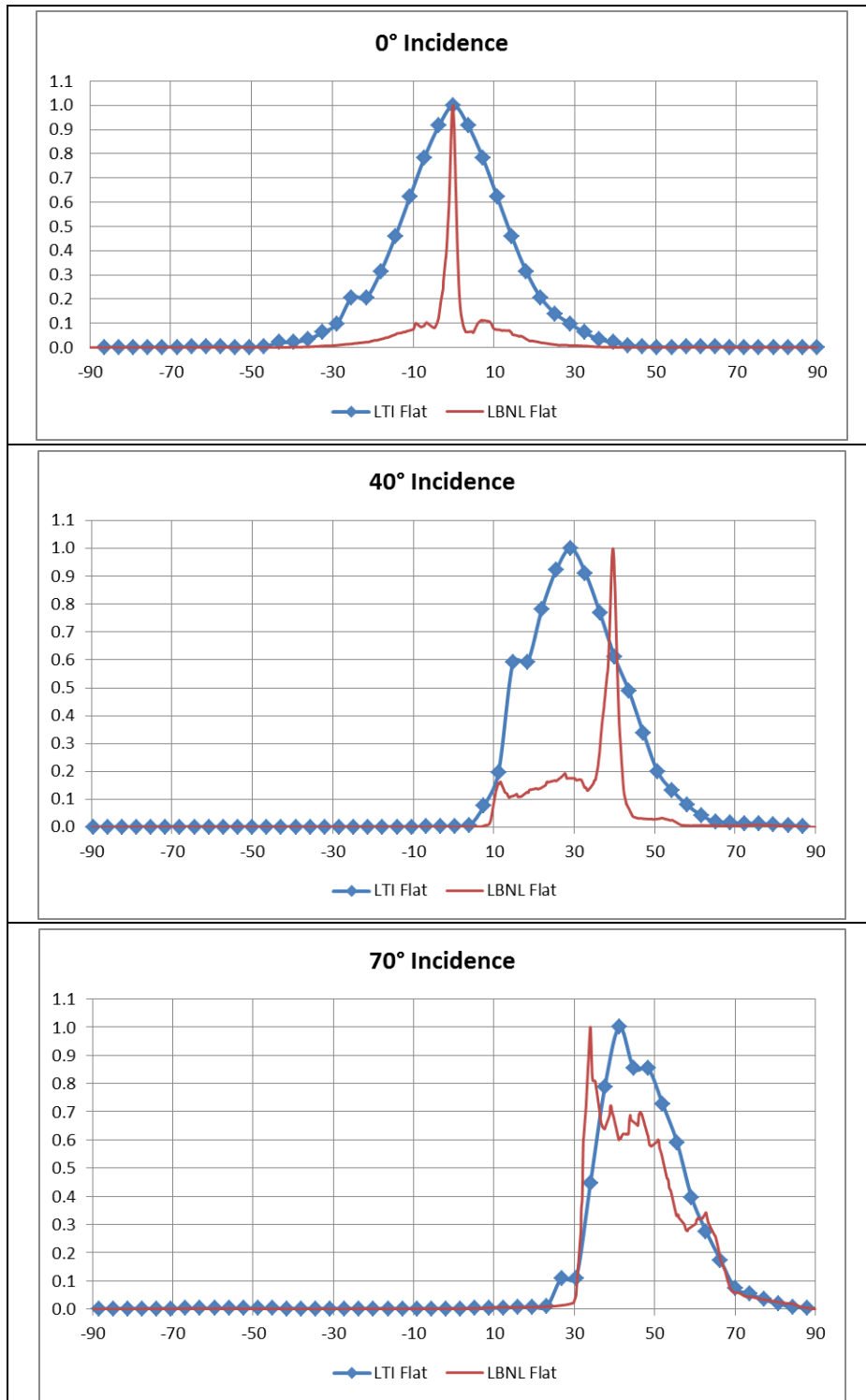


Figure 94: Comparison of SunOptics pyramid flat side transmittance measurements

Figure 95 plots the same data according to the theoretical, rounded prism, model. The shape of the data does resemble that of the measured data by LBNL, to some extent. The theoretical model seems to show greater spread at normal incidence and less spread at the higher angles.

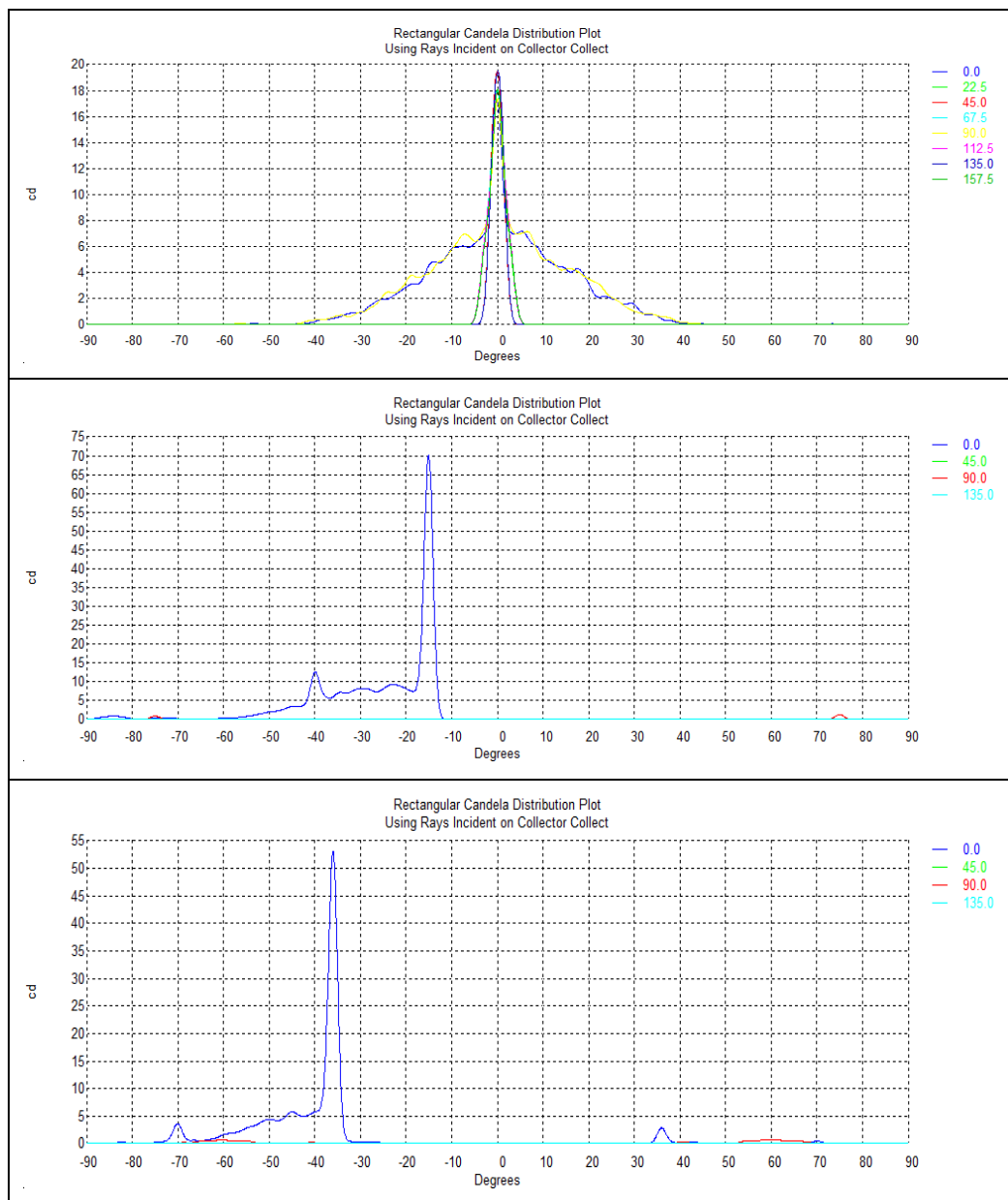


Figure 95: Theoretical prism flat side Transmittance Measurements

One of the most noticeable differences between the two lab's prismatic lens measurements is the sharper peaks, typically at specular or direct angles, exhibited in the LBNL data set. This is in a large part due to the averaging that occurs in LTI Optics data but also partly due to the section of data that is being reported. Consider an example of transmittance for a 50° incidence angle ($\phi_i = 0^\circ$ and $\theta_i = 50^\circ$) on the flat surface of the SunOptics lens. Figure 96 compares the incident plane, $\phi_s = 180^\circ$ and $\phi_s = 0^\circ$, of the two lab's output data to a full spherical set of raw data from LBNL for the same 50° incidence angle. Both the shapes seen in the planar data reported by the labs (a) can be seen in the full hemisphere scatter data (b). As expected, the LBNL planar data aligns with the 0° plane. The LTI optics data appears to be an average between the various output planes that likely represent the 0° plane for other incident directions of light.

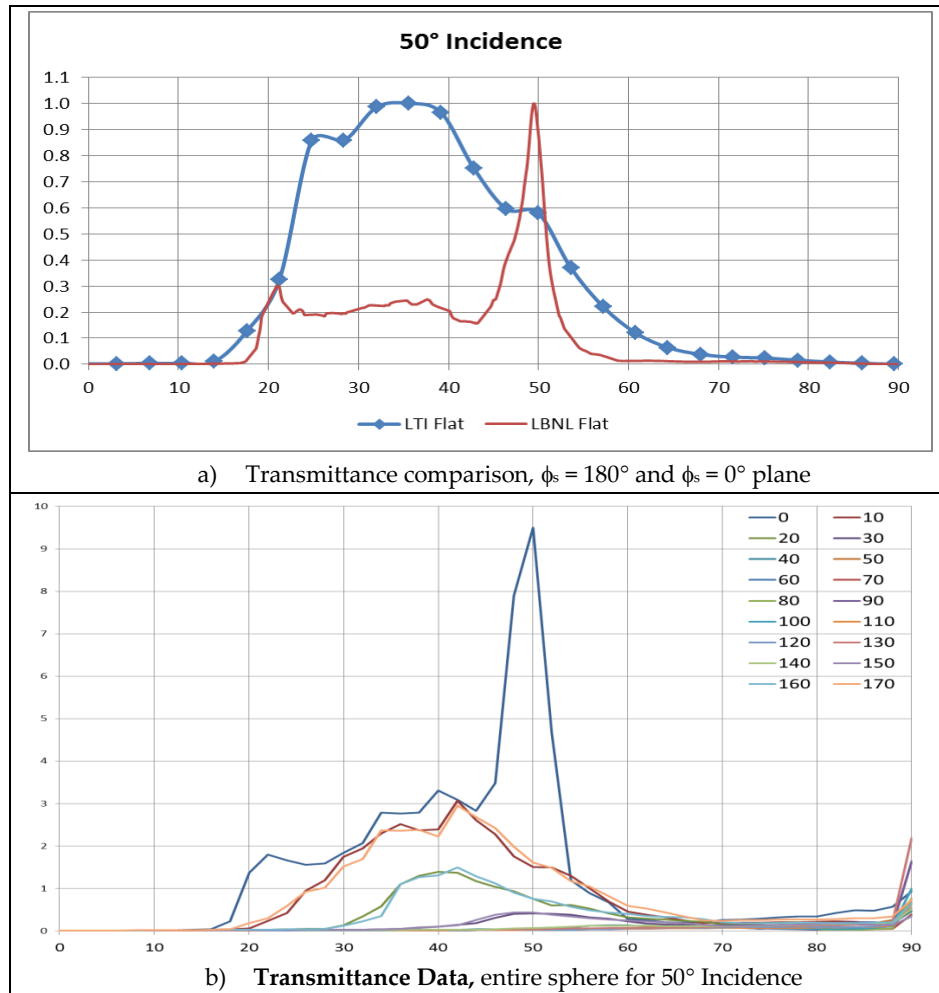


Figure 96: Comparison of symmetric and asymmetric scatter data

Figure 97 compares the reflectance measurements of the **flat** side of the Sunoptics prismatic lens. Being the flat side of this material, a significant level of specularity is expected, particularly at the higher incidence angles where total internal reflection would begin to occur. Both sets of data show specularity, more so at the higher angles. At normal incidence, they both show a wider spread is likely due to interaction with the prisms on the backside of the material. At the higher incident angles, the data shows specular spikes mostly corresponding with the mirror angle; however LTI Optics data seems to be shifted by about 5°. LTI Optics data also shows a wider spread partly due to more coarse resolution of the measurements and partly due to the averaging of the data.

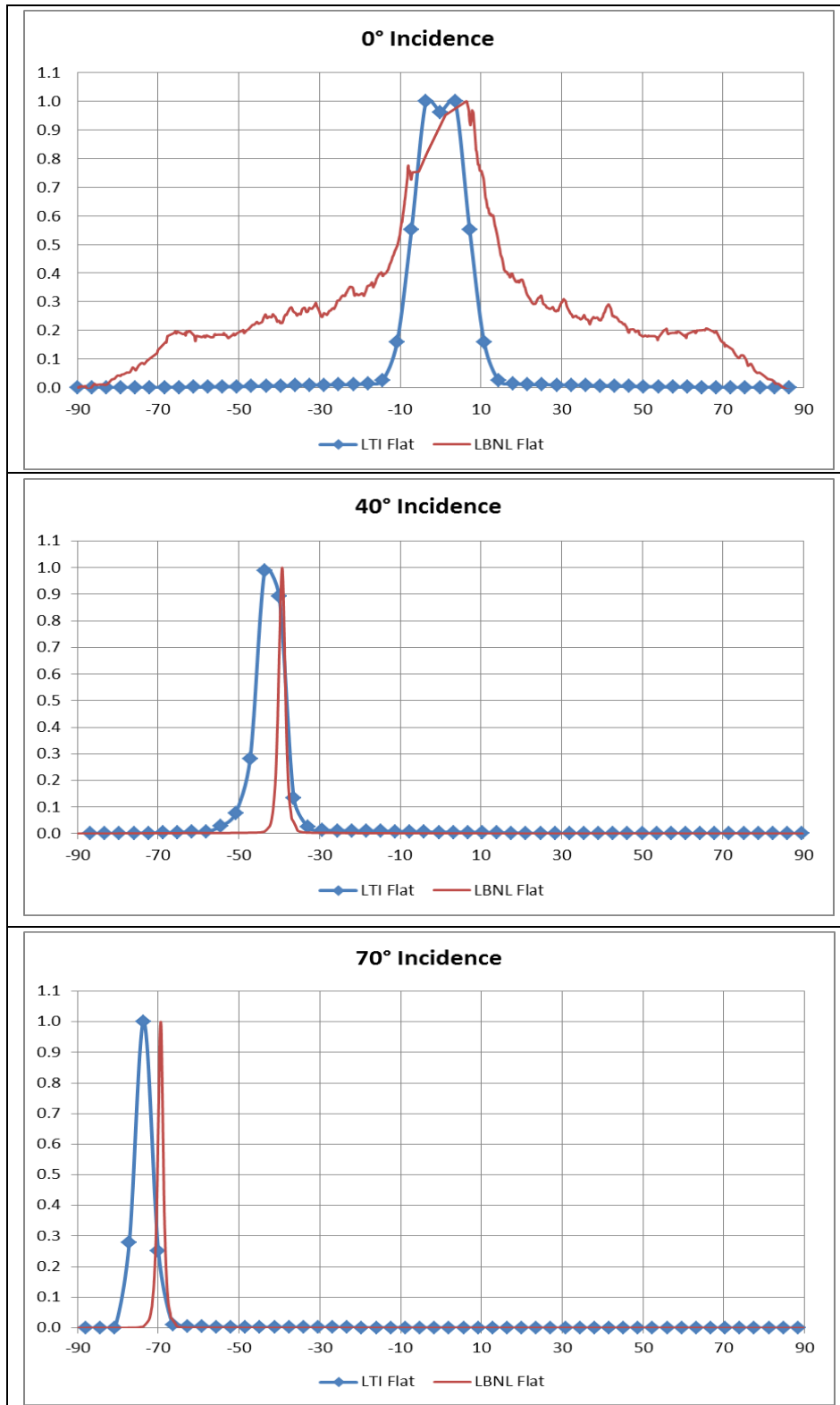


Figure 97: Comparison of SunOptics pyramid flat side reflectance measurements

Figure 98 compares the transmittance measurements for light incident on the **prism** side of the SunOptics lens material. Both data sets match up better, containing a spread of

light to either side of a direct beam. At the higher incidence angles, the LTI data starts to show more of a shift away from the direct angle towards the material normal: consistent with the theoretical studies. The data also exhibits less direct beam transmittance than the flat side of the lens which is also consistent with the theoretical studies which show more of a scatter when incident light is striking the pyramids directly.

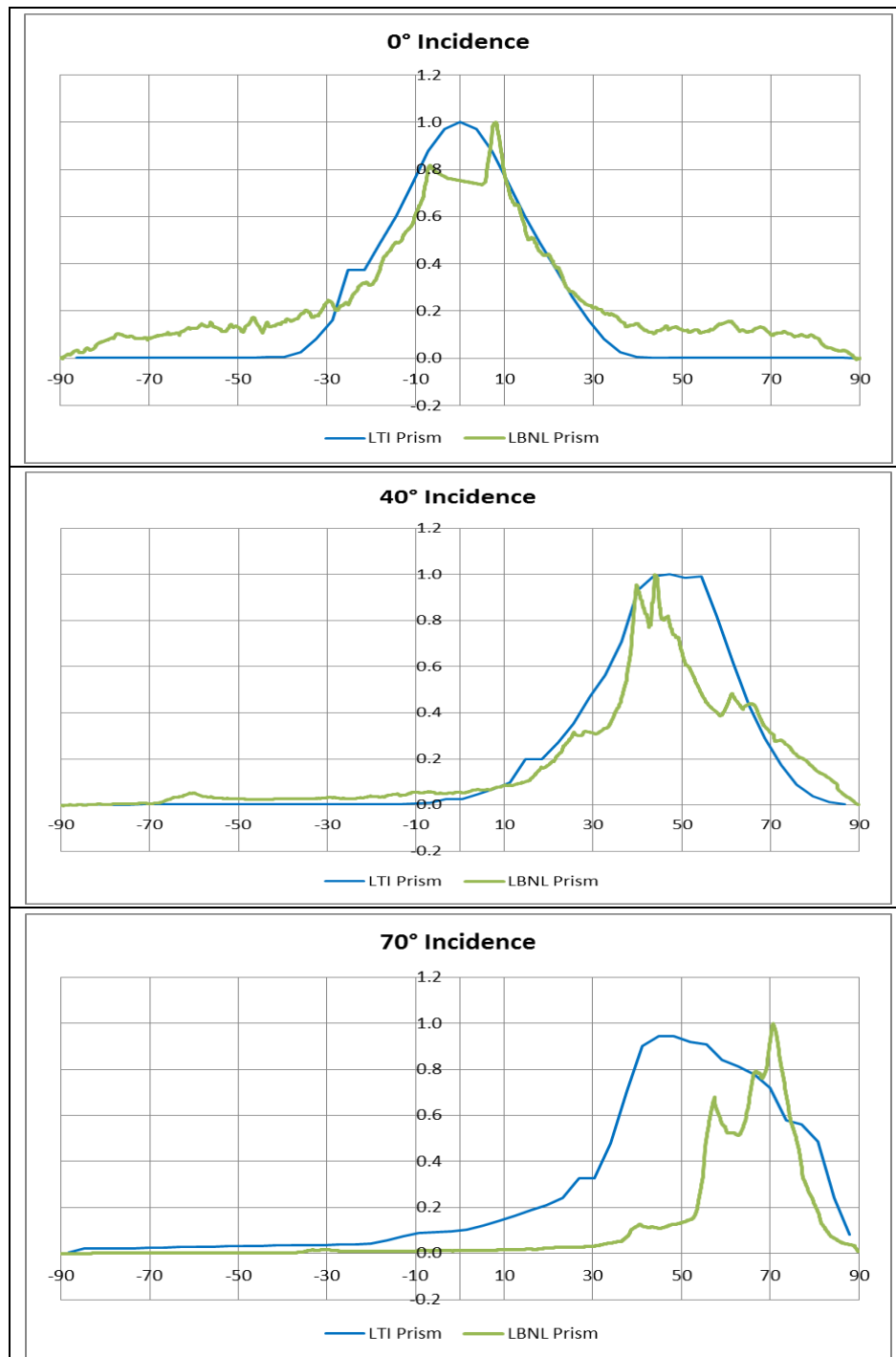


Figure 98: Comparison of SunOptics Pyramid prism-side transmittance measurements

Figure 99 compares the reflectance measurements for the **prism** side of the SunOptics lens material. One would expect very little to no specularity for this surface due to its prism texture, however, there is a strong specular component exhibited in LBNL data. Opposite of the flat side, the data shows more specularity at perpendicular angles shifting to more diffusion towards the normal at higher angles.

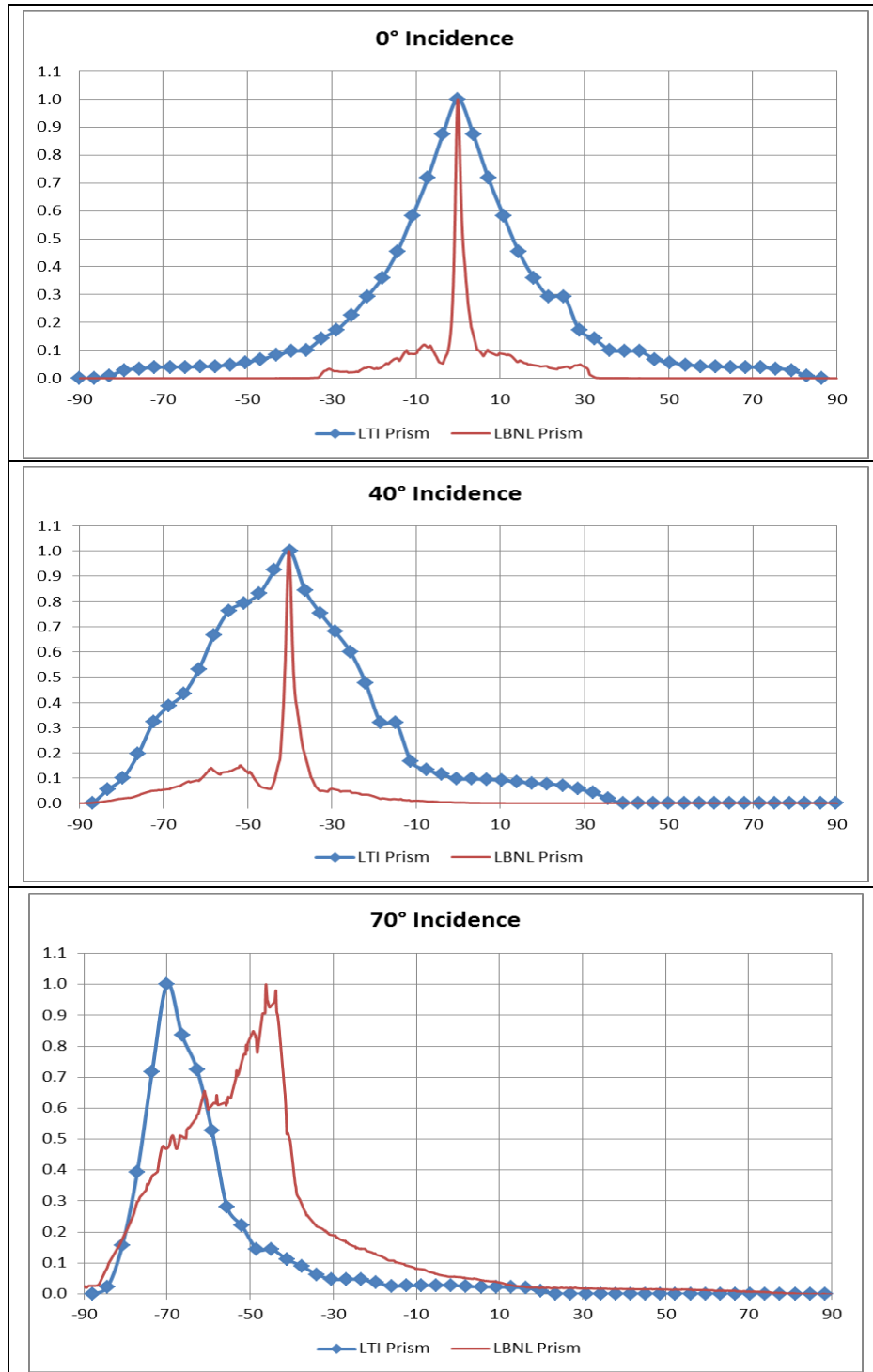


Figure 99: Comparison of SunOptics Pyramid prism-side reflectance measurements

Figure 100 shows the original BTDF information and samples measured.

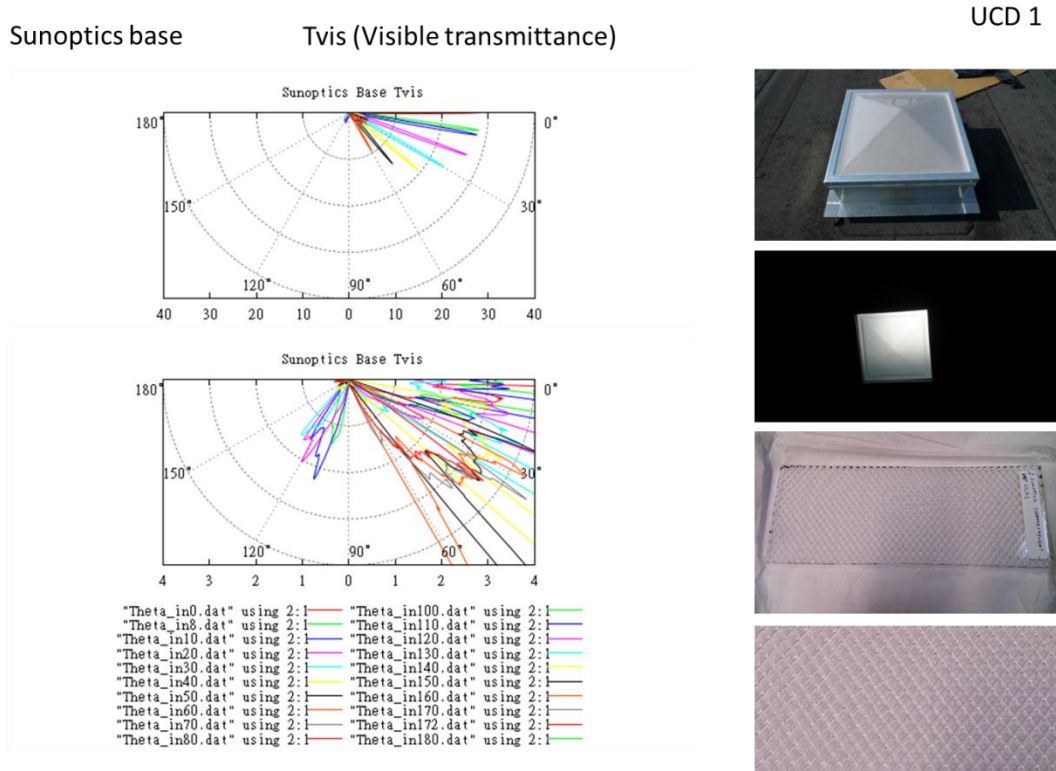


Figure 100: Sample results present the DAQ (BTDF/cos(theta_out)) of Sunoptics pyramid prismatic skylight base material

A.3 SunOptics Reflector

Sunoptics reflector

Rvis (Visible reflectance)

UCD 5

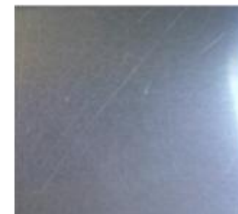
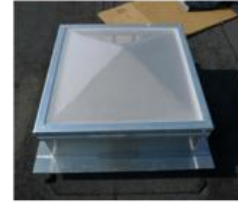
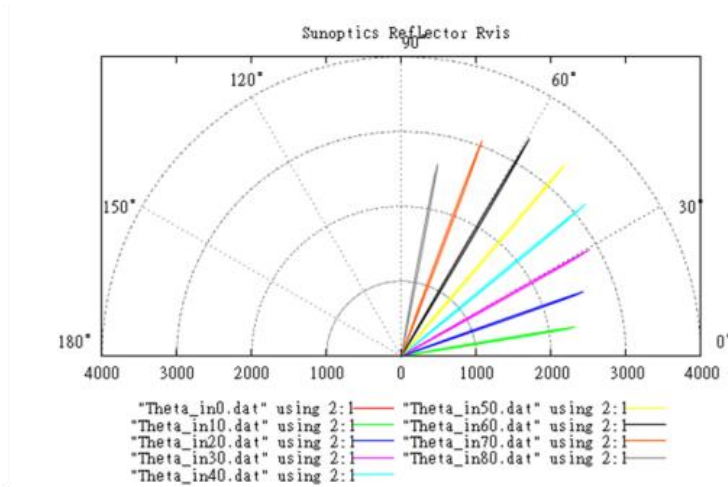


Figure 101: Sample results present the DAQ (BRDF/cos(theta_out)) of Sunoptics pyramid prismatic skylight reflector material

A.4 Suntunnel Base Diffuser

The following Figure 102 through Figure 105 show comparisons of the measured BSDF data for the SunTunnel lens material. Similar to the SunOptics lens there are a number of instances where the data does not align very well. Anisotropic definitions created via simulation were used in lieu of this data.

For the transmittance measurements of this material, there are often two or three peaks in both data sets. They are not always aligning with each other but indicate that both measurements picked up some level of split-beam behavior. The scatter also seems to shift so that it is roughly centered on the directly transmitted ray.

The reflectance measurements show some specularity off of the flat side of this material except for at a normal incidence where some spread of light is shown. The reflectance on the prism side of the material is much less specular as would be expected. There are often two or three peaks of reflectance that occur that also shift such that they are centered on a mirrored ray direction.

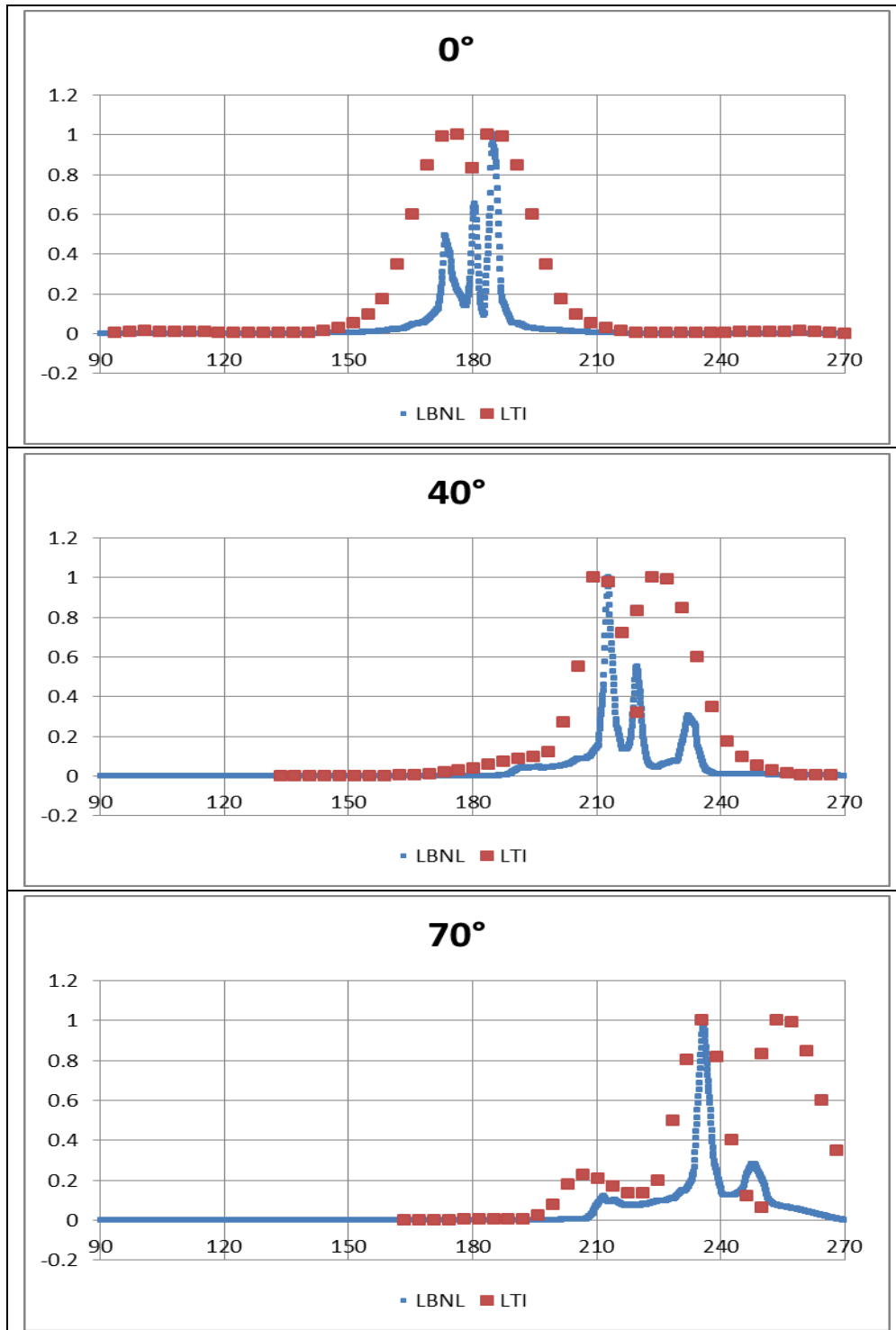


Figure 102: Comparison of SunTunnel Pyramid flat-side transmittance measurements

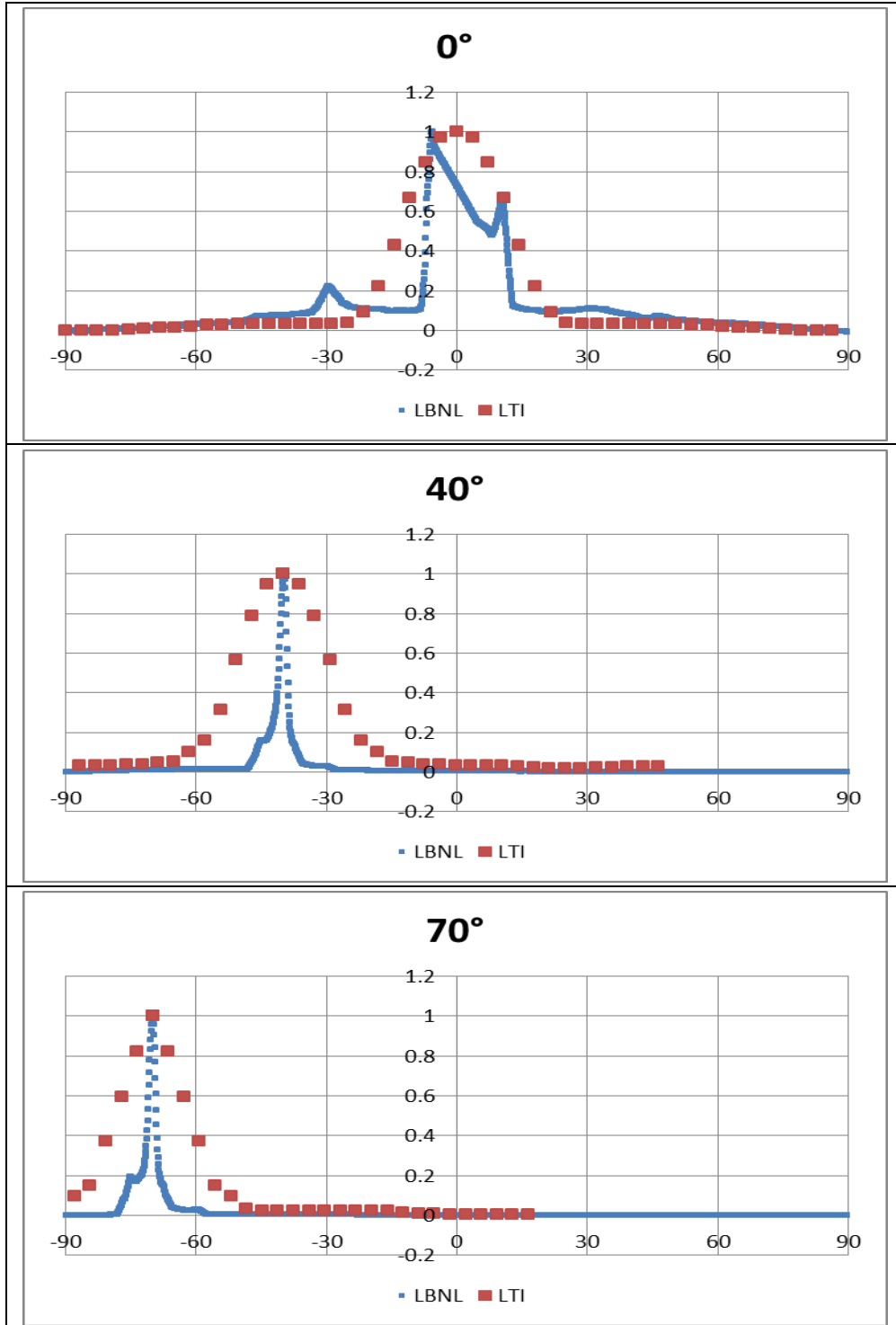


Figure 103: Comparison of SunTunnel Pyramid flat-side reflectance measurements

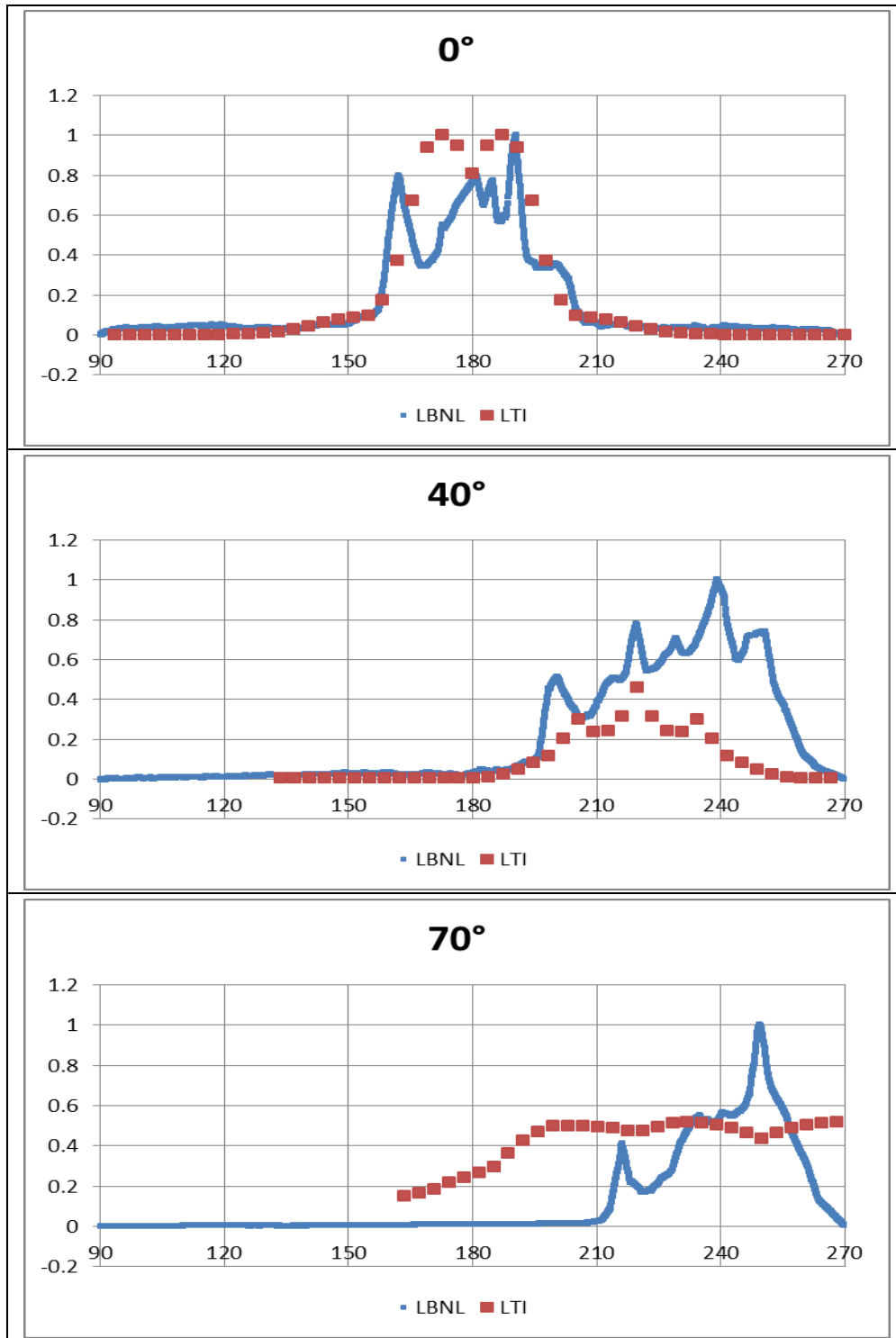


Figure 104: Comparison of SunTunnel Pyramid prism-side transmittance measurements

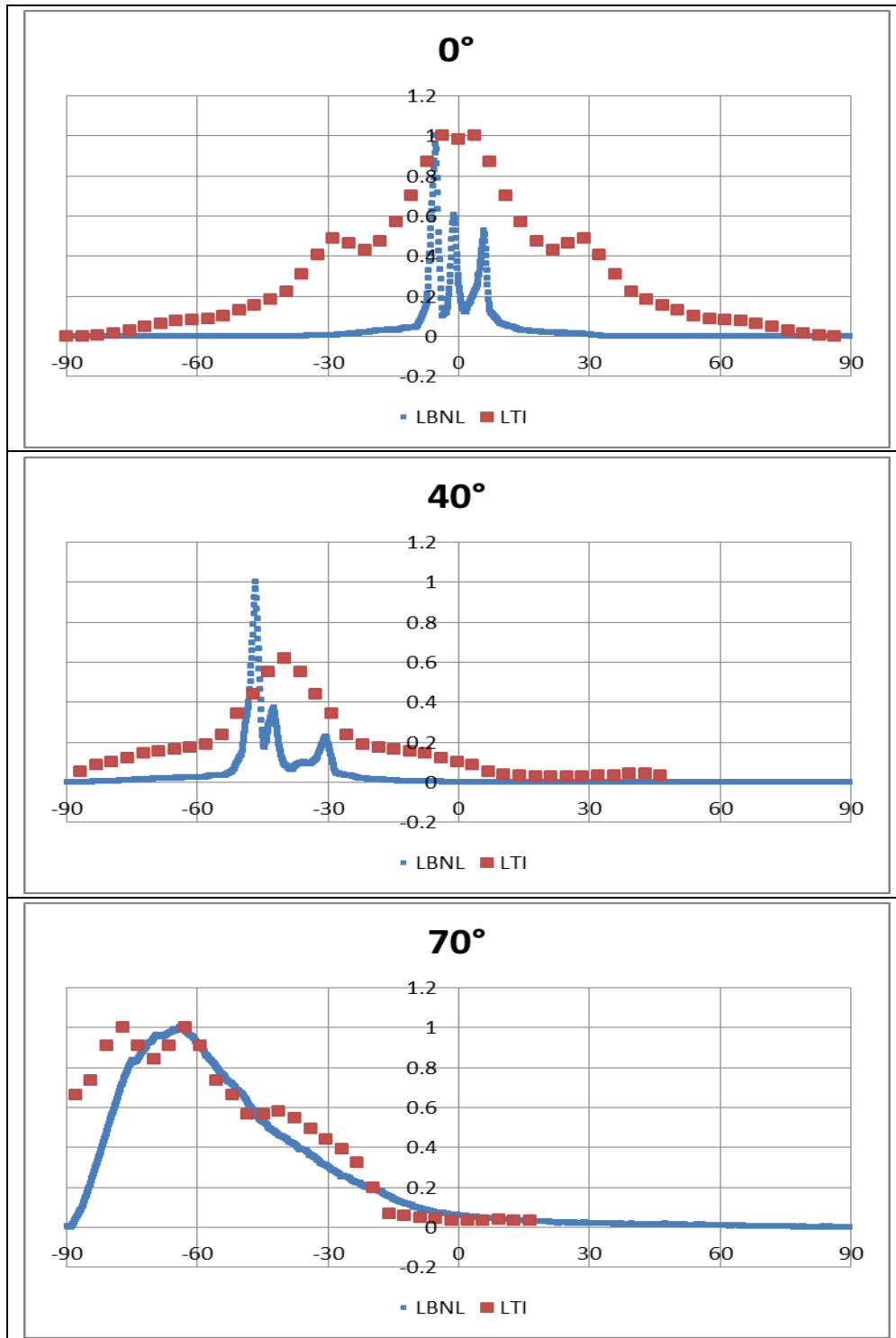


Figure 105: Comparison of SunTunnel Pyramid prism-side reflectance measurements

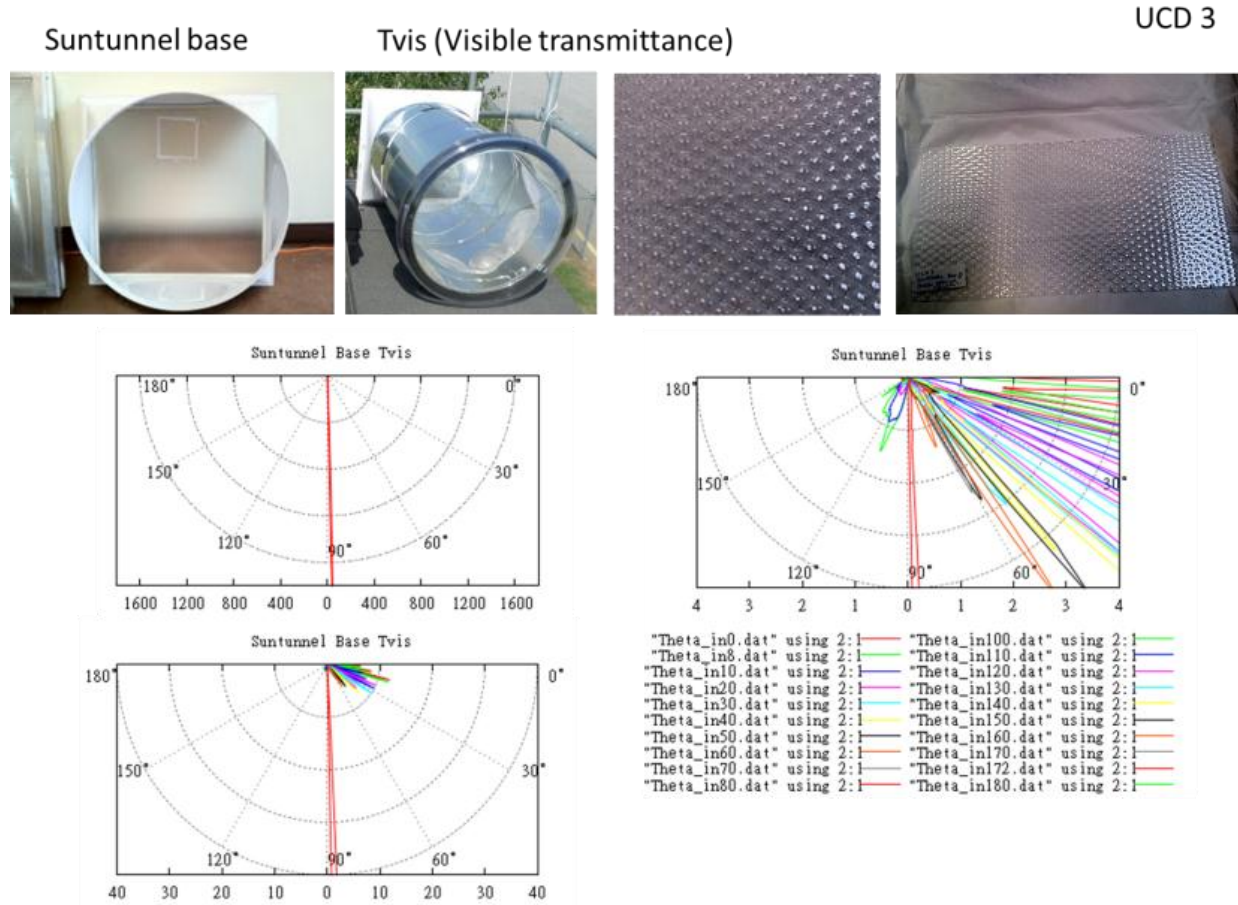


Figure 106: Sample results present the DAQ (BTDF/cos(theta_out)) of Velux SunTunnel base material

Suntunnel base

Rvis (Visible reflectance)

UCD 3

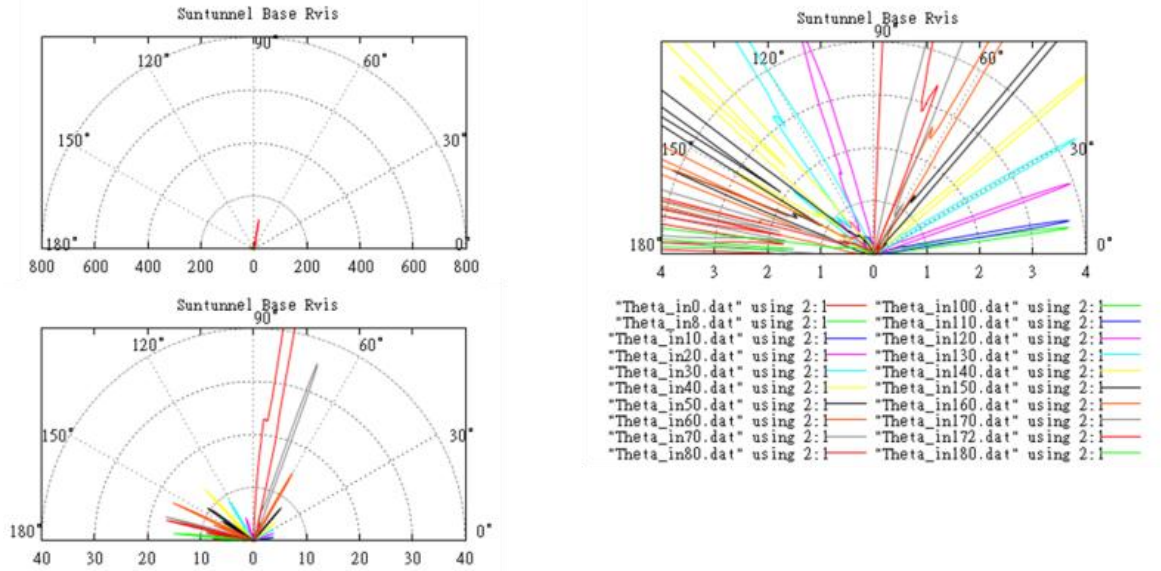


Figure 107: Sample results present the DAQ (BRDF/cos(theta_out)) of Velux SunTunnel base material

A.5 Suntunnel Tube Walls

Suntunnel reflector

Rvis (Visible reflectance)

UCD 6

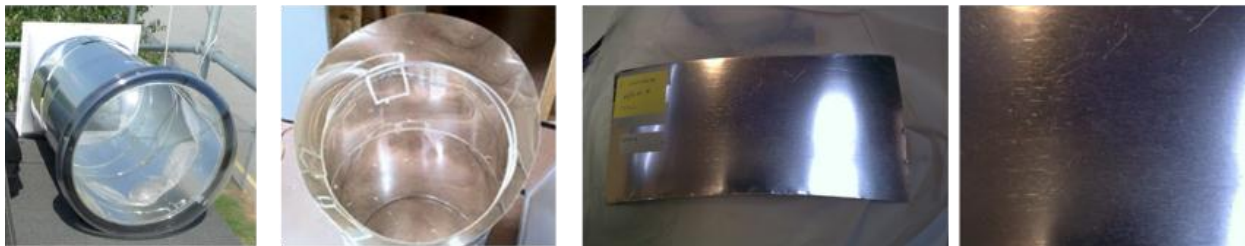
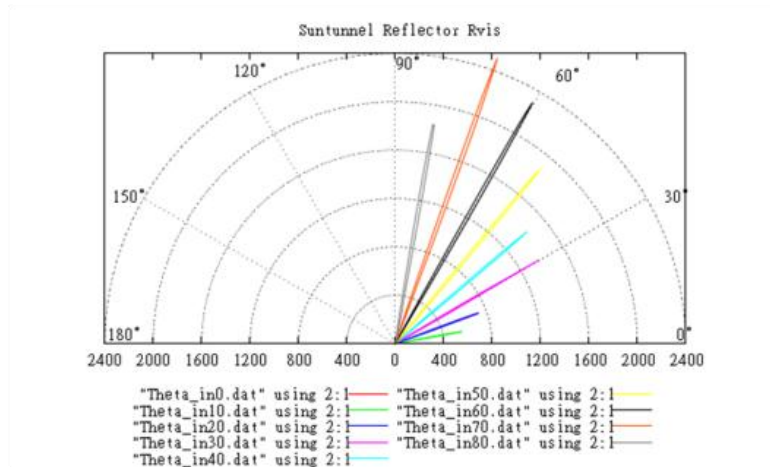


Figure 108: Sample results present the DAQ (BRDF/cos(theta_out)) of Velux SunTunnel reflector material

A.6 Suntunnel White Boot

UCD 4

Suntunnel bottom white Rvis (Visible reflectance)

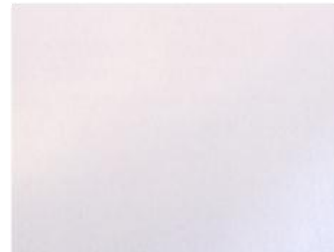
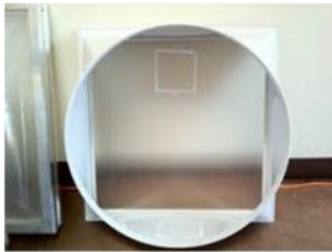
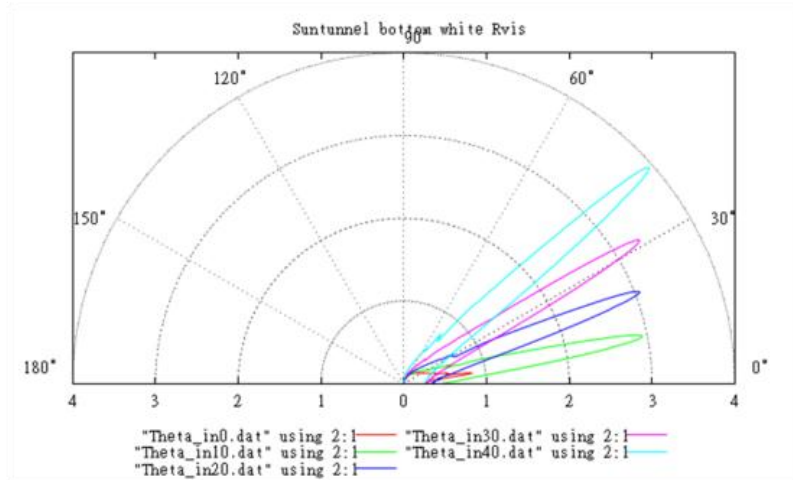


Figure 109: Sample results present the DAQ (BRDF/cos(theta_out)) of Velux SunTunnel white material

Appendix B: On-site Material Measurements

Material measurements were taken for any on-site elements that would impact the optics of the skylight system, particularly for any exposed wood in the roof and skylight framing, the floor and walls of the goniophotometer room. Reflectance was derived from luminance measurements of the material and of a reference white card. The luminance measured during the material reflectance measurements are shown below in Table 6.

Table 6: Measured reflectance for black wall, floor and Wood

Black Wall	Reference
41.45	2.04
41.81	2.06
35.63	1.6
34.67	1.55
35.09	1.55
Average 37.73	1.76

Black Floor	Reference
36	0.6
37.61	0.55
36.73	0.5
Average 36.78	0.55

Wood	Reference
2630	1297
2602	1369
2533	1352
2551	1348
6698	1906
6517	1873
6501	1942
Average 4290	1584

Appendix C: Illuminance meter calibration

Tables 10 and 11 below show the results of the illuminance meter calibration tests. They were repeated after it was found out that the Velux meter was not leveled. A correction factor will be determined for the measurements conducted before the Velux meter was leveled.

Table 7: Results of first illuminance meter calibration

Set 1		Set 2	
CLTC Meter	Velux Meter	CLTC Meter	Velux Meter
8203	8760	6217	5960
8227	8790	6214	5970
8170	8760	6222	5980
8194	8770	6230	5990
8196	8780	6257	6020
8106	8730	6275	6040
8078	8670	6272	6040
8032	8640	6256	6020
8060	8660	6251	6030
Average 8141	8729	Average 6244	6006

Table 8: Results of second illuminance meter calibration

Set 3		Set 4	
CLTC Meter	Velux Meter	CLTC Meter	Velux Meter
6642	6680	9147	9430
6635	6680	9151	9420
6644	6680	9140	9420
6652	6700	9121	9410
6646	6700	9135	9420
6659	6710	9111	9400
6675	6720	9102	9390
6683	6720	9069	9370
6684	6730	9076	9370
6694	6740	9053	9360
Average 6661	6706	Average 9111	9399

Appendix D: Sky Patching Study

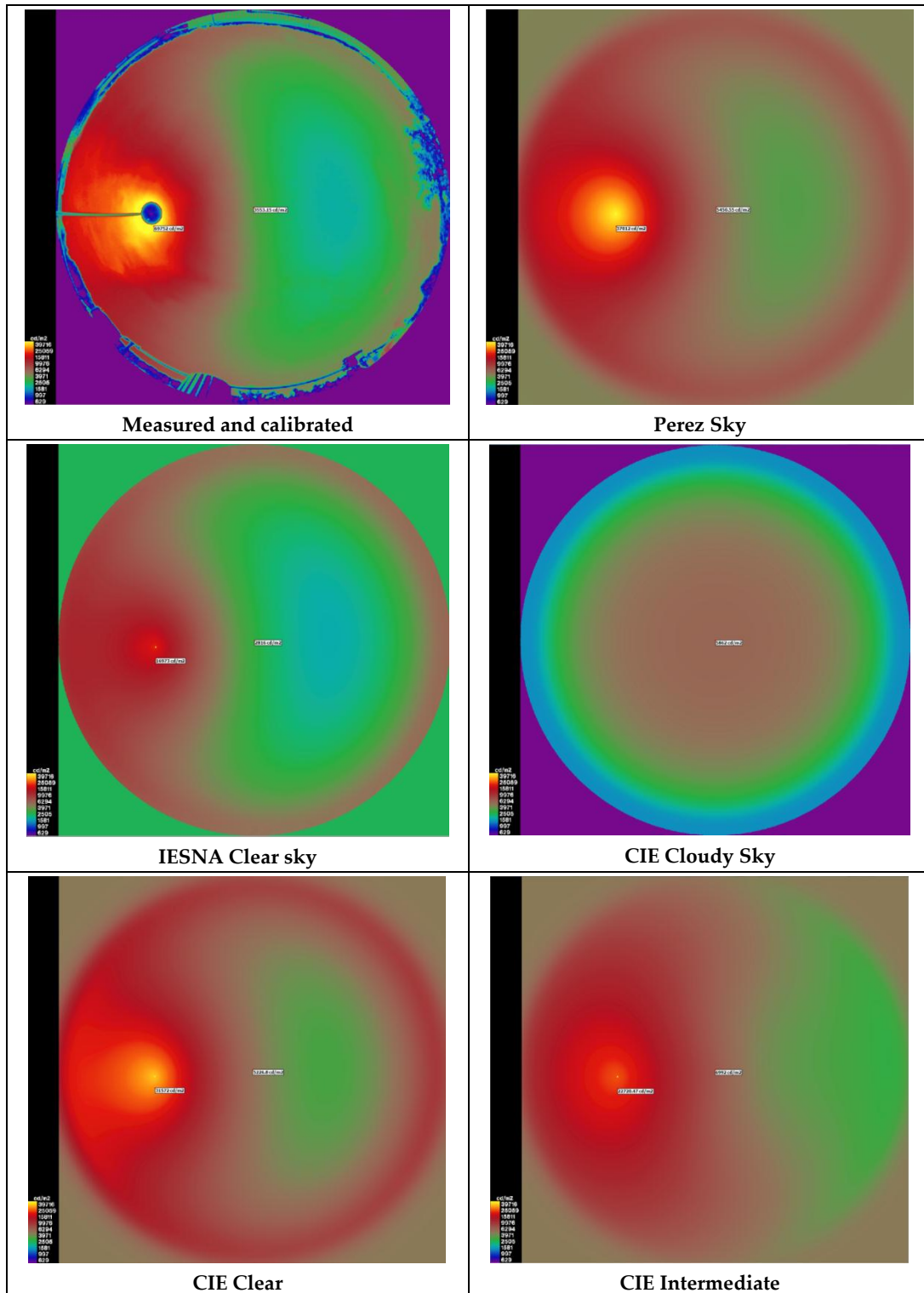


Figure 110: Standard sky types considered for shielded portion of measured sky

Appendix E: References

1. Committee, S.a.L.P.T.P., *Photometric Testing of Skylight and Tubular Daylighting Devices under Hemispherical Sky Conditions*, 2010, IESNA.
2. Thanachareonkit, A.F., L.; Papamichael, K., *Portable, durable instruments for sky luminance distribution field measurements*". IES Annual Conference, Toronto, 2010.
3. *Nikon fish-eye lens FC-E9 information page*. 2010 [cited 2010 July]; Available from: <http://imaging.nikon.com/lineup/accessory/converter/fc-e9/>.
4. E2387, A.S., *Standard Practice for Goniometric Optical Scatter Measurements*. 2005.
5. Apian-Bennewitz, P., *New scanning gonio-photometer for extended BRDF measurements*. SPIE Optics + Photonics, 2010.
6. International, A., *Plexiglas Acrylic Sheet Optical and Transmission Characteristics*.
7. Klems, J.H., *A New Method for Predicting the Solar Heat Gain of Complex Fenestration Systems I and II*. ASHRAE Transactions, 1993. **100**(1): p. 21.
8. Ward, G.M., R.; Lee, E.S.; McNeil, A.; Jonsson, J., *Simulating the Daylight Performance of Complex Fenestration Systems Using Bidirectional Scattering Distribution Functions within Radiance*. Leukos, 2011. **7**(4).
9. Ward, G., *A Variable-resolution BSDF Implementation*. Annual Radiance Conference, 2011.
10. Windows & Daylighting Group, B.T.P.L., *Window 6.2 / Therm 6.2 Research Version User Manual*. 2008. **LBNL-941**.
11. Ward, G., *Using the New Radiance BSDF Material Primitive*. Annual Radiance Conference, 2011.
12. Ward, G., *genBSDF Manual*. 2010.
13. Murray-Coleman, J.F.a.S., A.M., *The Automated Measurement of BRDFs and their Application to Luminaire Modeling*. Journal of the Illuminating Engineering Society, 1990(Winter 1990): p. 12.